

POPULATION PROCESSES AND PATTERNS ACROSS SCALES

A Dissertation

Presented to the Faculty of the Graduate School

of Cornell University

in Partial Fulfillment of the Requirements for the Degree of

Doctor of Philosophy

by

Hidetoshi Inamine

December 2017

© 2017 Hidetoshi Inamine
ALL RIGHTS RESERVED

POPULATION PROCESSES AND PATTERNS ACROSS SCALES

Hidetoshi Inamine, Ph.D.

Cornell University 2017

A major challenge in ecology and evolutionary biology is to understand how biological patterns at one scale are generated by a multitude of processes operating at various scales. Two approaches are especially powerful at linking these processes to patterns: mathematical modeling and using a citizen science dataset. This dissertation uses these two approaches to detect unobservable biological processes from observable patterns in three separate studies: monarch butterfly population dynamics in eastern United States, microbiota population dynamics in fly gut, and mating strategy dynamics in hybridizing species pairs. First, the dissertation tests whether a continental population decline of the monarch butterfly is caused by the scarcity of milkweed, as the milkweed decline has been shown to locally impact monarch population. The study concludes that the milkweed scarcity is not the cause of the continental monarch decline. An observation made at a microscopic scale cannot be extrapolated to explain the pattern at a macroscopic scale. Second, the dissertation develops novel method to understand population dynamics of ingested bacteria from fecal time-series taken from its host. Application of this method to experiments using *Drosophila* shows that bacterial population is regulated over larger gut area in the host as the density of bacteria increases. Information on processes at a microscopic scale may be preserved at a macroscopic scale. Third, the dissertation develops a model to understand how unequal population sizes between hybridizing species pairs influence the evolution of mate choosiness in

these species. An observation of greater choosiness in a smaller population has often been interpreted as evidence for reinforcement, but our results suggest that this interpretation is not valid. Some microscopic processes may dominate others to generate macroscopic patterns. Lastly, this dissertation highlights the importance of scale not only in basic science, but also in applications such as conservation and medicine.

BIOGRAPHICAL SKETCH

Hidetoshi Inamine was born and raised in subtropical biodiverse island of Okinawa, Japan. He enjoyed collecting and rearing insects and plants as a child, but never fathomed a research career in ecology as a possibility. He completed his B.A. in Biological Sciences (with specialization in Neuroscience) at the University of Chicago in 2009. His undergraduate thesis (advised by Paul Vezina) focused on dissecting a molecular pathway underlying amphetamine sensitization in laboratory rats, an area far removed from theoretical ecology and evolutionary biology. Yet, Hidetoshi enjoyed courses in ecology and evolutionary biology at Chicago, especially the mathematical and theoretical aspect of the field.

To assess whether he wanted to pursue a research career in this field, Hidetoshi worked under Joy Bergelson between 2009 and 2011, on a project investigating gene-for-gene interaction between a model plant *Arabidopsis thaliana* and a pathogen *Pseudomonas syringae*. During this time, he also studied insect-predator-pathogen population dynamics under Greg Dwyer. These experiences cemented Hidetoshi's academic interests.

In 2011, Hidetoshi moved to Cornell University to pursue a Ph.D. in ecology and evolutionary biology (with a minor in applied mathematics) under Stephen Ellner. Since attending the Complexity Science Summer School at the Santa Fe Institute in 2012, he has been fascinated with understanding how ecological processes operating in one "scale" percolate across and create patterns in another "scale". Over the years, this interest morphed into the diverse projects forming this dissertation. Hidetoshi begins a post-doctoral position at the Pennsylvania State University with Katriona Shea and Angus Buckling after Cornell.

To my parents, Naoko and Morio Inamine, and my siblings.
And to Dan.

ACKNOWLEDGEMENTS

Throughout my time at Cornell, I have benefitted from generous support from mentors, scholars, and friends. I am extremely grateful to the members of my dissertation committee for their unwavering attention and advices: Steve Ellner, John Guckenheimer, and Kerry Shaw. Steve has been extremely charitable with his time, intellect, and support, and I could not have asked for a better advisor than him. John and Kerry have been insightful and challenged me to carefully crystalize my thoughts. Committee meetings were always intellectually gratifying and importantly, fun.

I am thankful to Rick Harrison for being a caring mentor and a sharp scholar. He helped shape my view on speciation, and was an instrumental member of the dissertation committee. You are truly missed.

Ellner lab and the reading group has been an exciting and engaging bunch. I am thankful for wonderful discussions and warm rapport.

Cornell University provided ample opportunities for collaborations, and I am especially grateful to Anurag Agrawal, Angela Douglas, and Nicolas Buchon for taking me into their labs and for their mentorships. The collective “we” used in this dissertation reflects the fruitful interactions I had at Cornell. I am fortunate to have worked with and learned from these scholars over various projects: Steve Ellner, Anurag Agrawal, Angela Douglas, Nicolas Buchon, Jim Springer, Peter Newell and Yuan Luo. Many discussions, constructive critiques, and enthusiastic support have transformed these projects into products that would have been impossible to achieve on my own. The whole is greater than the sum of its parts.

Atkinson Center for a Sustainable Future, the Cornell Graduate School, the Cornell Department of Ecology and Evolutionary Biology, the Orenstein Family,

Presidential Life Sciences Fellowship, and the Santa Fe Institute have provided generous support. This endeavor was made possible by the help and support from the administrative staff in the department.

Many friends from Cornell and Ithaca made my time here special. From karaoke to intellectual arguments and out-of-town trips, all are unforgettable. Thank you. Despite years of absence, I am grateful that my family back in Japan has continuously been encouraging and believing in me.

Last but not least, I would like to thank Daniel DellaPosta for traveling down this unique journey with me and for supporting me throughout.

TABLE OF CONTENTS

Biographical Sketch	iii
Dedication	iv
Acknowledgements	v
Table of Contents	vii
List of Tables	ix
List of Figures	x
1 Introduction	1
2 Linking the continental migratory cycle of the monarch butterfly to understand its population decline	6
2.1 Abstract	6
2.2 Introduction	7
2.3 Methods	11
2.4 Results	18
2.5 Discussion	26
2.6 Acknowledgements	31
3 Spatiotemporally heterogeneous population dynamics of gut bacteria inferred from fecal time-series data	32
3.1 Abstract	32
3.2 Introduction	33
3.3 Results	35
3.4 Discussion	50
3.5 Methods	54
3.6 Acknowledgements	62
4 Speciation by reinforcement: dynamics of choosiness evolution under asymmetric population sizes	63
4.1 Abstract	63
4.2 Introduction	64
4.3 Model	68
4.4 Results	75
4.5 Discussion	80
4.6 Acknowledgements	88
A Supplementary information to Chapter 2	89
A.1 Summary of analyses examining quality and potential biases in the NABA dataset.	89
A.2 Statistical analyses to examine temporal change in the relationship between stages of the annual migratory cycle.	103

B	Supplementary information to Chapter 3	117
B.1	Experimental materials and methods	117
B.2	Derivation of theoretical egestion time statistics from models . . .	134
C	Supplementary information to Chapter 4	157
C.1	Mating rate μ	157
	Bibliography	159

LIST OF TABLES

2.1	Regression analyses between stages of the annual monarch migratory cycle	19
2.2	Results from model selection to address the role of migratory inputs and temporal trends in pairwise regional links of the monarch's annual migratory cycle	23
2.3	Proposed threats to the sustainability of the eastern monarch butterfly annual migration	29
3.1	Fate of <i>A. tropicalis</i> ingested by <i>D. melanogaster</i> following administration of <i>A. tropicalis</i> at Low density	47
4.1	Experimental and observational studies with either Howard or Hubbs mating pattern	66
4.2	Asymmetric (<i>i.e.</i> species-specific) parameters in the model and their biological interpretation	76
A.1	A summary of the annual census data used in analyses	90
B.1	Hypothetical microsphere and microbial populations used in numerical examples	151

LIST OF FIGURES

2.1	The annual multigenerational migratory cycle of the monarch butterfly	8
2.2	Temporal decline in the overwintering colony size of the monarch in Mexico	9
2.3	NABA count locations for three regions (NE, MW, and S), and mean population index for each region across years	12
2.4	Continent-wide population links in the annual migratory cycle of the eastern monarch butterfly	21
2.5	Temporal pattern of monarch abundances in the overwintering colonies in Mexico, southern USA, and four independent summer northern indices	24
3.1	Stability of bacteria in mono-association with <i>Drosophila</i>	36
3.2	Schematic of transfer and sampling protocol for <i>Egestion Time Experiment</i> and <i>Microbial Fate Experiment</i>	38
3.3	<i>Egestion time dynamics in Egestion Time Experiment</i>	39
3.4	Compartment diagram for a model with arbitrary number of compartments, and inference scheme based on the model	43
3.5	Proportion of bacteria egested and egestion time statistics from <i>Egestion Time Experiment</i>	45
3.6	Abundance of bacteria in the fly whole body 1 and 5 h post-ingestion in <i>Microbial Fate Experiment</i>	49
4.1	Mating behavior of populations 1 and 3 when K differs between the two populations, and all other parameters remain equal	76
4.2	Transient dynamics of $m(z)$ for populations 1 and 3 when K differs between the two populations, and all other parameters remain equal	77
4.3	Mating behavior of populations 1 and 3 when γ differs between the two populations, and all other parameters remain equal	79
4.4	Mating behavior of populations 1 and 3 under asymmetric population sizes and asymmetric γ_x	81
4.5	Mating behavior of populations 1 and 3 under asymmetric population sizes and asymmetric α_x	82
4.6	Mating behavior of populations 1 and 3 under asymmetric population sizes and asymmetric s_x	83
A.1	Number of counts in NABA dataset across NE, MW, and S	92
A.2	Fraction of data points taken in each month, out of the total number of data points in a given year	93
A.3	Fraction of the year where there was at least one data point in the 7-day window	95

A.4	The number of years with a count in the 7-day window for each date	96
A.5	Correlation between original population index and the truncated population index for NE and MW	97
A.6	Raw data counts for the NE and MW	98
A.7	Number of monarchs observed with varying party hours in NE and MW, from year 1997 and 2012	102
A.8	Ripley's K function for the spatial locations of NABA population counts in each year.	104
A.9	Ripley's K function as a function of year for the NE and MW regions	104
B.1	Density of <i>A. tropicalis</i> colonies from fly homogenates plated on mMRS media with and without tetracycline	119
B.2	Consistency between manual and automated counts of microspheres and bacteria	120
B.3	Compartment diagram for one, two, and three compartments models	136
B.4	Cumulative distribution function and statistics of the bacteria egestion time from simulating bi-directional model	154
B.5	Some examples of possible functional forms for f and g	155
B.6	Egestion time statistics from a simulation and experiments	156

CHAPTER 1

INTRODUCTION

Population dynamics are driven by various ecological processes such as competition, predation, and reproduction. These processes, however, may operate at spatial, temporal, and organizational scales different from that at which the dynamics are observed. A major challenge in ecology and evolutionary biology is to elucidate how biological patterns at one scale are generated by a multitude of processes operating at various scales [1].

Biological processes are partitioned into different scales to simplify and better understand biological systems. For example, ecological, microevolutionary, and macroevolutionary processes are traditionally considered to be at an ascending order of timescales, where processes dominating the dynamics at one scale are considered weak in another scale [2]. A focus on a particular scale does not mean that the weaker processes are absent, but assumed to be constant in the background. Separation of scales allows ecologists and evolutionary biologists to ignore unobservable processes such as heterogeneous selection pressure over population dynamics, population dynamics over geological timescale, *etc.*

Processes, however, percolate across scales and modify patterns. For example, Yoshida and co-workers [3] showed that rapid evolution occurring on ecological timescales can leave a distinct signature (*i.e.* half-period phase lags) in predator and prey population dynamics. In a different example, Murdoch and co-workers [4] showed that the degree of interactions between predator and prey (*i.e.* generalist *vs.* specialist predator) generates specific cycle periods of the predator (*i.e.* period much longer than the generation time of either predator or prey); pattern at the population level results from processes at the

community level.

These two examples highlight some common themes in the problem of scale. First, mathematical models are powerful tools to link processes to patterns across scales [1, 5]. In these examples, models gave clear signatures of unobserved processes, guiding the authors to look for previously unrecognized patterns. Second, understanding how processes percolate across scales in one system allows us to test the generality of this percolation in other systems. For example, a follow-up study on rapid evolution [6] showed that rapid evolution occurs widely across various empirical systems. Evolution can no longer be ignored in ecological studies. Similarly, [4] showed that the degree of interactions between predator and prey was consistently reflected in cycle periods across 108 time series of natural population. The community context of a predator must be considered when studying its population dynamics. By studying how processes generate patterns across scales, we can start to understand what kind of biological information is necessary for different level of theoretical abstraction [7].

This dissertation is interested in understanding how biological patterns are generated due to unobserved processes at various scales. We present three independent studies centered around this question: studies on monarch butterfly population dynamics, microbiota population dynamics, and mating behavior evolution in hybridizing species. Complementing mathematical models, we also employ a citizen science dataset, a recent approach to uncover processes operating at a scale that was previously unobservable [8].

Chapter 2 presents an empirical study on monarch butterfly (*Danaus plexippus*) population dynamics that examines whether microscopic processes (*i.e.* decline of host plants in the Midwest) can be extrapolated to explain a pattern

observed at macroscopic scale (*i.e.* continental population decline of monarch butterflies). Specifically, we use a long-term citizen science dataset to test a widely-held hypothesis in monarch butterfly conservation: Monarch butterflies are declining precipitously in eastern United States because the abundance of milkweed, the only host plant that the butterflies rely on, is declining, especially in the agricultural Midwest (the “milkweed limitation hypothesis”). This hypothesis stems from studies showing that milkweed decline (caused by increased use of genetically modified herbicide-resistance crops) locally impacts butterfly and caterpillar abundance. However, whether we can extrapolate from these studies to explain the continental scale population decline has been unclear. Using retrospective analysis, we find that the decline of local milkweed population is not the cause of the continental decline of the butterfly population. Instead, we argue that monarch success during the fall migration and re-establishment strongly contributes to the butterfly decline. This chapter illustrates how citizen-science data allow for investigations at “large spatial scales, where important processes not detectable at local scales may dominate dynamics” [8]. Importantly, this chapter highlights the problem and difficulty of scale in biological conservation.

Chapter 3 presents an experimental and methodological study on bacterial population dynamics that detects microscopic processes (*i.e.* heterogeneous interactions in the host gut) from macroscopic patterns (*i.e.* fecal time-series data). A major challenge in microbiological research is to understand the heterogeneous interactions between the host and the community of microorganisms that it harbors (microbiota). Yet, direct observation of these interactions is difficult due to the microscopic scale of the interactions and the spatio-temporal variation in host responses as well as the microbiota composition. We are therefore

presented with an “inverse problem”, where observable data must be used to infer unobservable processes. These hurdles necessitate a development of ecological theory where “patterns must be understood as emerging from the collective behaviors of large ensembles of smaller scale units” [1]. In this chapter, we derive statistics from mathematical models that link bacterial population dynamics from fecal time-series data (a type of data widely-collected) to the bacterial population dynamics in the host gut. Applying these statistics to experiments on *Drosophila melanogaster* and its microbiota, we find that the host fly regulates its microbiota over a larger area of the gut as the density of the ingested bacteria increases. These models help us recognize changes in a previously unstudied pattern as providing information about changes in host-microbe interactions. Furthermore, this chapter suggests the potential importance of ecological theory in medicine.

Lastly, Chapter 4 presents a theoretical study on speciation of a hybridizing species pair, examining what kind of macroscopic patterns (*i.e.* mating patterns over evolutionary timescale) are generated through microscopic processes (*i.e.* mate choice under unequal population sizes). Evolution of choosiness for mates in order to reduce hybridization (“reinforcement”) is considered to be an important driver of speciation. Two lines of arguments make contradicting predictions on how choosiness evolves when species with different population sizes hybridize. Past empirical studies support both predictions, but the processes underlying these outcomes have not been studied systematically. We focus on a trade-off between opportunity to mate and mating with a wrong partner, to understand how choosiness evolves. We find that, all else being equal, the species with larger population size becomes more discriminating than the species with smaller population size. An observation of greater choosiness in a smaller pop-

ulation has often been interpreted as evidence for reinforcement, but our results suggest that this interpretation is not valid. Inequalities in encounter rate and cost of hybridization should both be considered in order to understand the mating strategy of hybridizing species.

CHAPTER 2
LINKING THE CONTINENTAL MIGRATORY CYCLE OF THE
MONARCH BUTTERFLY TO UNDERSTAND ITS POPULATION
DECLINE

2.1 Abstract

Threats to several of the world's great animal migrations necessitate a research agenda focused on identifying drivers of their population dynamics. The monarch butterfly is an iconic species whose continental migratory population in eastern North America has been declining precipitously. Recent analyses have linked the monarch decline to reduced abundance of milkweed host plants in the USA caused by increased use of genetically modified herbicide-resistant crops. To identify the most sensitive stages in the monarch's annual multi-generational migration, and to test the milkweed limitation hypothesis, we analyzed 22 years of citizen science records from four monitoring programs across North America. We analyzed the relationships between butterfly population indices at successive stages of the annual migratory cycle to assess demographic connections and to address the roles of migrant population size versus temporal trends that reflect changes in habitat or resource quality. We find a sharp annual population decline in the first breeding generation in the southern USA, driven by the progressively smaller numbers of spring migrants from the overwintering grounds in Mexico. Monarch populations then build regionally during the summer generations. Contrary to the milkweed limitation hypoth-

This chapter is based on the publication "Linking the continental migratory cycle of the monarch butterfly to understand its population decline" by Hidetoshi Inamine, Stephen P. Ellner, James P. Springer, and Anurag A. Agrawal [9].

esis, we did not find statistically significant temporal trends in stage-to-stage population relationships in the mid-western or northeastern USA. In contrast, there are statistically significant negative temporal trends at the overwintering grounds in Mexico, suggesting that monarch success during the fall migration and re-establishment strongly contributes to the butterfly decline. Lack of milkweed, the only host plant for monarch butterfly caterpillars, is unlikely to be driving the monarch's population decline. Conservation efforts therefore require additional focus on the later phases in the monarch's annual migratory cycle. We hypothesize that lack of nectar sources, habitat fragmentation, continued degradation at the overwintering sites, or other threats to successful fall migration are critical limiting factors for declining monarchs.

2.2 Introduction

Cross-continent animal migrations are some of the most spectacular ecological phenomena and are severely threatened [10]. A major hurdle in conceptualizing and conserving animal migrations is understanding the demographic connectivity and population dynamics over the migratory cycle, especially in the face of large spatial movements over long time scales. For hundreds of years the annual migration of the monarch butterfly (*Danaus plexippus*) from Mexico to the northern USA and Canada has captured the imagination of scientists and non-scientists alike [11]. Like many other migratory animals, monarch butterflies have a complex multigenerational cycle and changes in any one of the stages can affect their population dynamics (Figure 2.1).

Monarchs have a history of 10-fold or larger annual population fluctua-

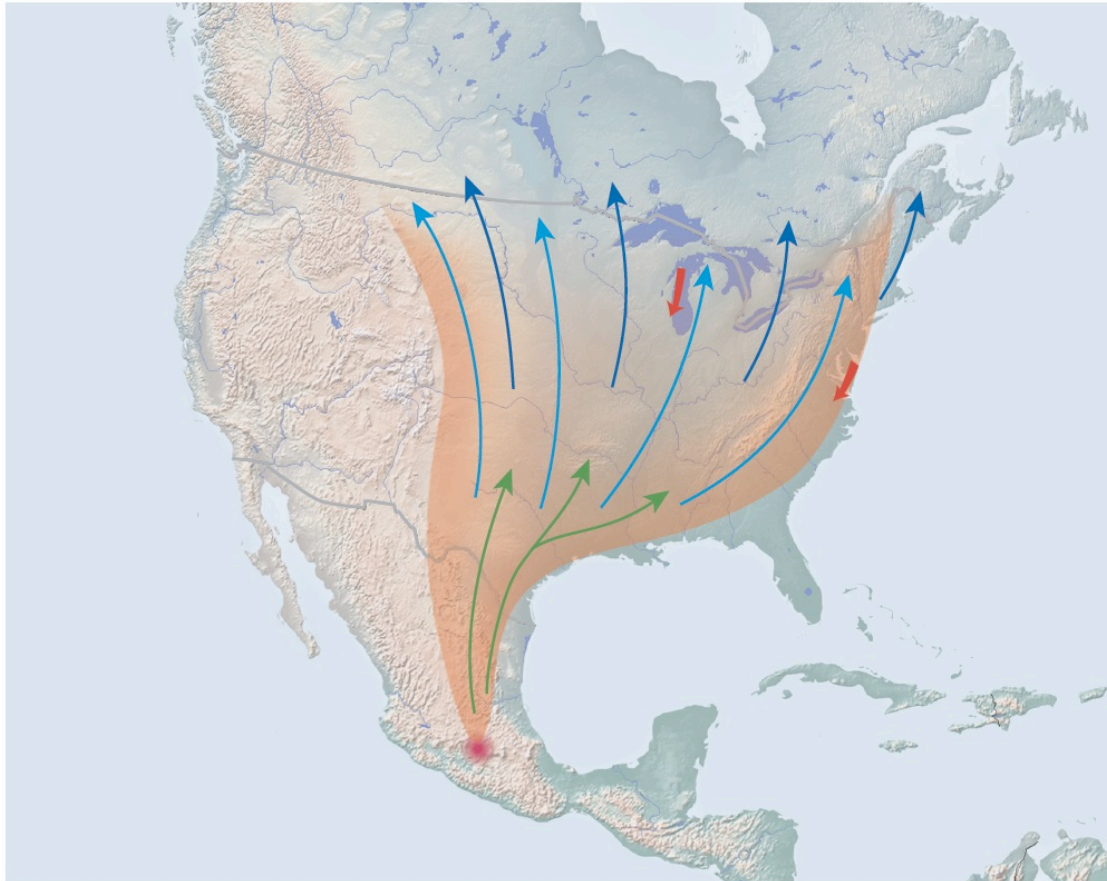


Figure 2.1: The annual multigenerational migratory cycle of the monarch butterfly. The southernmost red dot indicates the high elevation overwintering grounds (generation 0). North pointing arrows indicate spring and summer migration (green = generation 1, followed by 2–3 additional generations). The top of the solid red arrows indicate two funnel points of south flying monarchs for which we have count data, whereas the larger diffused red envelope indicates the overall southern migration. There are smaller monarch populations in Mexico, California, and Florida, but they are not depicted here.

tions [12–14]. Yet, a 2011 study based on 17 years of data revealed a precipitous long-term population decline at the overwintering sites in Mexico [13, 15] and the rate of decline may be increasing over time (Figure 2.2; [16]). Nonetheless, two independent fall monitoring programs that enumerate returning monarchs from the northern USA and Canada did not show a decline over the same time period [17, 18]. Understanding the complex population dynamics of monarchs

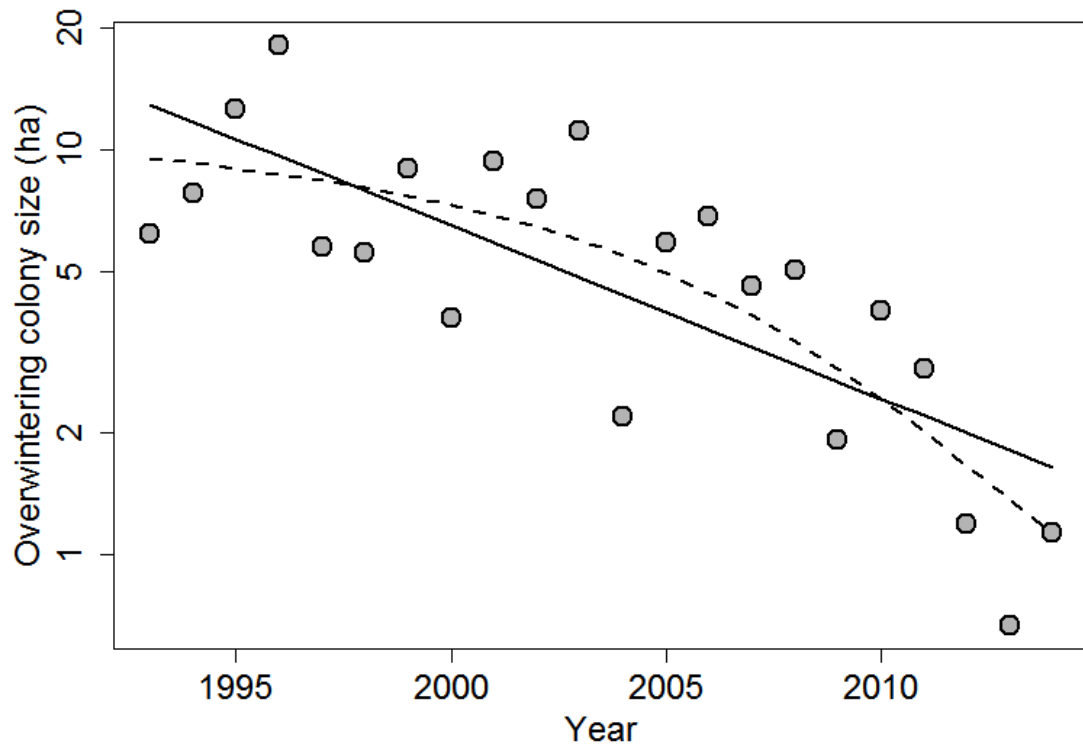


Figure 2.2: Temporal decline in the size of the overwintering colony in Mexico (ha). Note the logarithmic scaling of the y-axis. The fitted linear regression (solid line) is significant ($p < 0.001$) and corresponds to an average decrease of slightly over 9% per year. A fitted spline regression (dashed curve, fitted with the `gam` function in the `mgcv` library) suggests an accelerating decline; the nonlinearity is statistically significant ($p = 0.02$, F -test). Data from [13].

over space and time therefore remains an important ecological as well as conservation challenge.

From a conservation perspective, it is critical to identify key stage(s) influencing population dynamics. The classic case of loggerhead sea turtle conservation exemplifies this issue, as initial efforts emphasized life stages (eggs and hatchlings) that were unlikely to substantially benefit the population [19]. The monarchs' annual cycle has several potentially critical stages [20, 21]. In late winter, overwintering butterflies mate and fly from Mexico north to the southern USA, where most individuals lay eggs on emerging milkweeds, and

die (Figure 2.1). The next generation migrates north, expanding into southern Canada on both sides of the Appalachians, but east of the Rocky Mountains. Additional generations breed in these northern regions. Beginning in late August, unmated butterflies siphon through several funneling points and migrate up to 4000 km back to the overwintering grounds in Mexico. Millions of monarchs ultimately concentrate on about a dozen mountaintops, in an area less than 800 km² [22].

Since the discovery of the overwintering grounds in Mexico, numerous threats to monarchs and their migration have been identified, which largely involve human activities such as logging and agriculture [21, 23–25]. Recent analyses have specifically implicated the decline of milkweed host plants due to increased use of genetically modified herbicide-resistant crops, especially in the agricultural Midwest USA (the “milkweed limitation hypothesis”; [15, 26, 27]). Given that monarch caterpillars exclusively feed on milkweed, it is not surprising that the milkweed decline appears to be locally impacting butterfly and caterpillar abundance [27–29]. These local demographic effects were recently incorporated in prospective models for the monarch’s migratory cycle [30], where a stage-structured matrix projection model for the monarch life-cycle was combined with spatial structure and migration.

Here we take an alternative approach, using multiple data sets covering 22 years of monarch monitoring programs across North America to retrospectively investigate associations between population dynamics in different regions, and to identify stages contributing to the recent population decline. Using count data reported to the North American Butterfly Association (NABA) and other citizen scientist data, we sought to follow the cycle from overwintering abun-

dance, to spring and summer breeding populations, and finally to fall migrating butterfly counts. Our analyses and findings overlap, in part, with other recent analyses of monarch population trends [16–18,31]. However, our study is the first to link the entire annual migratory cycle, and the first to analyze temporal trends in population indices and stage-to-stage relationships through the migratory cycle. Thus, our analyses are uniquely positioned to address the milkweed limitation hypothesis by understanding demographic connectivity at larger temporal and spatial scales.

2.3 Methods

2.3.1 NABA citizen science data

The North American Butterfly Association (NABA) has compiled butterfly counts from participating citizens across North America since 1975. The dataset consists of thousands of observations on the number of adult monarchs, the location, number of participants, and total hours spent in the field for each census. We focus on > 6000 records from 1993–2014, as each of these years had a substantial number of counts (mean of 290 counts/year) and matches the census records available from the Mexico overwintering grounds. Although census locations are not fixed, butterflies are counted across the regions of interest (Figure 2.3A), and should represent regional sums of adults across small scale habitat variation. We scaled each count by total group hours [16, 31, 32]. In Appendix A.1, we show that our results are robust to alternative ways of normalizing counts for observer effort.

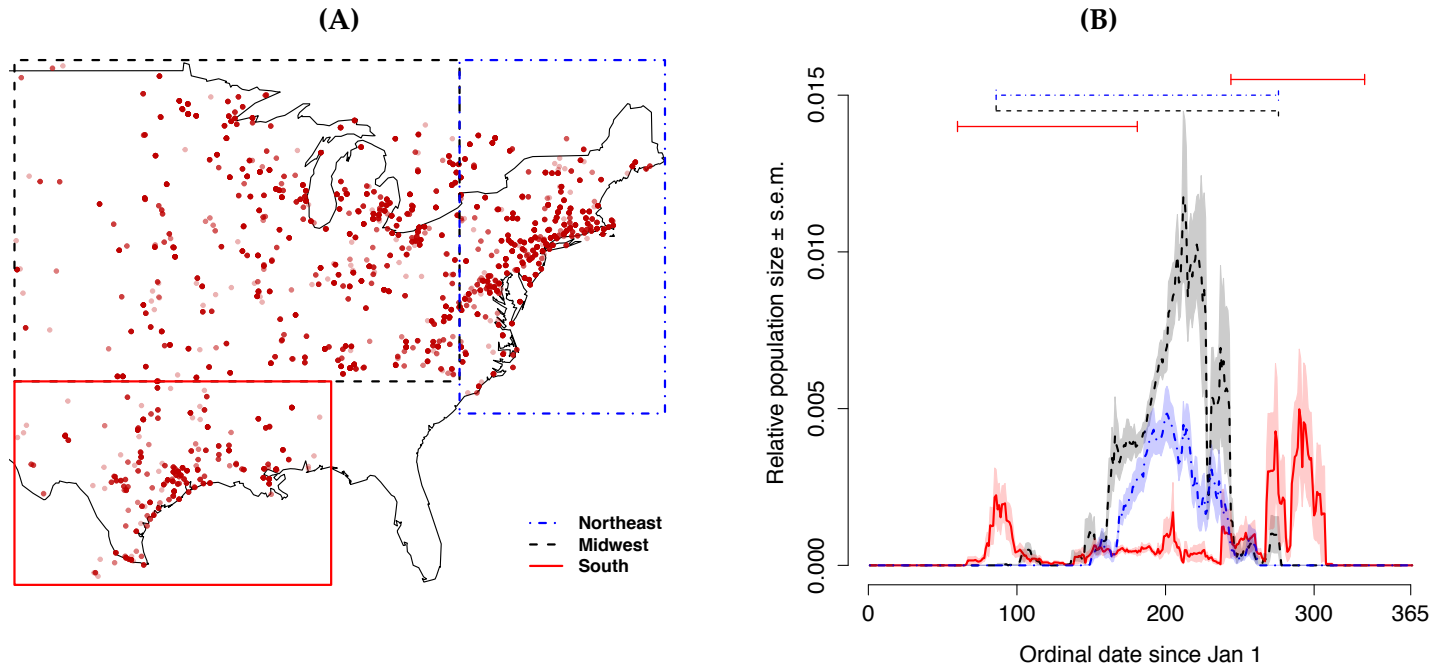


Figure 2.3: (A) Locations of North American Butterfly Association citizen science counts of monarch adults east of the Rocky Mountains, and separated into three regions: South (south of 34.5°N and west of Appalachians, excluding Georgia, South Carolina, and Florida where monarchs are largely non-migratory), Midwest (west of Appalachians), and Northeast (east of Appalachians) (1993–2014). Red dots indicate count locations and increasing color intensity indicates overlapping count points across years. A few count points located outside of this region were included in the analyses, but are not shown on the map. (B) Mean \pm s.e.m. (across years) moving average of the relative monarch population index over days of the year in the three regions. Shown above the curves are the windows of dates for which we used data to estimate the annual population index, with colors and line types corresponding to regions. Note that South is divided into spring and fall populations. The proportional abundance reflects the regional population density, not regional total population size. The relative indices here are therefore not directly comparable.

To focus on the long-range migration of the eastern monarch population, we eliminated some regions from the NABA dataset. We removed counts west of 105°W corresponding to the largely separate migratory “Californian” populations [32] and counts from Georgia, South Carolina, and Florida corresponding to the mostly non-migratory “Gulf Coast” populations [33]. The NABA dataset was then subdivided into three spatially distinct regions (Figure 2.3A): South (south of 34.5°N and west of 79°W), Northeast (north of 34.5°N and east of 79°W , corresponding to the Appalachian mountain divide), and Midwest (north of 34.5°N and west of 79°W). Northeast and Midwest include dates from March 27th to October 3rd, corresponding to the entire summer breeding season. South was further temporally subdivided into two groups: Spring South (March 1st–June 30th, corresponding to reproducing migrants moving north), and Fall South (September 1st–November 30th, corresponding to returning migrants moving south).

The NABA citizen science dataset has spatially and temporally variable sampling effort, and its quality has been challenged [34]. We therefore based our population abundance indices on a temporal moving average for each region [35]. For each date, we calculated an equally weighted average of all the counts in the region falling in a 7-day window, centered around that date. This approach alleviates biases in the population index due to temporal variation in sampling intensity. Ripley’s K function shows that there is no evidence for increased clustering of census points over time (Appendix A.1). We assessed and addressed other potential biases in the NABA dataset (varying sampling intensity, missing butterfly arrivals, etc.) in multiple ways (Appendix A.1).

The total monarch index for a given year was calculated by summing the

population index within a region during the time periods defined above. Northern populations have temporally overlapping and variable numbers of generations, so we calculated season-wide sums of observations in the Midwest and Northeast (99 % of the counts taken June–August). The same number of days was used for a season each year, so sums and averages are equivalent.

2.3.2 Assessing butterfly phenology in NABA data across years

Seasonal populations trends over the 22 years in the NABA dataset were estimated by calculating the proportional number of monarchs for each day (population index at each date/total index for that year across all regions). This value indicates the proportional abundance of butterflies seen each day. To assess whether the NABA dataset captured the known pattern of annual migratory phenology, we plotted the mean daily proportional abundance trends with the standard error calculated across the 22 years.

2.3.3 Additional data from repeatedly-measured sites

Cape May Point, New Jersey, is a major funneling point for southern migrating monarchs from the northeastern USA [18, 36]. Transect counts are conducted three times daily on a defined route, and the counts are normalized by hours of observation. Weekly averages are reported over 9 weeks from September 1st to October 31st (1992–2014). We summed the weekly averages to get a population size index reflecting the total number of butterflies migrating south.

Peninsula Point, Michigan, is a funneling point for southern migrating

monarchs from eastern and potentially Midwestern Canadian populations [18,37]. Transect counts are conducted one or two times daily on a defined route, and the counts were normalized by hours of observation. We obtained original data sheets from the Peninsula Point Monitoring Project. We averaged the daily counts for each week and summed the weekly averages to get our population index. The count period runs from early August to late September (1996–2014), so the population index for each year is based on the number of butterflies passing through over 8 weeks. Two years (1996 and 1998) were missing from the original data sheets, but were presented in another study using a slightly different estimation method [18]. We used regression analysis of the data from the 17 years included in both studies to predict values for the two missing years.

Mexican overwintering sites are monitored by the World Wildlife Fund. A December estimate of total hectares occupied by roosting butterflies is reported for 1993–2014 as a proxy for population size [13].

Finally, United States Department of Agriculture collects data on the adoption of herbicide resistant crops and we used the mean of adoption rates for corn and soybean from 1996–2015. We expected that increase adoption of herbicide resistant crops leads to increased herbicide use and consequently, decrease in milkweed abundance. We therefore employ this dataset as a proxy for milkweed abundance in the agricultural fields [27]. To move beyond the simply association between herbicide resistant crop adoption and monarch populations, we test whether year-to-year changes in adoption correlate with year-to-year changes in monarch population estimates.

2.3.4 Analyzing relationships between regions

We used regression analysis to test for relationships between annual population indices at successive stages in the migratory cycle (from “donor” to “recipient”, respectively): Mexico to Spring South (overwintering butterflies migrating north); Spring South to Northeast and Spring South to Midwest (butterflies migrating further north, while population size builds up over 2–3 generations); Northeast to Cape May and Midwest to Peninsula Point (fall migration South); Cape May to Fall South, Peninsula Point to Fall South, and Fall South to Mexico (migration further South); Midwest to Mexico, and Northeast to Mexico (bypassing Fall South). All analyses were performed in **R** version 2.15.1. [38].

The one NABA census that limited sampling was Fall South (we only have counts beginning in 2002 and 2014 was the single year with a count in November. The mean number of counts from 2002 to 2014 is 8.85). When we summarized the NABA regions, between-year variability was substantially higher for Fall South than for the Midwest and Northeast summer indices (see Section 2.4 and Figure 2.3B). These patterns call into question the quality of the fall South index perhaps due to much-reduced sampling. Nonetheless, we include the fall South index in analyses, but we do not base conclusions strictly on those results. In addition, we include regressions between the northern censuses and Mexico.

Given our knowledge of the migratory cycle, finding the expected positive relationship between successive pairwise stages indicates reasonable data quality and provides a basis for further analyses of the demographic links between the indices (WWF Mexico, NABA, Cape May, Peninsula Point) that were collected independently using different protocols. We tested for the link between overwintering and the spring migration by regressing the NABA Spring South

population index against the Mexico population index. Spring South counts did not include March and April for 1993–2004, thereby missing the crucial first-generation migrants from Mexico (Appendix A.1). Accordingly, for this link we focus on 2005–2014. We determined the link between summer breeding and the fall migration by regressing the Cape May index against the NABA Northeast index, and the Peninsula Point index against the NABA Midwest index, respectively. Our strong *a priori* expectation was to find a positive relationship between population indices of the “donor” and “recipient” regions based on the monarch’s known annual cycle. Therefore, although we present two-tailed *p*-values, we consider *p*-values below 0.1 to be significant for these tests. If a data point had a studentized residual over 3 in magnitude, it was considered a possible outlier [39]. In such cases, results are presented with and without the possible outlier.

2.3.5 Testing for temporal trends in population relationships

We conducted forward and backward model selection and used *F*-tests to address whether the cause of any observed population decline at a “recipient” stage in the cycle was due to declining inputs (population index at the “donor” stage), or due to a decline in the relationship between population indices at these two stages. We used “donor”, “year”, and “donor-by-year” interaction, as predictors. We performed model selection based on AIC, and used *F*-tests to assess whether a potential predictor significantly improves the model’s fit. Additional details of the analysis and complete output of the model selection procedure are presented in Appendix A.2. In four such analyses we detected a single outlier, and present results with and without the outlier.

2.4 Results

2.4.1 Citizen Science data captures the annual migratory cycle

Figure 2.3B shows a moving-average index of relative population size across each year, based on the 6376 records in the NABA dataset, separated into three geographical regions. The daily population indices clearly captured the monarch's continental migration: a spring wave of population increase and decrease in the southern USA, followed by a similar but extended summer pattern in the Midwest and Northeast as the butterflies move north, and then a fall wave of returning butterflies in the south flying to Mexico. The trend varies somewhat (standard errors indicated by shaded regions) but the major features are consistent across years.

Next we assessed whether the population indices reflect the known links in the migratory cycle. Despite using distinct monitoring methods, the overwintering population index linearly predicted the Spring South population index based on NABA counts ($p < 0.001$, adjusted $R^2 = 0.753$; Table 2.1, Figure 2.4A), reflecting the first breeding generation in the southern USA. The annual Spring South index predicted the subsequent Midwest and Northeast NABA-based indices ($p = 0.04$, adjusted $R^2 = 0.346$ and $p = 0.06$, adjusted $R^2 = 0.291$, respectively; Table 2.1, Figure 2.4B,D). Although there may be spatial biases in these NABA counts (*e.g.*, we lack data on whether surveys were conducted in crop fields), the high mobility of monarchs and the large geographic area of sampling in the Midwest and Northeast (Figure 2.3A) are likely to alleviate these issues. The Midwest and Northeast indices are also correlated with each other ($n = 22$, $r = 0.682$, $p < 0.001$), suggesting that variation in spatial sampling

Table 2.1: Regression analyses between stages of the annual monarch migratory cycle. Statistical significance is indicated by *** $p < 0.001$, ** $p < 0.01$, * $p < 0.05$, and + $p < 0.1$ (two-tailed tests).

	Independent	Dependent	n (years)	Slope	Adj R^2
Spring migration	Mexico ¹	Spring South	10	10.465***	0.753
Summer breeding (first generation)	Spring South	Northeast	10	1.855+	0.291
	Spring South	Midwest	10	2.403*	0.346
Summer breeding (up to 3 generations)	Northeast	Cape May	22	5.713**	0.283
	Midwest	Peninsula Point	19	0.598 ²	0.018
Fall migration	Midwest	Fall South	13	0.195	0.018
	Northeast	Fall South	13	0.195	<0.001
	Peninsula Point	Fall South	13	-0.059	<0.001
	Cape May	Fall South	13	0.034	0.01
	Fall South	Mexico	13	0.004	<0.001
	Midwest	Mexico	22	0.003	<0.001
	Northeast	Mexico	22	-0.01	<0.001
	Cape May	Mexico	22	0.001	<0.001
	Peninsula Point	Mexico	19	0.001	<0.001

among NABA volunteers has not greatly biased these indices.

Links between summer indices and the single-location counts of fall southward flying migrants again involve distinct data sets. The NABA-based summer Northeast index predicted the Cape May, NJ fall migration count ($p < 0.01$, adjusted $R^2 = 0.283$; Table 2.1, Figure 2.4E). The Midwest index predicted, although less strongly, the fall migration through Peninsula Point, MI ($p = 0.06$, adjusted $R^2 = 0.15$ on log-transformed data; $p = 0.05$, adjusted $R^2 = 0.17$ with one potential outlier (2014) removed; Figure 2.4C). These results are what we

¹Although this is the most direct test of a relationship between overwintering monarch numbers in Mexico and the spring populations in the USA, it is limited by 10 years of data. If we skip this first breeding generation (Spring South) and examine the 22-year relationship between Mexico and either the Midwest or Northeast, there is no significant relationship in either case ($p > 0.4$). The visual suggestion (not shown) of a hump-shaped relationship in scatterplots of the data is not statistically supported ($p > 0.35$ in all cases, for quadratic regression or nonparametric spline regression of Midwest or Northeast on the prior Mexico population).

²With a single outlying year (2014) removed, this relationship was significant at $p = 0.050$ (Adj $R^2 = 0.171$). The 2014 census for Peninsula Point was a statistically significant outlier (studentized residual > 3.1), see [39].

would expect if the fall migration counts at Cape May and Peninsula Point are representative of the total adult butterfly source populations in the Northeast and Midwest regions, respectively. Overall, these statistical linkages (from Mexico through the fall migration counts) are strong evidence for data quality and expected demographic links between Mexico, spring and summer breeding generations, and fall migration indices.

In contrast, our Fall South index (2002–2014), representing butterflies returning to Mexico through the southern USA, showed no relationship with the end of summer indices (Cape May and Peninsula Point) or with the overwintering population in Mexico (Table 2.1, Figure 2.4F–H). Given the lack of relationship with fall South, we also regressed the Mexico overwintering population index against summer indices (Midwest, Northeast, Peninsula Point, and Cape May) (*e.g.*, Figure 2.4I; all analyses in Table 2.1). We used all four indices to independently test the relationship, yet the only significant relationship was between Peninsula Point and Mexico when an outlier was removed, with a slope that decreased over time ($p < 0.01$, adjusted $R^2 = 0.62$; Appendix A.2).

2.4.2 The milkweed limitation hypothesis is not supported

None of the four northern indices (or the fall South index) showed a statistically significant decline across the full 22-year period covered by the NABA counts (Figure 2.5). This suggests that northern populations were able to build up during the breeding generations, despite the overwinter decline. Admittedly, the Northeast and Midwest indices do show some visual indication of a decline beginning in 2005. To address this, we examined the temporal trends begin-

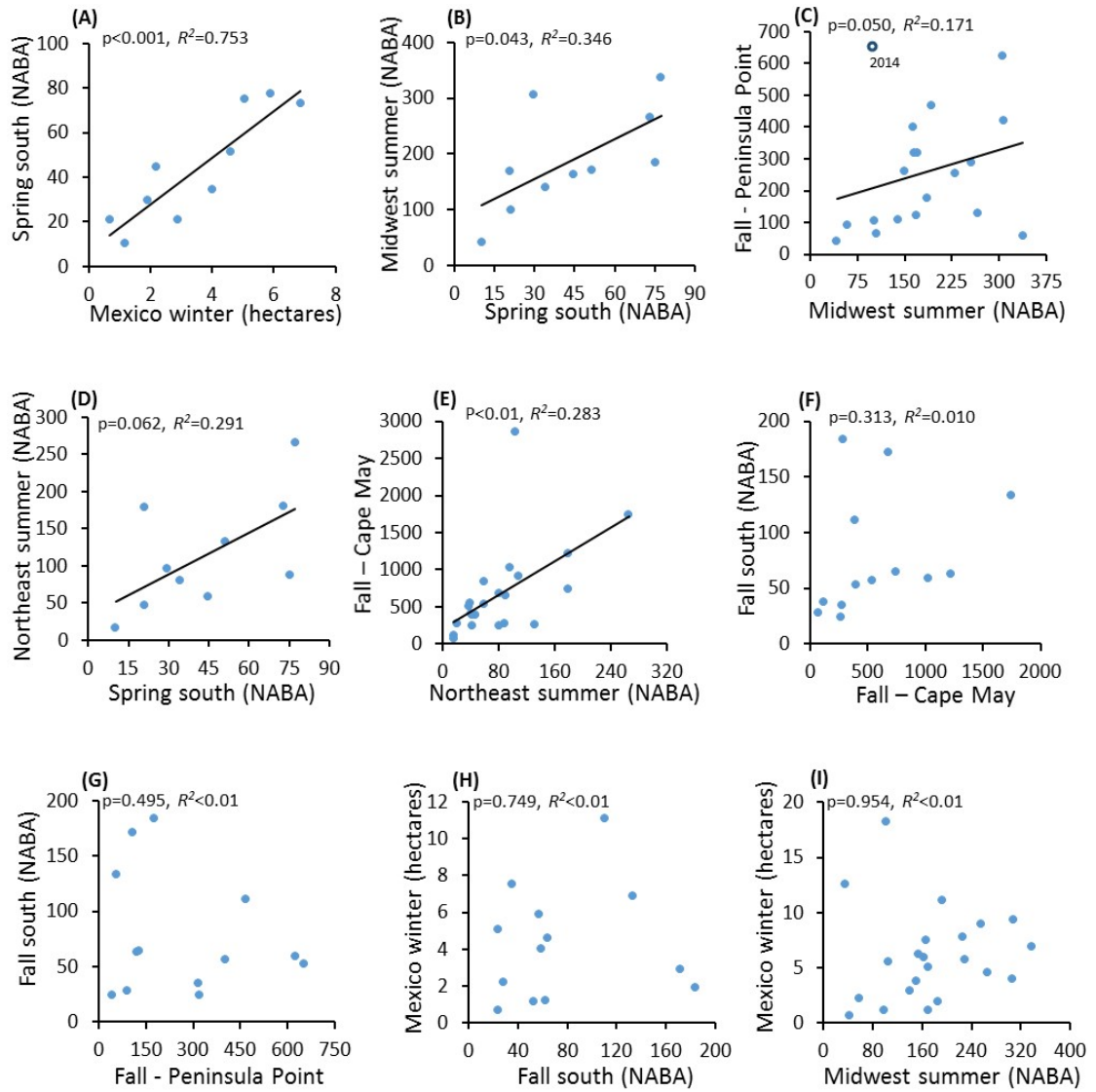


Figure 2.4: Continent-wide population links in the annual migratory cycle of the eastern monarch butterfly. Representative links are shown here, but others are detailed in Table 2.1. Regression lines are only shown for statistically significant slopes (in panel (C), the outlying year 2014 is indicated and was excluded, see Table 2.1 for statistical justification of outlier removal). Both NABA and Fall Peninsula Point counts were normalized by sampling effort. Units for NABA counts are the sum of daily estimates from a moving average, while Fall Peninsula Point units are the sum of weekly average counts (all are normalized by effort, see Section 2.3).

ning then, but only found marginally significant declines since 2005 (Adjusted $R^2 = 0.15$, $p = 0.15$ and adjusted $R^2 = 0.31$, $p = 0.055$, for Northeast and Midwest respectively, Figure 2.5). Additionally, over the same time period the declines were more severe in Mexico and in the first generation in the south (the fitted linear regressions of population index v. year correspond to decreases of 92.4 % over the time period for Mexico, 78.5 % for spring South, 62.1 % for Midwest and 64.9 % for Northeast), and there was no statistically significant trend in the Cape May, Peninsula Point, or Fall South indices. The steep decline in Mexico is reflected in subsequent northern indices, as we expect from the annual cycle, but the impact is progressively attenuated at each step of the cycle (Figure 2.5).

We next asked if the year-to-year changes in overwintering monarch population estimates are correlated with year-to-year changes in adoption of herbicide-resistant crops. We use differenced data, rather than directly correlating monarch populations with herbicide-resistant crop adoption, because any two variables showing a trend over the same time will be correlated. If the relationship is causal, however, annual differences in adoption should correlate with annual differences in monarch populations. No such correlation is observed ($n = 21$, $r = 0.03$, $p = 0.897$, Table A.1). As a case in point, the peaks of the summer Midwest and Northeast population indices both occurred in 2006, following a 10-year period in which use of herbicide-tolerant crops rose steadily from 0–62.5 % of corn and soybean acreage (Table A.1).

Table 2.2: Results from model selection without an outlier (see Appendix A.2 for full details) to address the role of migratory inputs and temporal trends in pairwise regional links of the monarch’s annual migratory cycle in eastern North America.

Recipient (Dependent Variable)	Donor (Independent Variable)	Best Model
Spring South	Mexico	Spring South ~ Mexico + Mexico × YEAR
Midwest	Spring South	Midwest ~ Spring South
Northeast	Spring South	Northeast ~ Spring South
Peninsula Point	Midwest	Peninsula Point ~ Midwest
Cape May	Northeast	Cape May ~ Northeast
Mexico	Midwest	Mexico ~ YEAR
Mexico	Northeast	Mexico ~ YEAR
Mexico	Peninsula Point	Mexico ~ Peninsula Point + Peninsula Point × YEAR
Mexico	Cape May	Mexico ~ YEAR

2.4.3 Where is the break in cycle?

We used a model selection approach to test for temporal trends in the stage-to-stage relationships between population indices (Table 2.2 and Appendix A.2). This procedure evaluates whether the population at “recipient” stage (*e.g.*, Midwest) was driven by inputs from the previous “donor” stage (*e.g.*, monarchs migrating from the South), or by “year”, which represents an unspecified directional effect on the stage being predicted (*e.g.*, habitat degradation, decline of milkweed). A significant interaction between “year” and “donor” indicates a relationship changing over time. If milkweed reduction is the main factor in the monarch decline, we expect to see changing relationships in stages where breeding occurs. Instead, we found temporal trends at stages where the population is not building and not dependent on milkweed (Table 2.2).

Along the northern migration, the “donor” stage was the most important predictor of the “recipient” stage, and the interaction term was at most marginally significant (Table 2.2, Appendix A.2). For example, the Midwest summer population index is best explained by the input population size from

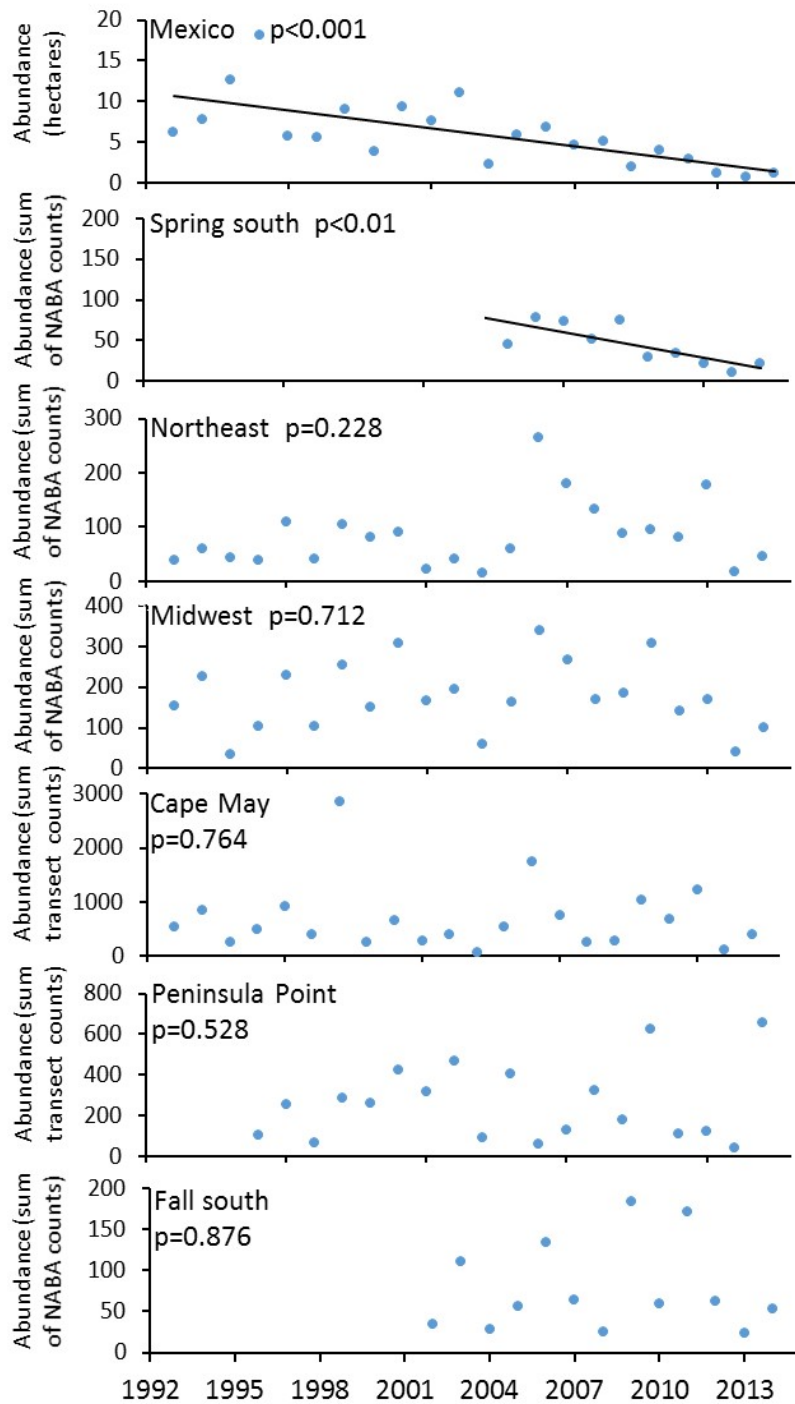


Figure 2.5: Temporal pattern of monarch abundances in the overwintering colonies in Mexico, southern USA, and four independent summer northern indices (1993–2014). Units for NABA counts are the sum of daily estimates from a moving average, while Fall Peninsula Point and Cape May units are the sum of average weekly transect counts (all are normalized by effort, see Section 2.3). Only significant regression lines are shown.

Spring South.

Similar results hold for the beginning of the southern migration, when the butterflies fly south through funnel points such as Cape May and Peninsula Point (Appendix A.2). However, along the southern migration, “year” is a significant predictor of the Mexican overwintering population, indicating a decline at this stage, with three out of four northern USA indices failing to explain additional variation in the overwintering population index. The one exception was the relationship between migrants from Peninsula Point and Mexico with an outlier removed. Here, both the “donor” and interaction terms were statistically significant, indicating a declining relationship over time. Importantly, Peninsula Point captures migrating butterflies and therefore a decline in the slope predicting the population size in Mexico is independent of milkweed. Lastly, our analyses show some evidence for an interaction between Fall South and “year” in predicting monarch populations in Mexico. Again, these adult butterflies do not depend on milkweed, suggesting a temporal change in migratory success.

Ries and co-workers [31] found a significant positive correlation between summer peak populations (estimated from NABA counts) and the subsequent overwintering population in Mexico after the latter data were detrended for their annual decline. We therefore tested for associations between our summer indices and detrended Mexico data (*i.e.*, the residuals from the nonlinear trend plotted in Figure 2.2). The correlations of Mexico with our Midwest index (which is most similar to the region considered by [31]) and with Peninsula Point were positive and marginally significant ($r = 0.40$, $p = 0.07$ and $r = 0.37$, $p = 0.12$ respectively). In other words, the Midwestern index weakly predicts

the numbers arriving to Mexico, but only after the downward trend in Mexico is removed. We found no significant correlations between de-trended Mexico data and the Northeast, Cape May, or Fall South indices ($r > 0$ but $p > 0.2$ in all cases). Taken together, our results are consistent with failed migration or re-establishment at the overwintering grounds impacting the population decline in Mexico.

2.5 Discussion

The current literature on monarch population dynamics and declines is rife with inconsistent patterns and interpretations [15, 18, 27, 40, 41]. While the monarch population is clearly declining in Mexico, a similar pattern is not observed in many northern regions. We have attempted to make sense of these inconsistencies by connecting the demographic dots of the annual monarch migratory cycle. Although none of the datasets employed is perfect, they represent the bulk of the available data, and we linked them in new ways. Citizen-science data allow for investigations at “large spatial scales, where important processes not detectable at local scales may dominate dynamics” [8].

Although limited sample size (10–22 years for population indices) and variability in the data limit the statistical power of any one test, we used several different approaches to examine population trends and the milkweed limitation hypothesis. Several trends during the years covered by our data conflict with expectations of the milkweed limitation hypothesis. The lack of an overall decline in the two NABA summer regional indices, and the two fall migratory indices covering the same years, suggest that the milkweed decline is not limiting

the production of adult butterflies. Similarly, Crewe and McCracken [42] found that the fall migrant counts at the Long Point, Ontario funneling point decreased at roughly half the rate of the decline in Mexico. Taken together these results indicate a substantial recovery, during the breeding season, from population bottlenecks. We found no correlation between annual increases in the adoption of herbicide-resistant crops (the hypothesized causal agent of milkweed declines) and annual decreases in the Mexico overwintering population. For the summer population indices, where milkweed limitation should be most evident, monarch populations actually increased substantially over the decade that included 2/3 of the total increase in herbicide-resistant crop acreage (through the mid 2000s).

Our stage-to-stage regression analyses show that monarch population changes are predictable along the annual cycle from Mexico through to the summer breeding grounds; the annual population index at each step reflects the index of the previous step. Furthermore, model selection confirmed that the regional links are sufficient to explain the population dynamics up to the fall migration. For example, the decline in the overwintering population fully accounts for the decline in the first generation in the southern USA. However, there is a break in predictability beginning with the fall migration. That three out of four northern indices fail to predict the numbers arriving in the south conflicts with our most basic expectations about monarch population dynamics and suggests an external factor, but it occurs at a stage when milkweed is not utilized. Badgett and Davis [17] also hypothesized that diminished fall migration success is an important factor in the overwintering population decline, but this was based solely on the lack of a decline in the Peninsula Point counts, and was predicated on the assumption that Peninsula Point is representative of the

total northern breeding population. Our analysis of the successive links across the entire migratory cycle more completely addresses this issue and is concordant with the hypothesis that the population decline is most strongly driven by events after monarchs rely on milkweeds.

Our model selection analysis indicates that over the years, populations of adult monarchs consistently build up during the summer, beginning in the first (southern USA) breeding generation. There is some evidence that the density of monarch eggs has declined since 2007 [28], and that larval survival has also declined [43]; these results, however, are inconsistent with the trends in summer adult counts and initial number of fall migrants (Figure 2.5). We believe that adult counts are complementary to egg and larval counts, but are more useful in analyses such as ours because the adult stage represents migrants after egg and larval mortality (which is typically very high in the field). Our analysis indicates that an unknown, annually increasing effect, is impacting the monarch population by the time they reach Mexico, producing a consistent decline over the past two decades.

One way in which lack of milkweed could drive monarch declines is if the monarchs that reach Mexico are a small geographical subset of those breeding in the USA during the summer months. It has been suggested that the Midwestern USA is the critical area for monarch breeding that populates the overwintering grounds [27,30]. Although NABA counts are not typically conducted in agricultural fields where milkweed declines are strongest [26,27], our regional population indices sum over large areas (Figure 2.3A), and predict the numbers flying south in the fall that are drawn from all habitats (Figure 2.4). Results from stable isotope work and tagging are variable, but indicate that well over

Table 2.3: Proposed threats to the sustainability of the eastern monarch butterfly annual migration.

Proposed threat	References
Habitat destruction / logging at the overwintering sites	[15,21,50]
Habitat destruction / reduced nectar availability on southern migration	[24,51]
Disease, predation, and parasitoids	[23,52]
Climate change / extreme weather	[15,25]
Herbicides / genetically modified herbicide tolerant crops (loss of milkweed)	[27,29,30]
Insecticides / genetically modified insecticidal crops	[49]
Automobile accidents, especially during the migration	[53]
Electromagnetic fields / microwave emissions	[54]
Trap plants	[55,56]

half of the monarchs making it to Mexico are derived from outside the agricultural Midwest [20,44,45]. Few eastern coastal migrants reach the overwintering sites, but non-coastal migrants east and west of the Appalachians are more successful [46,47].

Many factors have been suggested to explain the overwintering population decline of the monarch butterfly (Table 2.3). Our analyses point to the fall migration and re-establishment on the wintering grounds as key issues. Uncovering the cause of the trends at these stages may be critical to understanding the decline in Mexico. The severe “100-year” drought in Texas (2010–2015) likely had a strong impact on spring and fall migrants, corresponding to the lowest monarch numbers on record [33,48]. Factors such as sub-lethal insecticide effects in the breeding grounds [49] or lack of nectar sources during the fall [24] may be important in driving a wedge between summer and overwintering populations. Milkweed is typically no longer flowering during the fall migration, and other plant species (many in the *Asteraceae*) serve as nectar sources. However, the condition of fall migrants might be affected by the environments they experience early in life, including milkweed shortage, insecticides, or other changes in habitat quality.

Other aspects of the breeding and migratory behavior of monarchs are changing, and their roles in population dynamics are unknown. The sex ratio of monarchs at the overwintering sites has changed over the past three decades from 53 % female to 43 % female [57]. As well, the pace of the fall southern migration has sped up over the past decade [58]. We currently have few estimates of the sub-lethal impacts of poor quality summer breeding habitat, insecticide residues, and intensified agriculture on the monarchs' migratory success. Predator, parasitoid, and disease impacts can also be severe [23,52]. Determining the extent to which these and other factors contribute to the dynamics of eastern monarchs is a high priority.

2.5.1 Conclusion: conservation and controversy

The past two years have seen tremendous media attention and scientific discourse on the population decline of the monarch butterfly [34, 59–62]. While there has been consistency in some of the analyses, other research and interpretations has called into question the extent to which we truly understand fluctuations in monarch population sizes, especially given the complex annual migratory cycle [31,41,63]. We hope that our analysis linking the annual population steps has shed light on this important conservation issue, and moreover that our approach will be useful in understanding the similar challenges faced by many long-distance migrants [10].

The monarch butterfly is far from being threatened, but the eastern USA migration, one of the most spectacular animal migrations in the world, may be an endangered phenomenon [15]. To identify and manage the risk factors associ-

ated with its decline, deeper critical analyses of the existing data are essential. We do not dispute that milkweed is essential for larval monarchs, and might serve as a buffer against further aggravation. Yet our analyses indicate that other stages are critical, so milkweed conservation alone is unlikely to be sufficient to preserve the migration. Additional resources are necessary to study and improve the transition between summer breeding in the USA and overwintering in their highland forested habitats in Mexico.

2.6 Acknowledgements

This work was improved by discussions with S. Altizer, C. Brassil, L. Brower, B. Dalziel, A. Davis, P. Dubin, C. Edwards, T. Flockhart, K. Gustafsson, A. Hastings, L. Arcila-Hernandez, M. Holden, G. Jander, P. Jones, B. Lewenstein, S. Mou, K. Oberhauser, E. Patrick, R. Petipas, J. Pleasants, L. Ries, O. Taylor, J. Thaler, S. Wolf, E. Wurtz, M. Zalucki, T. Züst, and anonymous reviewers. Funding was entirely provided by the Atkinson Center for a Sustainable Future at Cornell University.

CHAPTER 3

SPATIOTEMPORALLY HETEROGENEOUS POPULATION DYNAMICS OF GUT BACTERIA INFERRED FROM FECAL TIME-SERIES DATA

3.1 Abstract

A priority in gut microbiome research is to develop methods to investigate ecological processes shaping microbial populations in the host from readily accessible data, such as fecal samples. Here, we demonstrate that these processes can be inferred from the proportion of microorganisms egested and their egestion time distribution using general mathematical models that link within-host processes to statistics from fecal time-series. We apply this framework to *Drosophila melanogaster* and its gut bacterium, *Acetobacter tropicalis*. Specifically, we investigate changes in their interactions following ingestion of a food bolus containing bacteria, in a set of treatments varying key parameters: the density of exogenous bacteria ingested by the flies (Low/High) and association status of the host (axenic or mono-associated with *A. tropicalis*). At 5 h post-ingestion, $\approx 35\%$ of the intact bacterial cells have transited through the gut with the food bolus and $\approx 10\%$ are retained in a viable and culturable state, leaving $\approx 55\%$ that have likely been lysed in the gut. Our models imply that lysis and retention occur over a short spatial range within the gut when the bacteria are ingested from low density, but more broadly in the host gut when ingested from high density, for both gnotobiotic and axenic hosts. Our study illustrates how time-series data complement analysis of static abundance patterns to infer ecological

This chapter is based on the manuscript (accepted at *mBio*) "Spatiotemporally heterogeneous population dynamics of gut bacteria inferred from fecal time-series data" by Hidetoshi Inamine, Stephen P. Ellner, Peter D. Newell, Yuan Luo, Nicolas Buchon, and Angela E. Douglas.

processes as bacteria traverse through the host. Our approach can be extended to investigate how different bacterial species interact within the host, to understand the processes shaping microbial community assembly.

3.2 Introduction

Many animals harbor in their gut a microbial community [64] that is diverse and variable, both over time in one animal host and among different hosts. The microbiota can influence many important phenotypic traits of its animal host including nutrition, immunity, and behavior [65–69]. In turn, the diversity and abundance of microorganisms are influenced by host traits, especially the immune system, among-microbial interactions, and the availability of microbial taxa in the external environment [70–74]. There is increasing interest in applying ecological concepts to elucidate the processes underlying within-host microbial population and community patterns (*e.g.* demographic processes, competition, and migration [74–77]). Analysis of the temporal dynamics of populations is particularly valuable, for example to infer the processes underlying demographic fluctuations and to discriminate between niche and neutral theories of community assembly [78,79]. Generally, past studies have used the microbial composition of fecal samples as a convenient proxy for within-gut processes (*e.g.* [80–82]), with time-series data obtained by repeated fecal sampling from individual hosts, although a few systems (notably, the transparent zebrafish larva and *C. elegans*) are amenable to within-gut analysis in real-time [83,84].

The basis for this study was the prediction that the ecological insights that can be gained from analysis of fecal time-series data may be constrained by

a lack of ecological theory. Our first goal therefore was to develop general mathematical models that link within-host ecological processes to statistics that are measurable from microbial abundance in fecal time-series data. We then tested the theory using the amenable gut microbiome system in *Drosophila melanogaster*. This association is facultative for both the host, which can be reared under axenic (germ-free) conditions over multiple generations, and for the microbial partners, which are generally readily culturable; standardized associations with one or multiple microbial taxa can be generated by feeding axenic insects on the desired microorganisms [85, 86]. Previous research has revealed considerable temporal and among-host variation in community composition [87–91], including non-persistent taxa that transit repeatedly between the fly and food via fecal-oral cycling [92]. To facilitate the analysis, our experiments were conducted on a mono-association, *i.e.* with a single bacterial partner, and we investigated how the bacterial population dynamics within the host is altered by the density of administered bacteria (High/Low density) and microbial status of the host (Gnotobiotic/Axenic). We predicted that the Axenic fly gut, empty of competitors, may be more readily colonized than Gnotobiotic flies; and that flies which ingest large numbers of bacteria (High density) are likely to display a heightened immunological response, suppressing bacterial colonization, relative to flies that ingest fewer bacteria (Low density). Based on the first experiments of this study, we selected a strain of *Acetobacter tropicalis* isolated from *D. melanogaster* for this analysis. Our experiments reveal that the fate of ingested *A. tropicalis* is not uniform: although some cells transit through the gut with the food (as previously described, [92]), other cells are lost, possibly lysed in the gut, and others are retained for extended periods. Furthermore, the dynamics of egestion time through the gut suggest that the fate of the cells is

dictated by processes occurring in a spatially-restricted location within the gut.

3.3 Results

3.3.1 Dynamics of bacterial populations in *Drosophila*

Our first experiment investigated the stability of bacterial populations in the gut of *Drosophila* using the published procedure of frequent transfers to sterile medium, which depletes the populations of microorganisms with high rates of fecal-oral cycling [92, 93]. We reared *Drosophila* from birth in mono-association with five bacterial species of the genera *Acetobacter* and *Lactobacillus*, isolated previously from the guts of the same *Drosophila* strain as used in this study [94]. At 5–6 d after reaching adulthood, the bacterial density in the flies varied significantly between species, from $(0.880 \pm 0.147) \times 10^3$ per fly (*L. brevis*) to $(175.0 \pm 17.1) \times 10^3$ per fly (*L. fructivorans*) (ANOVA on log-transformed data: $F_{4,20} = 54.6$, $p < 0.001$). The flies were then transferred to sterile food thrice-daily over 6 d to reduce bacterial cycling between flies and food. The change in bacterial density in the flies varied significantly with bacterial species (ANOVA interaction term: $F_{4,37} = 33.47$, $p < 0.001$). Analysis by Tukey's *post hoc* test revealed that the density of three species (*A. tropicalis*, *L. brevis* and *L. plantarum*) did not differ over the 6-days experiment, but *A. pomorum* declined 18-fold, and *L. fructivorans* by nearly 200-fold (Figure 3.1). These data suggest that the relationship between the bacterial populations in the food and flies varies with the bacterial species. *L. fructivorans* was particularly dependent on oral replenishment, while *A. tropicalis*, *L. plantarum* and *L. brevis* maintained stable popula-

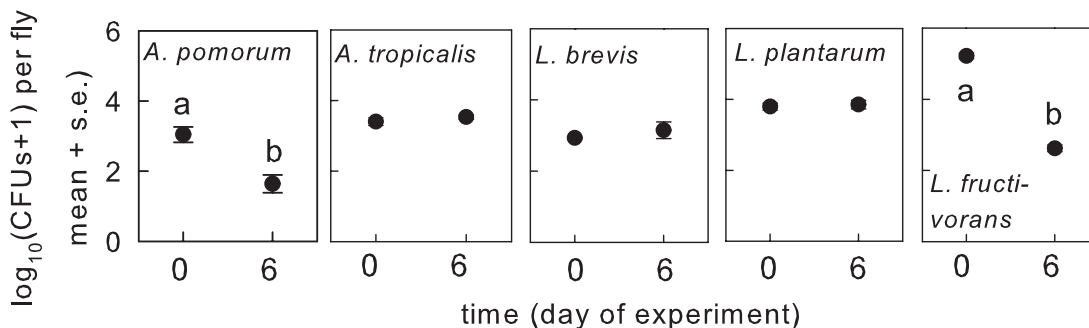


Figure 3.1: Stability of bacteria in mono-association with *Drosophila* over 6-day experimental period. The *Drosophila* were raised from egg in mono-association with the bacteria indicated. Density (CFU/fly) is shown at day 0 (5-day-old adults) and at day 6 (11-day-old adults), after thrice-daily transfers to fresh diet. Different letters indicate significant differences between the two time-points.

tions in the flies under the experimental conditions.

Our second experiment investigated the short-term dynamics of bacteria that maintain stable populations under thrice-daily transfers to sterile diet. Of the three species with these dynamics (Figure 3.1), we focused on *A. tropicalis* because this bacterium is readily amenable to genetic transformation [95]. Specifically, we transformed *A. tropicalis* with pCM62-GFP plasmid, allowing us to track the cells by fluorescence. We confirmed that GFP expression is stable in *A. tropicalis* for at least 15 d, both in culture and following ingestion by *Drosophila* (Appendix B.1.1 and Figure B.1), and the fluorescing cells are reliably identified in our method (Appendix B.1.2 and Figure B.2). Our experiments monitored the abundance of the GFP-labeled *A. tropicalis* cells recovered from the feces of *Drosophila* (Figure 3.2). Four treatments were used: Axenic flies and Gnotobiotic flies (mono-associated with *A. tropicalis*) that were fed on bacteria at High or Low density, enabling us to determine how these factors affect the population dynamics of *A. tropicalis*. To control for variation in the number of bacterial cells ingested and to ensure that the bulk flow of food through the gut was also

quantified, fluorescent microspheres that transit through the gut with the food were mixed with the inoculum of bacterial cells.

We scored the abundance of intact GFP-labeled bacteria and fluorescent microspheres in the feces of flies that were transferred hourly to sterile food over 5 h (Figure 3.2: Samples for *Egestion Time Experiment*). Most of the bacterial cells and microspheres (mean of 76 %) were egested in the first 2 h, and their abundance in the feces tapered to low numbers by 5 h in all treatments (Figures 3.3A and 3.3B). Very small numbers of GFP-labeled bacteria and microspheres (mean \pm s.e.m. = 1.0 ± 0.3 and 0.40 ± 0.11 % of the ingested bacteria and microspheres, respectively) were present in the 24 h fecal samples. We inferred that 5 h sufficiently captures bacteria that are egested with the bulk flow of food. The flies were further cultured to 48 h with a single transfer to sterile food at 24 h (Figure 3.2). The condition of bacteria egested from the flies in 48 h samples was different from those scored at 1–5 h: whereas the bacteria at 1–5 h were isolated and easy to count, the bacteria at 48 h were aggregated, making it impossible to score number of bacterial cells. Using the index of presence/absence of bacteria in each fecal sample, we scored bacterial colonies in 20–80 % of the fecal samples collected at 48 h, whereas bacteria were detected in only one sample at 24 h (in Low density treatment administered to Axenic flies; Figure 3.3C). The proportion of 48 h samples containing bacteria was significantly higher for flies that had ingested *Acetobacter* from Low density inoculum, relative to High density inoculum (70 and 36 %, respectively; $p = 0.038$ Fisher's exact test), but did not differ significantly between the Axenic and Gnotobiotic flies (58 % versus 47 %: $p = 0.56$ Fisher's exact test).

Taken together, our results indicate that some cells of *A. tropicalis* pass

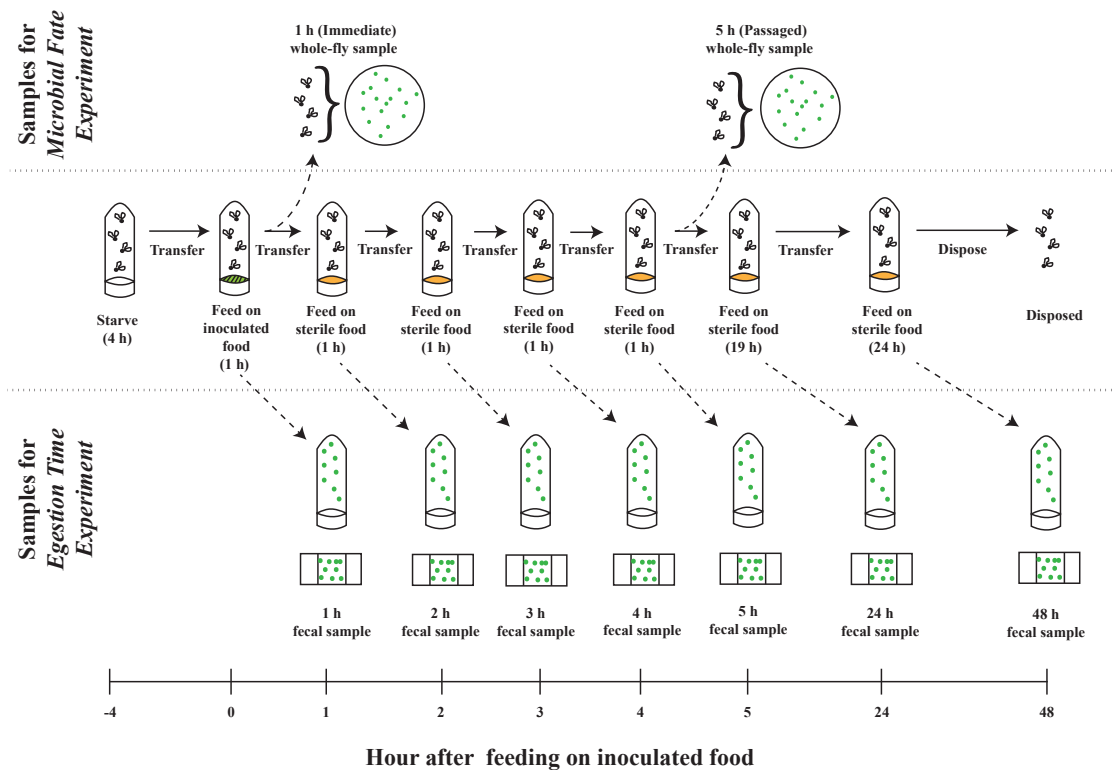


Figure 3.2: Schematic of transfer and sampling protocol for *Egestion Time Experiment* and *Microbial Fate Experiment*. To calculate the egestion time of bacteria and microspheres in *Egestion Time Experiment*, each sample of 50 male flies was transferred to a series of fresh vials (solid line). After transfer, feces from the vials were processed and the number of particles were quantified under fluorescent microscope (straight dashed line). To calculate the proportion of bacteria egested, *Microbial Fate Experiment* followed the same transfer protocol as the *Egestion Time Experiment*, but some samples were sacrificed for quantification of CFU. The experimental timeline (bottom of the figure) shows the number of hours after feeding on food inoculated with GFP-transformed *A. tropicalis*. See Section 3.5 for details.

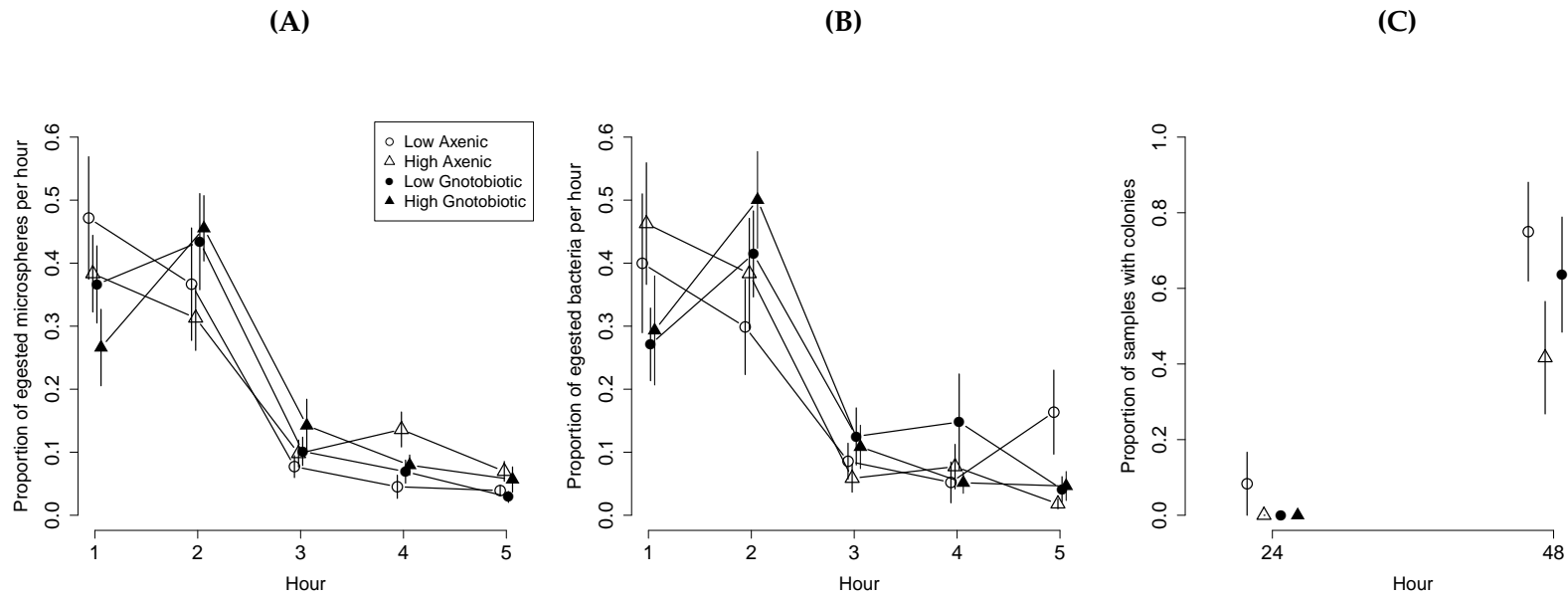


Figure 3.3: Egestion time dynamics in *Egestion Time Experiment*. Proportional mean \pm s.e.m. of egested (A) microspheres and (B) bacteria in each sample were calculated from initial 5 h (see Section 3.3.1). (C) Proportion of samples with microbial colonies present \pm s.e.m. Samples at 24 and 48 h were scored for presence/absence of microbial colonies. Symbols and colors represent different treatments as described in the legends (white circle: Low Axenic; white triangle: High Axenic; black circle: Low Gnotobiotic; black triangle: High Gnotobiotic).

through the host intact with the bulk flow of food but a proportion of cells are retained, giving rise to the bacterial cells that are shed at a later time. These data suggest that population processes occurring in the first few hours after ingestion play a crucial role in the overall dynamics of the *A. tropicalis* populations in the *Drosophila* gut. To guide this analysis, we constructed mathematical models of the population dynamics of microorganisms in the gut.

3.3.2 Theoretical predictions: ecological inference from the mean and the variance of particle egestion times

We constructed two classes of models: compartment models and a structural model. Compartment models are differential equation models with specific functions and parameters describing reproduction, death or retention, and movement of microorganisms (such as bacteria) within the gut. We built a series of compartment models, and derived formulae for the mean (μ) and the variance (σ^2) of microbial egestion times as a function of model parameters (Appendix B.2.1 and Figures B.3 and B.4). The structural model is a generalization of the compartment models with qualitative assumptions rather than fully specified process-rate functions. We used this model to show that our qualitative results from the compartment models hold widely across different models (Appendix B.2.2 and Figure B.5). Our models do not distinguish between death and retention of a microorganism within the gut, because we assume in both cases that it disappears from the bulk flow in the compartments tracked by our model.

For a compartment model with $n + 1$ compartments (*e.g.* foregut, midgut,

hindgut; Figure 3.4A), we derived $\mu = \sum_{i=0}^n 1/(m_i - r_i)$ and $\sigma^2 = \sum_{i=0}^n 1/(m_i - r_i)^2$, where m_i and r_i are per-capita emigration rate and net reproduction rate (birth rate b minus death or retention rate d) in the i^{th} compartment, respectively. In our study, we compare the egestion time statistics of a bacterium and inert microspheres of similar diameters (see Section 3.3.5 below). For microspheres, which have $r_i = 0$, $\mu = \sum_{i=0}^n 1/m_i$ and $\sigma^2 = \sum_{i=0}^n 1/m_i^2$. These formulae show how demographic processes affect μ and σ^2 . Specifically, increase in net reproduction rate (*i.e.* more birth than death or retention) would increase μ and σ^2 , whereas decrease in net reproduction rate (*i.e.* more death or retention than birth) would decrease both. The model also predicts that a decrease in emigration rate from compartments would increase μ and σ^2 . Our structural model shows that these results hold for a large class of models and parameters (Appendix B.2.2 and Figure B.5).

The results we obtained from theoretical models are intuitive. The more time a microorganism spends in the host, the higher its probability of disappearing in the host (*i.e.* death or retention) instead of egesting in feces. When this probability in the host is higher, a microorganism that transits rapidly through the host gut to the feces is more likely to be observed. We therefore expect to see a smaller μ with higher disappearance rate. Furthermore, increase in early egestion and decrease in later egestion should lead to a narrower distribution of bacteria egestion time. We therefore expect to see a smaller σ^2 with lower proportion of egested cells.

While an increase in death or retention decreases egestion time statistics, the magnitude of reduction in egestion time statistics depends on how abruptly (over space, but also over time due to peristalsis) additional death or retention

occur over the host gut (Appendix B.2.3 and Table B.1). For example, suppose that bacterial death and retention in the host gut reduces the proportion of bacteria egested. If the death and retention occur gradually (small effect across many gut compartments), then we observe large and empirically distinguishable reduction in egestion time statistics (compare “Microsphere” and “C” populations in Table B.1). However, if the death and retention occur abruptly (large effect in small number of compartments), then we observe minor reduction in egestion time statistics that may be difficult to observe empirically (compare “Microsphere” and “B” populations in Table B.1). Therefore, proportion of bacteria egested and egestion time statistics can be used together to make inferences about within-host processes without sampling the populations within the host (Figure 3.4B). Within treatment, we compare proportion of bacteria egested to the proportion of microspheres egested, and egestion time statistics of bacteria (μ_b and σ_b^2) to microspheres (μ_0 and σ_0^2), to differentiate the bacterial population dynamics from the microsphere dynamics. Between treatments, we compare proportion of bacteria egested and normalized statistics for bacteria (relative to microspheres; $\mu_{norm} = \mu_b \div \mu_0$ and $\sigma_{norm}^2 = \sigma_b^2 \div \sigma_0^2$) from one treatment to another, to assess the effects of prior interaction of the host with the bacterium (Gnotobiotic v. Axenic flies) and bacterial density (Low v. High density) on bacterial population dynamics.

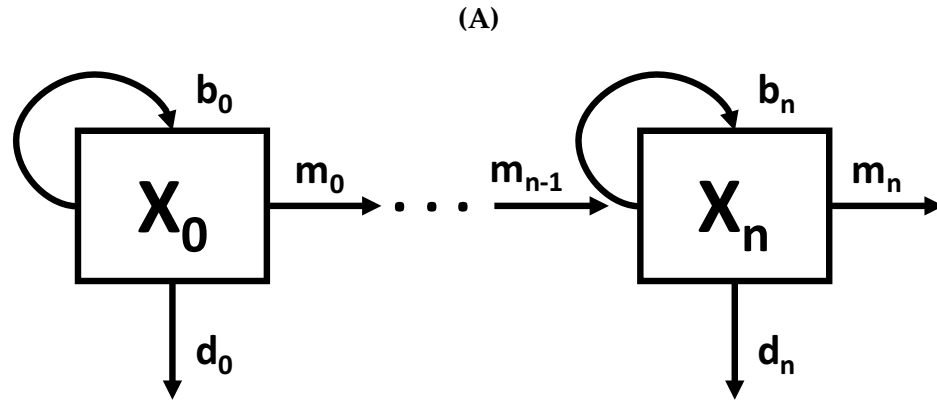


Figure 3.4: (A) Compartment diagram with arbitrary number of compartments. Each compartment corresponds to a population of bacteria in a gut region (*e.g.* foregut), and X_i is the microbial population size in the i^{th} compartment of the gut. The parameters $r_i (= b_i - d_i)$ correspond to per-capita net reproduction rate of the bacteria in the i^{th} compartment, and m_i correspond to per-capita migration rate from the i^{th} compartment to the $(i+1)^{\text{th}}$ compartment. (B) Inference scheme based on the compartment model with arbitrary number of compartments. Based on this model, we interpret comparisons within a treatment (bacteria v. microspheres) or between treatments (bacteria v. bacteria). Four demographic patterns can be inferred based on proportion of particles egested and statistics of the egestion time. Lower proportion egested and/or lower mean and variance of egestion time are expected consequences from different patterns of mortality or retention in the fly gut.

3.3.3 Proportion of *A. tropicalis* egested from the host in *Egestion Time Experiment*

To apply our theoretical predictions, we first calculated the proportion of *A. tropicalis* cells egested, compared to the number ingested by the host (rows in Figure 3.4B). Over the 5 h, the total number of egested bacteria was less than the estimated number ingested (Figure 3.5A). The proportion egested was significantly lower than 1 for three treatments: *A. tropicalis* administered at Low density to both Axenic flies (LA) (t -test: mean \pm s.e.m. = 0.25 ± 0.12 , $p = 0.003$) and Gnotobiotic flies (LG) (0.30 ± 0.18 , $p = 0.02$), and High density administered to Gnotobiotic flies (HG) (0.45 ± 0.16 , $p = 0.03$), but not for *A. tropicalis* administered at High density to Axenic flies (HA) (0.69 ± 0.3 , $p = 0.35$). However, no statistically significant differences among the treatments were evident by Type II or Type III ANOVA (bacterial density: $p = 0.164$, Axenic/Gnotobiotic treatment: $p = 0.652$, interaction: $p = 0.474$), or by stepwise model selection [96] based on AIC [97] and F -tests. These results demonstrate that a significant proportion of ingested *A. tropicalis* are not detected in the feces, suggesting that 30–75 % of ingested *A. tropicalis* cells are retained or lysed within the host, irrespective of the density of ingested cells and prior colonization of the flies with *A. tropicalis*.

3.3.4 The fate of bacterial cells not egested by the fly: *Microbial Fate Experiment*

Following our finding that many ingested bacterial cells do not pass to the feces with the bulk flow of food through the gut (Figure 3.5A), we investigated

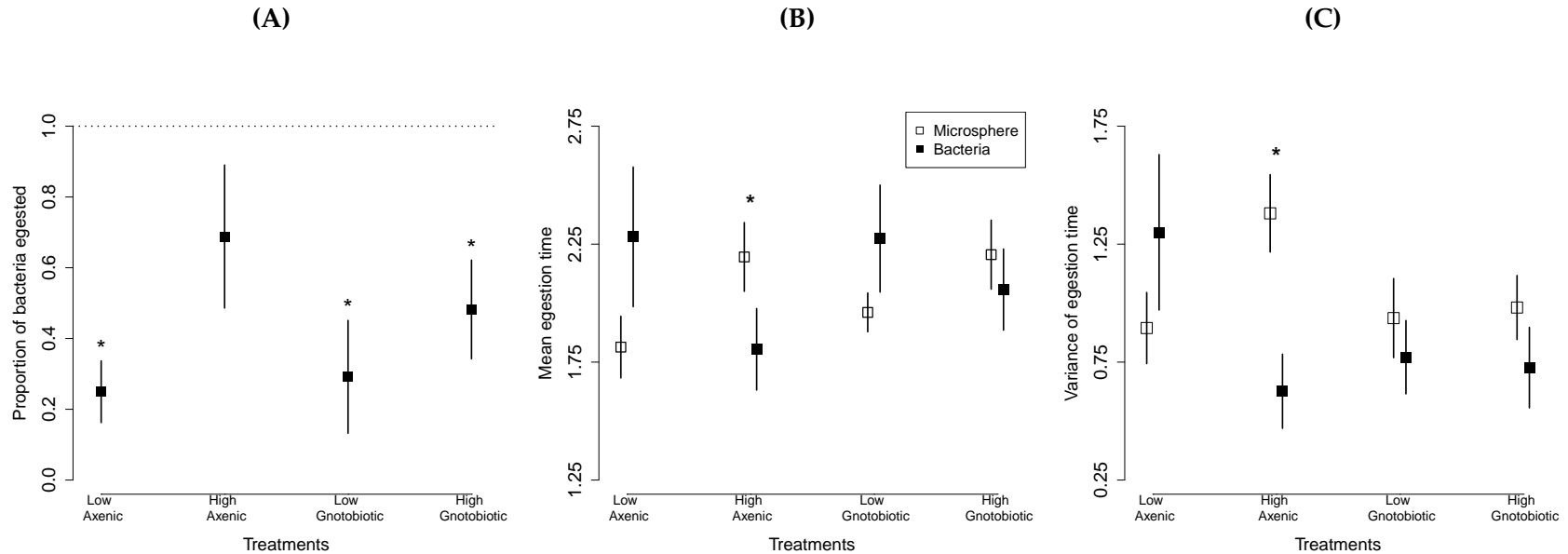


Figure 3.5: (A) Mean \pm s.e.m. for proportion bacteria egested in the four different treatments. Dotted line (proportion egested = 1) corresponds to the number of microbial cells predicted from number of microspheres in the feces. Asterisk indicates proportion bacteria egested significantly lower than 1 ($p < 0.05$). Sample mean \pm s.e.m. of: (B) mean egestion time and (C) variance of egestion time for microspheres (white square) and bacteria (black square). Statistics were calculated by using the proportional abundance at each hour (to 5 h) as the probability distribution of egestion times. See text for further details. Asterisk indicates significantly different statistics between microspheres and bacteria ($p < 0.05$).

how many ingested *A. tropicalis* cells are retained in the host intact and viable 5 h post-ingestion. We conducted an additional set of experiments (*Microbial Fate Experiment*, Section 3.5.7 and Figure 3.2), using the Low-density treatments (LA and LG) described above. The number of viable cells was quantified as the number of colony forming units (CFU) on tetracycline-plates, using the *tetR* gene on the pCM62-GFP plasmid borne by these bacteria, and compared to the total number of ingested bacteria.

For each of three separate replicate experiments, the number of bacteria per fly was reduced by 1–2 orders of magnitude over 5 h in the host body (Figure 3.6). Interestingly, the coefficient of variation of the (un-transformed) number of bacteria per fly increased over time for each replicate experiment, perhaps reflecting among-host variation in the fate of *A. tropicalis* cells. Using these results, we estimated the fate of ingested bacteria to comprise: 35 % egested, 10 % retained alive in the host, and 55 % lost from the system (inferred to have been lysed, although we cannot exclude the possibility that some retained cells had adopted a viable-but-nonculturable condition; Table 3.1 and Appendices B.1.3 to B.1.6). Taken together, our data suggest that more than half of *A. tropicalis* cells are likely lysed during transit through the gut. In the next section, we apply our theoretical models to *Egestion Time Experiment* data, to investigate the pattern of retention and/or bacterial lysis in the gut.

Table 3.1: Fate of *A. tropicalis* ingested by *D. melanogaster* following administration of *A. tropicalis* at Low density. Across three separate replicate experiments, four samples from Axenic flies and two samples from Gnotobiotic flies were collected, and the proportions of bacteria egested, retained, and lysed were calculated (Appendices B.1.3 to B.1.6). Summary statistics (mean \pm s.e.m.) are calculated across the replicate experiments. The results presented for Axenic flies omit one outlier replicate experiment in which no bacteria were recovered from fecal samples; summary statistics for Axenic flies with the outlier included are shown in square brackets.

Replicate	Fly Treatment	Proportion of bacteria egested	Proportion of bacteria retained	Proportion of bacteria lysed
1	Axenic	0.11	0.09	0.80
1	Axenic	0.10	0.03	0.87
3	Axenic	0.26	0.09	0.65
<i>Mean \pm s.e.m.</i>		0.18 \pm 0.08 [0.12 \pm 0.08]	0.08 \pm 0.02 [0.07 \pm 0.01]	0.74 \pm 0.09 [0.81 \pm 0.09]
2	Gnotobiotic	0.64	0.10	0.25
3	Gnotobiotic	0.42	0.16	0.42
<i>Mean \pm s.e.m.</i>		0.53 \pm 0.11	0.13 \pm 0.03	0.34 \pm 0.09

3.3.5 Egestion time statistics for microspheres and bacteria in *Egestion Time Experiment*

The mean egestion time for the microspheres and intact GFP-labeled *A. tropicalis* was *ca.* 2 h. We first used these data to test and validate our models. The mean and the variance of the egestion time for the microspheres and bacteria exhibited relationships that are predicted by the models (Appendix B.2.3 and Figure B.6). We then used the data to infer the second key comparison in the bacterial population dynamics, the pair-wise differences in the mean and variance of the egestion time for the microspheres and bacteria in each treatment (columns in Figure 3.4B). For Gnotobiotic flies, μ_0 and μ_b (the mean egestion time for microspheres and bacteria, respectively) were similar at both bacterial densities (paired *t*-test: $p = 0.120$ for LG, and $p = 0.293$ for HG). In Axenic flies, there

was no significant difference at Low density (paired t -test: $p = 0.069$), but μ_0 was significantly higher than μ_b at High density (paired t -test: $p = 0.003$, mean difference of 0.39 h with 95 % CI = [0.164, 0.619] h). The variance data yielded the same patterns of significance: the variance for the microspheres and bacteria (σ_o^2 and σ_b^2) did not differ in Gnotobiotic flies (paired t -test: $p = 0.525$ and 0.190, respectively) or in Axenic flies at Low density (paired t -test: $p = 0.15$), but σ_o^2 was significantly larger than σ_b^2 at High density (paired t -test: $p < 0.0001$, mean difference of 0.754 with 95 % CI = [0.49, 1.01]).

Combining the data for the proportion of particles ingested (Figure 3.5A) and the mean and variance of the egestion time (Figures 3.5B and 3.5C), we inferred key processes shaping the population dynamics of *A. tropicalis* in the *Drosophila* gut. Specifically, a proportion of the bacterial cells is retained or lysed abruptly at small location in the gut for three treatments: *A. tropicalis* administered at High and Low density to Gnotobiotic flies, and at Low density to Axenic flies (bottom left cell in Figure 3.4B). In contrast, a proportion of the bacteria is retained or lysed gradually across the whole gut when *A. tropicalis* is administered at High density to Axenic flies (top right cell in Figure 3.4B). These results suggest that microbial population dynamics differ depending on the treatment. This variation could not have been detected from just the total number of bacteria egested.

To investigate further how the population dynamics of *A. tropicalis* vary with treatment, we compared the normalized egestion time statistics (relative to microspheres; *e.g.* μ_{norm} in HA = μ_b in HA \div μ_0 in HA) across the treatments. μ_{norm} is significantly reduced in flies administered *A. tropicalis* at High density, relative to Low density ($p < 0.001$ for Type II and Type III ANOVA; slope = -0.32 in

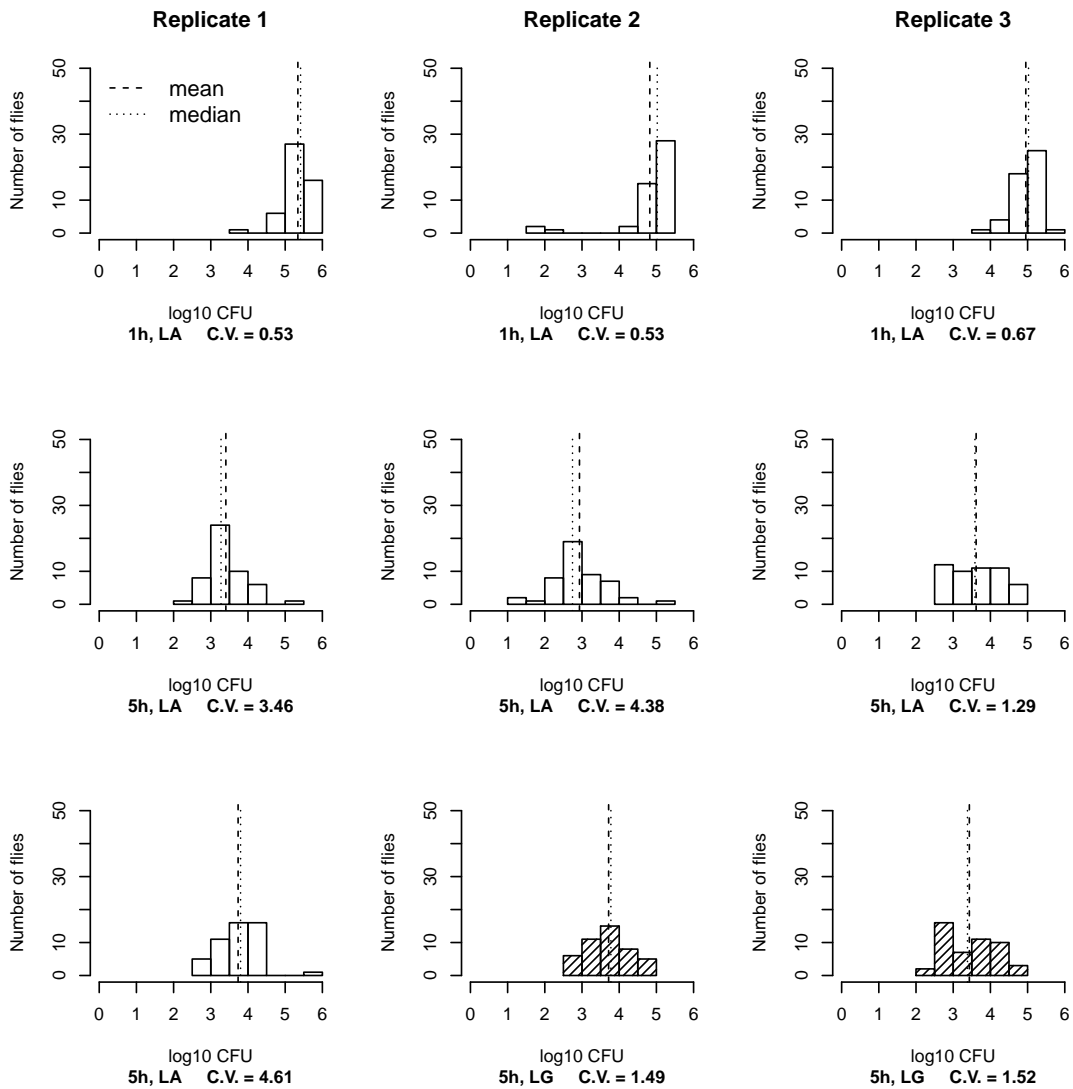


Figure 3.6: \log_{10} abundance of bacteria retained in the host body 1 h (first row) and 5 h (second and third rows) after exposure of Axenic (white bars) or Gnotobiotic (hatched bars) flies to Low density *A. tropicalis* in *Microbial Fate Experiment*. The three columns correspond to three different replicate experiments. Each histogram is data from a single vial with 50 flies (LA: Low Axenic; LG: Low Gnotobiotic). Vertical dashed and dotted lines are the mean and the median, respectively, of \log_{10} abundance of bacteria retained in the host body. Coefficient of variation for each vial was calculated using un-transformed abundance of bacteria retained.

simple linear regression, $p < 0.001$), but neither the Axenic/Gnotobiotic treatment ($p = 0.826$ for Type II and $p = 0.873$ for Type III ANOVA) nor the interaction term ($p = 0.199$ for Type II and Type III ANOVA) is significant. This pattern is also obtained for σ_{norm}^2 (bacterial density: $p < 0.005$ for Type II and Type III ANOVA; slope = -0.82 in simple linear regression, $p < 0.002$; Axenic/Gnotobiotic treatment: $p = 0.549$ for Type II and $p = 0.574$ for Type III ANOVA; interaction: $p = 0.434$ for Type II and Type III ANOVA). Taken together, these data suggest that lysis or retention of *A. tropicalis* in the gut is spatially more widespread at high inoculum density, irrespective of whether the flies are Gnotobiotic or Axenic (Figure 3.4B).

3.4 Discussion

The high diversity of microorganisms associated with most animals presents a complex system to decipher, as the interactions between the host and microorganisms are spatio-temporally heterogeneous. To understand the drivers structuring these communities, there is increasing interest in applying ecological theory to microbiomes. Cross-sectional studies based on static abundance or presence data highlight important ecological processes [77, 98], but replicate time-series from repeated measurements are becoming especially valuable to differentiate ecological processes from stochastic fluctuations within and among hosts [78]. Fecal time-series are widely collected [81, 82] and contain information on bacterial species interactions [79]. However, fecal communities can differ from within-gut communities and lack spatial information [80]. The novel mathematical methods developed in this study provide the basis to explain fecal time-series as patterns resulting from within-host processes. Specifically, we

were able to use the relationship between the spatial processes in the host and the temporal patterns in the feces to infer how spatio-temporal interactions between the *Drosophila* host and its microbiota vary under controlled experiments.

Our results come with two potential caveats. First, we calculated the number of bacteria retained in the host by counting the number of culturable bacteria. We therefore would have missed viable but nonculturable cells (VBNC). Although this issue cannot be excluded, its significance is likely minimal because we have not detected VBNC of the strain of *A. tropicalis* used in this study under a range of conditions. Second, in our compartment models, we assumed that parameters are constant over time. This may not be fully accurate because the ingested bacterial cells may induce immunological responses in the gut, including a rapid increase in reactive oxygen species and, more slowly, anti-microbial peptide production [99]. The magnitude and timescale of these immune responses are not well-known, making it difficult to quantify the extent to which our system deviates from the expectations of temporal stability. However, an indication that our theoretical results are robust to the assumption of constant parameters comes from our structural model, which shows that our qualitative results hold for wide range of parameters and functions, including time-varying parameters (Appendix B.2.2 and Figure B.5).

Despite substantial research on the gut microbiome in recent years, the population dynamics of gut microorganisms are very poorly resolved. Our theoretical results show that the complexity of the gut habitat can affect the dynamics of microbial populations, with substantial effects of the spatial distribution of host processes on egestion time distributions (Figure 3.4B). The implications of these effects are illustrated by our empirical data on *Drosophila*, which indicate

that many of the ingested bacterial cells are apparently lysed over a limited spatial scale. A strong candidate site is the proximal acidic region of the *Drosophila* gut (analogous to the mammalian stomach), which has been demonstrated to suppress the populations of both *Lactobacillus* and *Acetobacter* [100]. However, the lower mean and variance of bacteria (relative to microspheres) at High density (relative to Low density) indicates that high numbers of ingested bacteria can lead to more gradual population reduction as bacteria pass through the gut (top right cell in Figure 3.4B). We hypothesize that high bacterial density triggers inducible host immune responses through multiple compartments of the midgut [90, 101, 102], in addition to the constitutive low pH in the acidic region. Induced host immune response at high bacterial density may also explain the lower proportion of 48 h samples with bacteria present, compared to 48 h samples from Low-density treatments.

The high apparent mortality of the bacteria in the *Drosophila* gut raises the question of the benefits that *A. tropicalis* may receive from associating with this host. In the laboratory, *Acetobacter* density is depressed in the presence of flies relative to fly-free vials [88]. It is possible that *Drosophila* consumes and digests *Acetobacter* as part of its diet [92]. However, viable bacterial cells are consistently present in feces for hours to days post-ingestion, suggesting that *Acetobacter* may benefit from host-mediated dispersal of viable microbial cells ([103]; this study). *Drosophila* could act as a vector that transfers *A. tropicalis* between ephemeral resources, *e.g.* rotting fruit, decaying vegetable matter, thereby buffering the bacteria from regional extinction [104]. The relationship between *Drosophila* and *Acetobacter* may therefore be antagonistic (host nutritional benefit from bacterial prey) at the level of the individual bacterial cell, but mutualistic (host-mediated dispersal of bacteria) at the level of the bacterial popu-

lation. The relative significance of processes operating at different ecological scales may vary with ecological circumstance (*e.g.* composition and availability of food sources) and genotype of the host and bacteria.

The model developed here can also be applied to other systems where the shedding in the feces of ingested bacteria declines over time. For example, studies of egestion time distributions might provide information about interactions between two bacteria in a host. How would the presence of one bacterial strain affect the egestion time statistics of another? Competition for resources (*e.g.* space, nutrients), as well as interference competition through toxin production should lead to lower mean and variance of egestion time. On the other hand, cooperation and mutualism, both with other microbial taxa and with the host, is predicted to lead to higher mean and variance of egestion time. We further categorized population dynamics into four different spatio-temporal modes based on proportion of bacteria egested and the mean and variance of the egestion time. Our framework thus allows us to investigate how a microbial population behaves in a multispecies community, and furthermore, the spatial extent of the interaction along the host gut. For example, our approach can be used to answer the question: “To what extent do two bacteria species spatially overlap and compete over resources in the host?” Building simple microbial communities and investigating them through egestion time provides the basis for improved mechanistic understanding of the gut microbial ecology in various systems.

3.5 Methods

3.5.1 Within-host microbial population models

We constructed models for the dynamics of microbial population size within the host gut (Figure 3.4A) where X_i is the microbial population size in the i^{th} compartment of the gut (*e.g.* foregut, midgut, hindgut), r_i is the per-capita net reproductive rate of the bacteria in the i^{th} compartment, and m_i is the migration rate from the i^{th} compartment to the $(i + 1)^{\text{th}}$ compartment (except in the final compartment, where the bacteria “emigrate” to feces). Initially, we assumed that bacteria flow uni-directionally through an indefinite number of compartments in the host digestive tract. Within each compartment, bacteria are assumed to have constant per-capita birth, death and emigration rates. In Appendix B.2.1, we show the model equations, and derive the predicted mean and variance of egestion time of the bacteria. These statistics correspond to the mean and the variance calculated from time-series data for each sample. In Appendices B.2.1 and B.2.2, we further relax the assumptions of uni-directional movement and constant demographic rates to assess whether the same qualitative results hold for a general class of models. We used $n + 1$ compartment model to categorize inferences based on proportion of bacteria egested and egestion time statistics (Appendix B.2.3). It is important to note that our models do not distinguish between death and retention of a bacterium within a host, since a bacterium disappears in both cases from the compartments tracked by our model. We performed additional set of experiments to tease proportions of lysed and retained bacteria apart (Appendices B.1.3 to B.1.6).

3.5.2 Culturing of *Drosophila* flies and *Acetobacter tropicalis*

Wolbachia-free *Drosophila melanogaster* Canton-S flies were reared at 25 °C in a 12 h:12 h light-dark cycle on yeast-glucose diet (100 g l⁻¹ Brewer's yeast [inactive; MP Biomedicals], 100 g l⁻¹ glucose [Sigma], 12 g l⁻¹ agar [Apex], and preservatives comprising 0.04 % phosphoric acid and 0.42 % propionic acid [Sigma]). *Acetobacter tropicalis* DmCS006 derived from a single colony was grown overnight on modified MRS medium (mMRS, comprising 12.5 g l⁻¹ bactopeptone, 7.5 g l⁻¹ yeast extract, 20 g l⁻¹ D+ glucose, 2 g l⁻¹ potassium phosphate dibasic trihydrate, 2 g l⁻¹ ammonium citrate dibasic, 5 g l⁻¹ sodium acetate, 0.1 g l⁻¹ magnesium sulfate, 0.05 g l⁻¹ manganese sulfate) and concentrated to 10⁸ CFU/ml in sterile PBS. Axenic and gnotobiotic flies were prepared by the method of [94]. About 30 surface sterilized eggs were transferred to sterile food per vial. For each gnotobiotic fly vial, 50 µl suspension of *A. tropicalis* at 10⁸ cells/ml PBS was transferred directly onto the eggs.

All experiments were conducted on male flies at 5 days post-eclosion. One day before each experiment, axenic and gnotobiotic flies were sexed over sterile chilled aluminum foil and 50 male flies per vial were transferred to freshly-prepared sterile food. Female flies were homogenized in sterile PBS, and the suspension was spread onto MRS plates. Presence/absence of *A. tropicalis* was determined by presence/absence of bacterial colonies on the plate. Only axenic flies from vials with axenic females and gnotobiotic flies from vials with bacterial colonies were used for the experiments.

3.5.3 GFP-labeled *Acetobacter tropicalis*

GFP-labeled tetracycline-resistant *A. tropicalis* cells (*A. tropicalis*-pCM62-GFP) were created from *A. tropicalis* DmCS006, and the plasmid was confirmed to be stable (Appendix B.1.1). The colonies were streaked on mMRS plates with 5 g ml^{-1} tetracycline [Sigma-Aldrich], to select for the GFP strain. A single colony was grown overnight in mMRS without antibiotics, then collected by centrifugation and re-suspended into PBS at the desired density.

3.5.4 *Egestion Time Experiment*

To control feeding rate across samples, we adopted a protocol to obtain synchronous feeding on similar volume of food regardless of bacterial dosage [105] with minor modifications. Briefly, at the beginning of the light period, the flies were transferred to sterile 50 ml Falcon tubes and starved for 4 h without food or water at 29°C to synchronize and maximize feeding rate across samples (hour $-4-0$ in Figure 3.2). For each sample, $100 \mu\text{l}$ of dosing solution consisting of 10^8 or 10^9 CFU/ml *A. tropicalis* (Low and High density treatments, respectively), 10^9 beads/ml of microspheres ($1.0 \mu\text{m}$ diameter blue-green fluorescent FluoSpheres[®] polystyrene microspheres, Life Technologies F-13080), and 2.5 % sucrose were laid and dried on solidified sterile *Drosophila* food placed within the Falcon tube cap. *A. tropicalis* cells and the microspheres are of similar size ($0.5-0.7 \mu\text{m}$ by $1.8-2.0 \mu\text{m}$ size and $1 \mu\text{m}$ diameter, respectively). After starvation, each sample was exposed to the above treatment for an hour (hour $0-1$). Preliminary experiments showed, first, that every fly gut stained blue when exposed to Blue No.1 dye [Sigma] for an hour of feeding after the star-

vation condition above, indicating successful synchronized feeding (results not shown); and, second, that the number of egested microspheres recovered per fly across treatments was uniform, indicating that *Drosophila* fed on similar volume of food (Tukey's *post hoc* test: adjusted $p > 0.74$ for all comparisons). After hour 1, the samples were transferred to new sterile vials with sterile food, without the dosing solution. Samples repeatedly went through hourly transfer steps until the end of hour 5 for the short-term dynamics experiment. The flies were kept in a 29 °C incubator throughout the experiment except during the transfers. The number of surviving flies was recorded at the end of each hour interval.

After transfer, food caps were removed and the interior of the tubes was rinsed with 10 ml PBS. Tubes were reassembled with sterile caps, vortexed for 1 min and centrifuged at 5000 rpm for 10 min in 4 °C. The supernatant was carefully discarded, and the pellet was re-suspended in 100 µl PBS. Samples were transferred to sterile eppendorf tubes and stored in 4 °C for up to 6 h until microscopy. For the 24 and 48 h samples, the flies were maintained at 29 °C, with transfer to fresh, sterile food at 5 and 24 h. Samples were processed at 24 and 48 h exactly as for 1–5 h samples, except that the fecal pellets were scored for presence/absence of bacteria. Only samples with > 80 % fly survival at the end of hour 48 were used in the data analysis.

3.5.5 Quantification of egested GFP-labeled *A. tropicalis* and fluorescent microspheres from feces

Our goal is to quantify the ingested particle (GFP-labelled *A. tropicalis* cells or microspheres) abundance in feces from individual flies over time. We used a

Zeiss LSM500 fluorescent confocal microscope and the CellProfiler image analysis software to estimate the number of microspheres or bacteria per sample [106]. Specifically, 5 or 7.5 μl of the solution of re-suspended fecal matter was mounted on 24 mm \times 30 mm slide, and a field of scope (4753.7 μm \times 6040.2 μm) was randomly selected for microscopy. Fluorescent microspheres were identified as blue single fluorescent particles (acquired by wavelength 405 nm) and GFP-expressing intact bacteria were identified as green single fluorescent particles (acquired by wavelength 488 nm). To maximize precision and reduce spatial variability on a slide, a large area of slide was scanned, consisting of 100 tiles covering a surface of 4753.7 μm \times 6040.2 μm . The picture tiles were reassembled using Zeiss Zen. The number of particles was then quantified using CellProfiler, supplemented by manual counting for low-quality pictures. The CellProfiler and manual counting methods produced consistent values (Appendix B.1.2 and Figure B.2). From these measurements, we inferred the number of microspheres and bacteria from the initial sample, by scaling up first from the area under the field of scope to the total area of the slide, then up to the volume of aliquot used in preparation of the slide (*aliquot volume*), and lastly to the total volume. Particle abundance per fly was therefore calculated as the following:

$$\begin{aligned}
 \frac{\# \text{ Particles}}{\text{Fly}} &= \frac{\# \text{ Particles}}{\text{Scope}} \times \frac{\text{Scope}}{4753 \mu\text{m} \times 6040.2 \mu\text{m}} \times \frac{24 \text{ mm} \times 30 \text{ mm}}{\text{slide}} \\
 &\quad \times \frac{\text{slide}}{\text{aliquot volume}} \times \frac{\text{total volume}}{\# \text{ Fly}} \times \left(\frac{1000 \mu\text{m}}{1 \text{ mm}} \right)^2 \quad (3.1) \\
 &= \frac{\# \text{ Particles}}{\# \text{ Fly}} \times \frac{\text{total volume}}{\text{aliquot volume}} \times \frac{24 \times 30 \times 1000^2}{4753.7 \times 6040.2}
 \end{aligned}$$

The particle abundances in the inoculum used in the experiments were also quantified under the field of scope, in order to determine the relative number of microspheres to *A. tropicalis* cells in the solution used for each experiment.

3.5.6 Proportion of bacteria egested from feces in *Egestion Time*

Experiment

Using the number of bacteria recovered from feces over 5 h, we tested if *A. tropicalis* are egested passively without net reproduction or retention by the host. Specifically, we tested if the number of bacteria egested was equal to the number of bacteria ingested. Flies were exposed to a mixture of known microbial and microsphere densities in the experiments. Under the assumption that the flies ingested both particle types indiscriminately, the number of cells ingested relative to the number of microspheres ingested equals the number of cells in the inoculum relative to the number of microspheres in the inoculum. Similarly, we assume that both microspheres and bacteria were collected indiscriminately. Then, the number of cells egested relative to the number of microspheres egested equals the number of cells collected in the feces relative to the number of microspheres collected. We calculated the number of cells or microspheres recovered from feces by summing the number of *A. tropicalis* cells or microspheres in fecal samples over 5 h. Using the counts for microspheres and bacteria in inoculum and collected feces, we calculated the proportion of bacteria egested from feces as the following (see Appendices B.1.3 to B.1.6 for details):

$$\begin{aligned} \text{Proportion of bacteria egested} &= \frac{\# \text{ cells egested}}{\# \text{ cells ingested}} \\ &= \frac{(\# \text{ cells recovered from feces})/(\# \text{ microspheres recovered from feces})}{(\# \text{ cells in inoculum})/(\# \text{ microspheres in inoculum})} \end{aligned} \quad (3.2)$$

Proportion of bacteria egested therefore is the change in the number of cells relative to the number of microspheres, as both cells and microspheres traverse the fly gut.

The same inoculum was used repeatedly over multiple samples in a single day. Estimates of proportion egested from different samples on the same day are therefore not independent, so we averaged the estimated proportion egested for each treatment within a replicate experiment date.

We performed Student's *t*-test to assess if the averaged proportion egested differ from 1, where bacteria egested equals bacteria ingested. We then used ANOVA and model selection to assess whether our experimental treatments had any effect on the variation we observed in proportion egested across treatments.

3.5.7 *Microbial Fate Experiment*

To investigate if the ingested bacteria are retained or lysed in the host, we performed a separate set of experiments using Low density Axenic and Gnotobiotic treatments. The experiment followed the procedure of *Egestion Time Experiment*, but the flies were homogenized after feeding and passage (Figure 3.2). For each of the three replicate experiments, we had a whole-fly sample that was homogenized immediately after 1 h of feeding (Low density Axenic *Immediate* sample), and whole-fly samples that were homogenized after 5 h of hourly passage (Low density Axenic and Low density Gnotobiotic *Passaged* samples).

We calculated the proportion of bacteria egested as *Egestion Time Experiment*. To determine how many ingested bacteria were retained or lysed, we used the number of microspheres recovered to calculate the number of bacteria ingested (Appendices B.1.3 to B.1.6). To quantify the number of bacteria retained in the host whole-body, we surface sterilized the flies in 70 % ethanol, followed by

rinses in sterile water. We homogenized the whole-body flies and used a spiral plater to plate onto the mMRS plates with tetracycline (WASP-2 instrument, Microbiology International), selecting for GFP. Plates were incubated in 25 °C and the number of colonies (CFU) were counted 2 d after plating. Flies were homogenized individually to quantify inter-host variation over time. Homogenate microbial abundances were summed within a sample to calculate the mean *A. tropicalis* abundance per fly.

Microbial abundance from the fecal samples examined under a microscope (cells/fly) and from the whole-body homogenates on medium (CFU/fly) differ in units, and in the methods of quantification. To make a comparison between the two measurements, we calculated the conversion factor between the two units (Appendix B.1.5). We then calculate the proportion of bacteria retained and lysed.

3.5.8 Statistical analysis of egestion time from *Egestion Time*

Experiment

Our theory showed that mean and the variance of particle egestion time can be used to infer within-host population dynamics (Figure 3.4B, Appendix B.2.3, and Table B.1). We therefore calculated these statistics for each sample, and tested if the treatments led to different responses in the host. First, we compared the mean and the variance of microbial egestion time to microsphere statistics within each treatment. We performed paired *t*-tests between microbial and microsphere egestion time statistics, to understand the treatment effects on *A. tropicalis* with microspheres as controls. Second, we divided the mean and the vari-

ance of microbial egestion time by the mean and the variance of microsphere egestion time, respectively, to normalize the statistics across treatments. We performed forward model selection on linear models as well as ANOVA (Type II and III, to account for unbalanced sample size across treatments) to compare the normalized microbial statistics across treatments. In forward model selection, we used either the bacterial density or fly treatment as the starting covariate. We used `anova` function in **R** [38] to assess whether an additional covariate significantly improves the model.

3.6 Acknowledgements

H.I., S.P.E., N.B., and A.E.D. designed the study. H.I. performed theoretical work with guidance from S.P.E, and experiments with guidance from N.B and A.E.D. P.D.N. transformed *A. tropicalis* for the experiments. P.D.N and Y.L. performed microbiota stability experiment using 5 bacterial species, and validated H.I.'s experimental methods through independent experiments. H.I. wrote the initial draft, and all authors edited the paper. This work was improved by discussions with A. Agrawal, B. Lazzaro, and members in the Agrawal, Buchon, Douglas, and Ellner labs. We thank NSF DEB 1256719 and DEB 1353039 (to S.P.E.), NSF BIO 1241099 and NIH R01GM095372 (to A.E.D.), NSF BIO 1354421 and NSF BIO 1656118 (to N.B.), and Ruth L. Kirschstein NRSA postdoctoral fellowship (1F32GM099374-01) (to P.D.N.) for financial support. The funders had no role in study design, data collection and interpretation, or the decision to submit the work for publication.

CHAPTER 4

SPECIATION BY REINFORCEMENT: DYNAMICS OF CHOOSINESS EVOLUTION UNDER ASYMMETRIC POPULATION SIZES

4.1 Abstract

Reinforcement, the evolution of a preference for conspecific mates as a consequence of hybrid unfitness, is considered to be an important driver of speciation. When the hybridizing species have unequal population sizes, reinforcement theory [107] posits that the smaller population will evolve to be more choosy than the larger population (“Howard pattern”). An alternate hypothesis is that scarcity of conspecific mates will lead to less choosiness (“Hubbs pattern”, [108]). Experimental and field studies have found both patterns in hybridizing species pairs. We hypothesize that opportunity cost in mating (*e.g.* finite time available to find a partner) may limit the evolution of choosiness in the smaller population. We use a simple continuous trait-model to simulate the evolution of mating preferences when a choosing individual can mate once over each time step, but only has two chances to find a partner. Our model shows that, under unequal population sizes, the Howard pattern never evolves; the larger population becomes more choosy than the smaller population (Hubbs pattern). Other factors, such as unequal cost of hybridization, must be present in order to generate the Howard pattern. We therefore argue that observations of Howard pattern cannot be used as a support for reinforcement theory. Inequalities in encounter rate and cost of hybridization should both be considered in order to understand the mating strategy of hybridizing species.

4.2 Introduction

When individuals from two different “species” (or populations, ecotypes, *etc.*) mate, they frequently produce hybrids that are less fit than the parents [109]. To prevent wasting parental resources on hybrids and to direct them instead to more fit offsprings, choosiness for conspecific mates may be selected in potentially hybridizing species. The evolution of choosiness for mates as a consequence of reinforcing selection due to low fitness hybrids being weeded from the population (*i.e. reinforcement*) is considered to be an important driver of speciation [110–112].

However, hybridization can be a useful mating strategy if an individual cannot secure a conspecific mate. Specifically, “Hubbs principle” [108, 113, 114] states that hybridization between two species is favored when their population sizes greatly differ. Under highly unequal population sizes, individuals from a rare species (smaller population size) commonly encounter heterospecifics, but rarely encounter conspecifics. While hybrids are less fit, hybridization may be adaptive, as producing hybrid offspring is better than producing none.

Is hybridization always an evolutionarily advantageous strategy for individuals from rare species? Two contradicting predictions have been made in the literature, about how choosiness will evolve in the rarer species under population size asymmetry. On the one hand, reinforcement theory [107, 111, 115–119] predicts that because costly hybridization will be more common in rarer species, the selection pressure to increase choosiness will be stronger in rare species than in common species (hereafter, we call this the “Howard pattern”, where the rarer species is more choosy). On the other hand, Hubbs’ principle and its

extensions [108, 113, 120, 121] predict that if the high quality mates (*i.e.*, conspecifics) are scarce then less choosy individuals accepting lower quality mates (*i.e.* common heterospecifics) may have higher lifetime reproductive success than choosy individuals that only accept conspecific mates; hybridization may be an advantageous strategy in rare species, so choosiness should be weaker or less prevalent (hereafter, we call this the “Hubbs pattern”).

Experimental and observational studies across metazoans show mating patterns conforming to both the Howard and the Hubbs patterns (Table 4.1). Frequently in these studies, either reinforcement theory or Hubbs’ principle is invoked to explain the differential mating pattern of hybridizing species pairs, but the importance of the processes assumed to underlie the pattern are not evaluated. Therefore, the factors that have actually promoted one mating pattern over the other are unclear. Furthermore, the two Hubbs and Howard theories have developed independently without “cross-pollination”, even though they both employ adaptive arguments to explain differential mating patterns. For example, studies focusing on reinforcement see the gene flow resulting from hybridization as a passive homogenizing force that opposes reinforcement, rather than as an adaptive mating strategy that benefits the hybridizing individuals [122–124]. Similarly, studies focusing on Hubbs principle (synthesized in [113]) see hybridization as an immediately beneficial mating strategy, but the evolution of choosiness over longer timescale is not considered.

To gain a better conceptual understanding of how mating behavior evolves in hybridizing species, we construct a continuous trait-based population model that explicitly incorporates the potential costs and benefits of choosiness. We track population size and the distribution of a choosiness trait z in three pop-

Table 4.1: Experimental and observational studies documenting mating patterns between hybridizing species with asymmetric population sizes or geographic ranges. Mating patterns are categorized as “Howard” when the rarer population is more choosy, or “Hubbs” where the rarer population is less choosy. Hybrid cost is “Intrinsic” if hybrids have reduced viability or fertility, and “Extrinsic” if hybrids have a mating disadvantage or competitive disadvantage.

Common name	Species 1	Species 2	Asymmetry	Pattern	Hybrid cost	Reference
Invertebrates						
Fruit fly	<i>Drosophila pseudoobscura</i>	<i>D. persimilis</i>	Population size	Howard	Intrinsic	[115] ¹
Fruit fly	<i>Drosophila spp.</i>	<i>Drosophila spp.</i>				[116] ¹
	<i>D. paulistorum</i> Andean-Brazilian	<i>D. paulistorum</i> Transitional	Geographic area	Howard	Intrinsic	
	<i>D. paulistorum</i> Amazonian	<i>D. paulistorum</i> Centroamerican	Geographic area	Howard	Intrinsic	
	<i>D. yacuba</i>	<i>D. santomea</i>	Geographic area	Howard	Intrinsic	
	<i>D. persimilis</i>	<i>D. pseudoobscura</i>	Geographic area	Howard	Intrinsic	
	<i>D. paulistorum</i> Andean-Brazilian	<i>D. paulistorum</i> Orinocan	Geographic area	Howard	Intrinsic	
	<i>D. paulistorum</i> Andean-Brazilian	<i>D. paulistorum</i> Centroamerican	Geographic area	Howard	Intrinsic	
	<i>D. bipectinata</i>	<i>D. parabiepectinata</i>	Geographic area	Howard	Intrinsic	
	<i>D. melanogaster</i> (African only)	<i>D. simulans</i> (African only)	Geographic area	Howard	Intrinsic	
	<i>D. paulistorum</i> Amazonian	<i>D. paulistorum</i> Andean-Brazilian	Geographic area	Hubbs	Intrinsic	
	<i>D. paulistorum</i>	<i>D. tropicalis tropicalis</i>	Geographic area	Hubbs	Intrinsic	
Jewel wasp	<i>Nasonia vitripennis</i>	<i>Nasonia longicornis</i>	Geographic area	Howard	Intrinsic	[125] ¹
Walking stick	<i>Timema cristinae</i> (C. spinosus type)	<i>T. cristinae</i> (A. fasciculatum type)	Population size	Howard	Extrinsic	[123] ^{1,2}
Field crickets	<i>Gryllus texensis</i>	<i>G. rubens</i>	Population size	Hubbs	Extrinsic	[126]
Daphnia	<i>Daphnia galeata mendotae</i>	<i>D. rosea</i>	Population size	Howard	Intrinsic	[127]
Freshwater snails	<i>Viviparus ater</i>	<i>V. contectus</i>	Population size	Hubbs	Intrinsic	[128]
Vertebrates						
Swordtail fish	<i>Xiphophorus birchmanni</i>	<i>X. malinche</i>	Encounter rate ³	Hubbs	Likely ⁴	[129]
Minnows	<i>Notropis cornutus</i>	<i>N. chrysocephalus</i>	Population size	Hubbs	Intrinsic	[130]
Sunfish	<i>Lepomis spp.</i>	<i>Lepomis spp.</i>				[131]
	<i>L. macrochirus</i>	<i>L. cyanellus</i>	Population size	Hubbs	Intrinsic	
	<i>L. macrochirus</i>	<i>L. cyanellus</i>	Population size	Hubbs	Intrinsic	
	<i>L. macrochirus</i>	<i>L. cyanellus</i>	Population size	Hubbs	Intrinsic	
	<i>L. macrochirus</i>	<i>L. gulosus</i>	Population size	Hubbs	Intrinsic	
	<i>L. macrochirus</i>	<i>L. microlophus</i>	Population size	Hubbs	Intrinsic	
	<i>L. microlophus</i>	<i>L. macrochirus</i>	Population size	Howard	Intrinsic	
	<i>L. cyanellus</i>	<i>L. auritus</i>	Population size	Hubbs	Intrinsic	
Bass	<i>Micropterus punctulatus</i>	<i>M. dolomieu</i>	Population size	Hubbs	NA	[132]
Tree frog	<i>Litoria genimaculata</i> (N)	<i>Litoria genimaculata</i> (S)	Geographic area	Howard	Intrinsic	[133] ¹
Toads	<i>Bufo microscaphus</i>	<i>B. woodhousii</i>	Population size	Hubbs	NA	[134]
Sea turtles	<i>Cheloniidae spp.</i>	<i>Cheloniidae spp.</i>				[135]
	<i>Caretta caretta</i>	<i>Lepidochelys kempii</i>	Population size	Hubbs	Intrinsic	
	<i>Caretta caretta</i>	<i>Eretmochelys imbricata</i>	Population size	Howard	Intrinsic	
	<i>Caretta caretta</i>	<i>Chelonia mydas</i>	Population size	Howard	Intrinsic	
	<i>Eretmochelys imbricata</i>	<i>Chelonia mydas</i>	Population size	Howard	Intrinsic	
Chiffchaff	<i>Phylloscopus collybita</i>	<i>P. brehmii</i>	Population size	Howard	Likely ⁴	[136]
Darwin's finches	<i>Geospiza spp.</i>	<i>Geospiza spp.</i>				[137]
	<i>G. fortis</i>	<i>G. fuliginosa</i>	Population size	Hubbs	Extrinsic	
	<i>G. fortis</i>	<i>G. scandens</i>	Population size	Hubbs	Extrinsic	
Hares	<i>Lepus timidus</i>	<i>L. europaeus</i>	Population size	Hubbs	Likely ⁴	[138]
Fur seal	<i>Arctocephalus gazella</i>	<i>A. tropicalis</i>	Population size	Mix	Extrinsic	[139]

ulations: two parental species populations, and one hybrid population. In our model, each choosing individual sequentially encounters potential partners (with rate of encounter with population proportional to population size) and

¹These studies tested and confirmed reinforcement.

²This study also showed that substantial gene flow prevents reinforcement.

³This study performed an experiment where the fish were exposed to a potential mate over different time interval.

⁴Hybrid fitness cost likely, but not determined

decides whether or not to mate. An individual is given two chances to mate, but can mate only once during a time step in our model. Choosiness trait z determines the individual's behavior when her first encounter is with a hybrid partner. Higher choosiness increases the probability of the individual rejecting the hybrid partner, which gives the individual the second chance to encounter a conspecific partner. Lower choosiness increases the probability of the individual accepting the hybrid partner, which prevents the risk of encountering a heterospecific partner on the second chance. Our focus on a mating with a hybrid partner is the simplest possible scenario containing the essence of the costs and benefits of choosiness. A choosy individual is less likely to mate with hybrids and produce less fit offspring, but more likely to completely miss a chance to mate because no conspecific partner was found in the available time.

By explicitly incorporating the tradeoffs in choosiness, our model differs from previously published models in reinforcement literature (*e.g.* [119, 122]). Because an individual has limited encounters with potential partners over a time step, and mortality between time steps, the opportunity cost of mating may render hybridization as an adaptive mating strategy. Our model is therefore uniquely situated to directly compare the mechanisms underlying Hubbs and Howard patterns. Given these tradeoffs in choosiness, z evolves over time in each population depending on survival rates, fecundities, encounter rates, and population sizes of the three populations. We find that when parental species are symmetric in all parameters but asymmetric in population size, the model produces the Hubbs pattern. However, asymmetric fecundities between parental species can counteract asymmetric population sizes, switching the mating pattern from Hubbs to Howard.

4.3 Model

To construct our trait-based population model, we use an Integral Projection Model (IPM) [140–142] where individuals are cross-classified by species identity x , and a continuously varying (quantitative) choosiness trait z . If individuals are classified by a single trait z , an IPM takes the form:

$$\begin{aligned} n(z', t + 1) &= \int A(z', z)n(z, t)dz \\ &= \int s(z)[\mathcal{F}(z', z) + G(z', z)]n(z, t)dz \end{aligned} \tag{4.1}$$

where $n(z, t)$ is the population *density* of individuals with trait z at time t (such that $n(z, t)h \approx$ number of individuals in trait interval $[z, z + h]$ with small h) and the projection kernel A summarizes the contribution of trait z individuals now to the population of z' individuals after one time step. A is further partitioned into survivorship s , number of recruits \mathcal{F} , and trait change among adults G (e.g. growth or phenotypic plasticity).

We model three populations n_x where species identity $x = \{1, 2, 3\}$: n_1 and n_3 are population densities of the parental species and n_2 is population density of hybrids between the parental species. Individuals in each species are classified by choosiness z where higher z individuals are more discriminating than lower z individuals. Both x and z of an individual are established at birth, and they do not change over the individual's lifetime. We only track the choosy sex (female "individuals") with the assumption that the non-choosy sex (male "partners") are equally abundant. Applying Equation (4.1) to three populations, we have in

general:

$$\begin{aligned}
n_{x'}(z', t + 1) &= \sum_x \int A_{x'x}(z', z) n_x(z, t) dz \\
&= \sum_x \int s_{x'}(z') [\mathcal{F}_{x'x}(z', z) + G_{x'x}(z', z)] n_x(z, t) dz \\
&= s_{x'}(z') \left(n_{x'}(z', t) + \sum_x \int \mathcal{F}_{x'x}(z', z) n_x(z, t) dz \right)
\end{aligned} \tag{4.2}$$

Our goal is to explore how availability of partners and other factors affect the evolution of choosiness z . We therefore consider a model where trade-off in z occurs only through mating; individuals of the same population with different z incur fitness difference through fertility, but not through viability. We specify Equation (4.2) by the following assumptions. First, we assume that the survival probability $s_{x'}$ only depends on species identity x , and not on the choosiness. Therefore, $s_{x'}(z') = s_{x'}$. Second, we assume that the population sizes are regulated via intraspecific competition as follows: Each population is limited by $K_{x'}$ vacant space, which are first taken up by mature individuals. The remaining space are then proportionally shared among the offsprings with different traits. The space is vacated through death of the residing individual, and cannot be taken over while the individual remains alive. Taken together, we write:

$$n_{x'}(z', t + 1) = s_{x'} \left(n_{x'}(z', t) + \frac{(K_{x'} - \int n_{x'}(u, t) du) \sum_x \int F_{x'x}(z', z) n_x(z, t) dz}{\sum_x \iint F_{x'x}(u, z) n_x(z, t) dz du} \right) \tag{4.3}$$

where $F_{x'x}(z', z)$ describes the production of $\{x', z'\}$ offsprings by a $\{x, z\}$ individual, such that $F_{x'x}(z', z)h \approx$ the number of x' offspring in the range $[z', z' + h]$ produced by a x parent with trait z .

A $\{x, z\}$ individual can potentially mate with an $\{x'', z''\}$ partner of any type,

to produce offspring of various types $\{x', z'\}$. With whom an $\{x, z\}$ individual mates, however, depends on the partners encountered and the choosiness of $\{x, z\}$ individual (we assume that the male partners have a low mating cost and always accept the choosing individual's mating decision). Because encounter rates depend on the abundance of individuals at a given time, F varies over time. Therefore, we write F as:

$$\begin{aligned}
& F_{x',x}(z', z, t) \\
&= \sum_{x''} \int (\text{Mating rate } \mu \text{ between } \{x, z\} \text{ individual and } \{x'', z''\} \text{ partners at time } t) \\
&\quad \times (\text{Number of offspring } B \text{ produced when } \{x, z\} \text{ mates with } \{x'', z''\}) \\
&\quad \times (\text{Distribution } \Phi \text{ of } \{x', z'\} \text{ offspring when } \{x, z\} \text{ mates with } \{x'', z''\}) dz'' \\
&\equiv \sum_{x''} \int \mu(n_{x''}(z'', t), n_x(z, t)) B_{x''x}(z'', z) \Phi(\{x', z'\} | \{x'', z''\}, \{x, z\}) dz''
\end{aligned} \tag{4.4}$$

We simplify Equation (4.4) by making further biological assumptions. First, we assume that the number of offspring produced by a mating depends on the species identities of the parents, but not their choosiness. Furthermore, fecundity (expected offspring number) from a mating decreases as the genetic distance between the parents (*i.e.* $|x'' - x|$) increases:

$$B_{x''x}(z'', z) = B_{x''x} = b \exp(-\gamma_x |x'' - x|) \tag{4.5}$$

where γ_x is the species-specific fecundity cost of hybridization. Note that γ_x depends only on the species identity of the individual, not that of her partners.

Second, species identity x and choosiness trait z are inherited independently:

$$\Phi(\{x', z'\} | \{x'', z''\}, \{x, z\}) = \phi_x(x' | x'', x)\phi_z(z' | z'', z) \equiv \phi_{x'x''x}\phi_z(z' | z'', z) \quad (4.6)$$

where ϕ_x and ϕ_z are x and z trait distributions of the offsprings given the parents' identities and traits, respectively. Offspring species identity is inevitably just a consequence of parental species identities; the substantive assumption in Equation (4.6) is that transmission dynamics of choosiness are independent of species identity.

We assume that x follows Mendelian inheritance with some modifications. A backcross between hybrid and purebred individuals creates offsprings similar to the purebred species, *i.e.* half of the offsprings are purebreds and the other half are hybrids. However, a cross between two hybrid individuals creates hybrid offsprings. We further assume that x is not sex-linked (*i.e.* $\phi_{x'x''x} = \phi_{x'xx''}$), and therefore, we have 6 different mating combinations based on x :

$$1 \times 1 \left\{ \begin{array}{l} \phi_{111} = 1 \\ \phi_{211} = 0 \\ \phi_{311} = 0 \end{array} \right. \quad 1 \times 2 \left\{ \begin{array}{l} \phi_{112} = 0.5 \\ \phi_{212} = 0.5 \\ \phi_{312} = 0 \end{array} \right. \quad 1 \times 3 \left\{ \begin{array}{l} \phi_{113} = 0 \\ \phi_{213} = 1 \\ \phi_{313} = 0 \end{array} \right. \quad (4.7)$$

$$2 \times 2 \left\{ \begin{array}{l} \phi_{122} = 0 \\ \phi_{222} = 1 \\ \phi_{322} = 0 \end{array} \right. \quad 2 \times 3 \left\{ \begin{array}{l} \phi_{123} = 0 \\ \phi_{223} = 0.5 \\ \phi_{323} = 0.5 \end{array} \right. \quad 3 \times 3 \left\{ \begin{array}{l} \phi_{133} = 0 \\ \phi_{233} = 0 \\ \phi_{333} = 1 \end{array} \right.$$

For the trait inheritance distribution ϕ_z for crosses between purebred individuals (*e.g.* 1×1 and 1×3), we assume the infinitesimal model [143] in which the

offspring trait z has a Normal distribution centered at the average of the parents' trait values, with constant variance σ^2 :

$$\phi_z(z' | z'', z) \sim \mathcal{N}\left(z' \mid \mu = \frac{z'' + z}{2}, \sigma^2\right) \quad (4.8)$$

For the trait inheritance distribution ϕ_z between purebred and hybrid individuals (e.g. 1×2), we assume that offspring trait has a Normal distribution centered at the purebred parent's z , with constant variance σ^2 :

$$\phi_z(z' | z'', z) \sim \mathcal{N}(z' \mid \mu = z, \sigma^2) \quad (4.9)$$

We use different inheritance model for Equations (4.8) and (4.9) to allow z_3 and z_1 to evolve independently. Biologically, this means that the genes underlying population 1's preference for its conspecifics are different from the genes underlying population 3's preference for its conspecifics. The trait inheritance distribution ϕ_z between two hybrid individuals follow Equation (4.8).

Finally, we specify the mating rate μ . An individual can mate with an $\{x'', z''\}$ partner only if she encounters him. We describe this probability of encounter using encounter probability densities. In the next section, we first specify the encounter probability densities as functions of the population densities, and we then explain the mating rule as functions of the encounter probability densities.

4.3.1 Mating rate μ

To calculate the mating rates, we make the following assumptions. First, an individual encounters an $\{x'', z''\}$ partner with probability proportional to the pop-

ulation density of $\{x'', z''\}$. Second, each species has a species-specific encounter parameter $\alpha_{x''} \geq 0$. For example, some species may be more conspicuous than others, and therefore easier to be encountered. An increase in $\alpha_{x''}$ increases the probability of encountering an x'' individual. Taken together, the probability density of encountering $\{x'', z''\}$ partners is:

$$\alpha_{x''} E(n_{x''}(z'', t)) = \frac{\alpha_{x''} n_{x''}(z'', t)}{\sum_{x''} \alpha_{x''} \int n_{x''}(u, t) du} \quad (4.10)$$

In nature, a choosy individual who rejects a partner risks encountering a less compatible partner or not encountering a partner at all. In our model, we focus on the risk of encountering a less compatible partner. The probability density of encountering a partner therefore sums to 1 across all possible partners; an individual, when given a chance to mate, is guaranteed a partner. A model including the risk of not encountering subsequent partners for a choosy individual should lead to qualitatively similar results.

Second, to calculate the mating rates, we assume the following mating rules: Each individual can mate once at most during each time step, and is given two chances to encounter a partner. Any time an individual encounters a conspecific partner, they mate. The choosiness trait z determines the probability $m(z)$ that on the first chance, a purebred individual will mate with a hybrid partner:

$$m(z) = \frac{1}{1 + e^z}. \quad (4.11)$$

This is a decreasing function of z so that z is a measure of choosiness (large positive z is very choosy, large negative z is not choosy at all). A purebred individual never mates with a heterospecific on the first chance, because she is guaranteed a second chance and mating with heterospecific partner would produce the least

fit offsprings. On the second chance, an individual mates with any partner, because this is better than not mating at all during that time period. A hybrid individual mates with anyone it encounters on the first chance, because hybrids view parental species as its conspecifics.

Note that when z is low, an individual mates with a hybrid partner on the first chance, but not with a heterospecific partner. By doing so, the individual guarantees that they will mate during this time step, but forgoes a possible opportunity to mate with a conspecific partner on the second chance. The equations for the mating rates between each population are detailed in Appendix C.1.

4.3.2 Model simulation and analysis

We implemented the model in **R** [38], and ran the model until population distributions $n_1(z, t)$ and $n_3(z, t)$ numerically converged to a steady state. We then calculated the average $m(z)$ value (Equation (4.11)) for each population at the end of the simulation. We categorized a population to be “choosy” if its probability of mating with an encounter hybrid is $m(z) \leq 0.2$ and “non-choosy” if $m(z) \geq 0.8$. In our simulations, $m(z)$ always converged to either of these two extremes. We therefore obtain four possible mating patterns for populations 1 and 3: two convergent patterns (both populations are non-choosy or both are choosy) and two divergent patterns (“Hubbs” where the smaller population is non-choosy and larger population is choosy, and “Howard” where the smaller population is choosy and larger population is non-choosy).

To investigate how the mating behavior for populations 1 and 3 change with

parameters, we partitioned parameter space into the four possible mating patterns (*e.g.* Figure 4.1). To do so, we ran simulations at a grid of points across the parameter space, and computed their steady-state trait values. We then drew solid lines to connect the grid points at the boundary of the regions that contain the same mating pattern. We used unequal K_x values to create unequal population sizes, and focused on the three other population-specific parameters (α_x, γ_x, s_x ; Table 4.2) to introduce other asymmetries between the two purebred populations.

4.4 Results

To understand how unequal population size affects mating behavior, we increased the carrying capacity K for population 3 above that for population 1, while the carrying capacity for population 1 remained constant (Figure 4.1). Specifically, we varied K_3 from 8×10^4 to 3.2×10^5 while $K_1 = 8 \times 10^4$ and the other parameters remained equal between the species. We varied $\gamma_3 = \gamma_1 \equiv \gamma$ from 0.3 to 1.5. With no or small population size inequality ($K_1 \approx K_3$), both populations had similar mating behavior; both populations became choosy with high fecundity cost ($\gamma \geq 0.75$), and both populations became non-choosy with low fecundity cost ($\gamma \leq 0.6$). As population size asymmetry increased ($K_3 \gg K_1$), the larger population (N_3) became choosy whereas the smaller population (N_1) became non-choosy. The ratio of population sizes required for divergent mating patterns depends on cost of hybridization parameter, γ values (Figure 4.1). Nevertheless, all cases of divergent mating patterns followed the Hubbs pattern (rarer species is less choosy), rather than the Howard pattern (rarer species is more choosy).

Table 4.2: Asymmetric (*i.e.* species-specific) parameters in the model and their biological interpretation

Parameter	Biological interpretation
s_x	Adult and recruit survivorship over a timestep for x
K_x	Maximum vacant space (carrying capacity) for x
γ_x	Cost of hybridization on fecundity for x
a_x	Per capita encounter rate for x

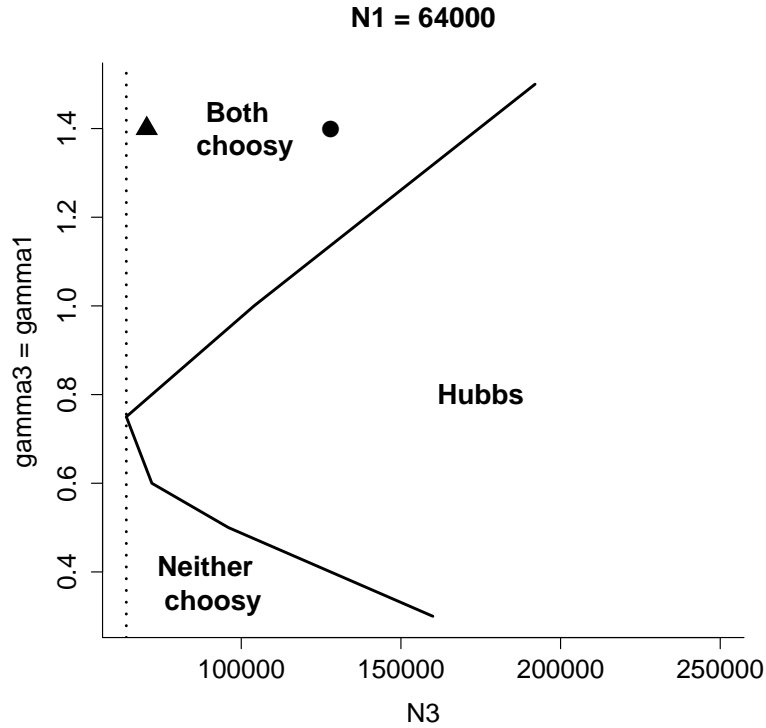


Figure 4.1: Mating behavior of populations 1 and 3 when K differs between the two populations, and all others remain equal. “Hubbs” refers to the pattern where the smaller population is non-choosy and the larger population is choosy. K_3 increased above $K_1 = 8 \times 10^4$ while $\gamma_1 = \gamma_3 \equiv \gamma$ varied. The parameter region to the left of the dotted line ($N_3 = N_1$) is mirror image to the parameter region to the right of the dotted line. In Figure 4.2, we plotted the transient dynamics for parameter values with low (triangle) and high (circle) population size asymmetries. Other parameters were set to: $b = 20$, $s_1 = s_3 = 0.8$, $s_2 = 0.6$, $\sigma^2 = 0.04$, $\alpha_1 = \alpha_2 = \alpha_3 = 0.1$, $K_2 = (K_1 + K_3)/2$, $\gamma_2 = (\gamma_1 + \gamma_3)/2$.

The Howard pattern did not emerge at the steady-state of our model simulations. Nevertheless, it is still possible that, as Howard originally suggested,

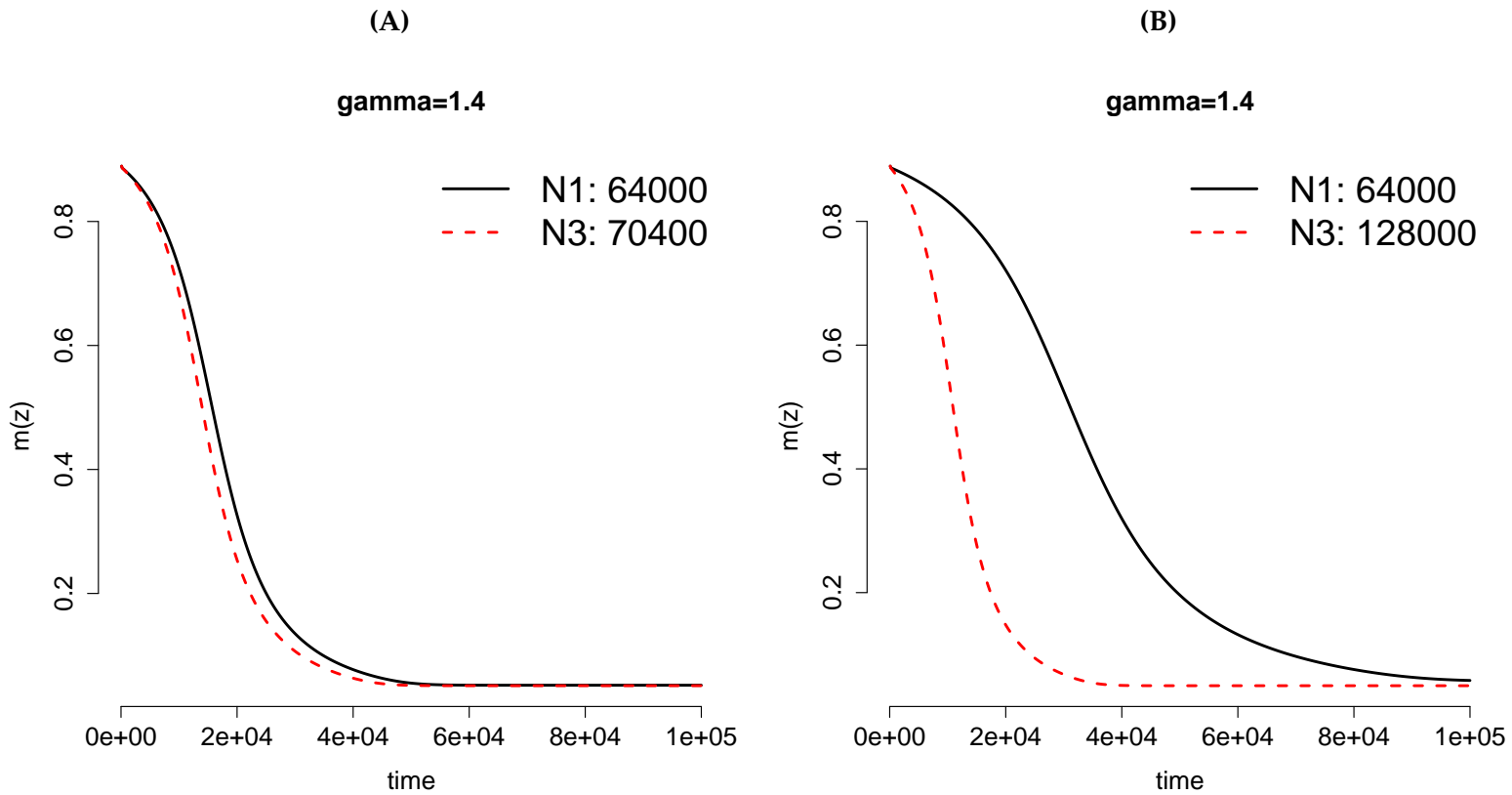


Figure 4.2: Transient dynamics of $m(z)$ for populations 1 and 3 (red-dashed and black-solid curves, respectively) when K differs between the two populations, and all other parameters remain equal. All individuals started with $m(z) = 0.9$, and the simulations ran for 10^5 time steps. Population 3 was larger than population 1 for the duration of the simulations. Parameter values were set to have (A) low (triangle in Figure 4.1) and (B) high (circle) population size asymmetries. The legends show population sizes at the end of 10^5 time steps.

the smaller population may evolve choosiness faster than the larger population, when both populations evolve towards choosiness (reinforcement). To test this, we selected points in the parameter space where both populations evolve choosiness with low and high population size asymmetries (triangle and circle in Figure 4.1, respectively). We started the simulations with $m(z) = 0.9$ for all individuals, and plotted the dynamics of choosiness $m(z)$ for the first 10^5 time steps of the simulations. Over the 10^5 time steps, the population with larger K always had larger population size than the population with smaller K . For both low and high population size asymmetries, the larger population evolved choosiness faster than the smaller population, and the difference in the rate of evolution increased with the magnitude of the population size asymmetry (Figures 4.2A and 4.2B).

Given that the ratio of population sizes required for divergent mating pattern depends on hybridization cost γ , we expect that differences in γ_x can also lead to divergent mating patterns. Holding all other parameters (including K) equal across species, we set $\gamma_1 = 0.75$ for population 1 and varied γ_3 from 0 to 0.75 (*i.e.* from no to equal fecundity cost). Across this range of γ_3 , population 1 remained choosy. Population 3, however, became non-choosy at $\gamma_3 \leq 0.6$ (Figure 4.3). As expected, mating behavior can also diverge due to differences in the cost for fecundity.

Next, we investigated the amount of difference in γ_x needed to counteract the effect of unequal population sizes. To do so, we held parameter values for population 1 constant but varied γ_3 and K_3 for population 3, with all other parameters the same as population 1. We ran two γ_x conditions: 1. γ_1 and γ_3 diverged with constant $\gamma_2 = \sqrt{\gamma_1\gamma_3} = 0.3$, and 2. γ_1 and γ_3 diverged with con-

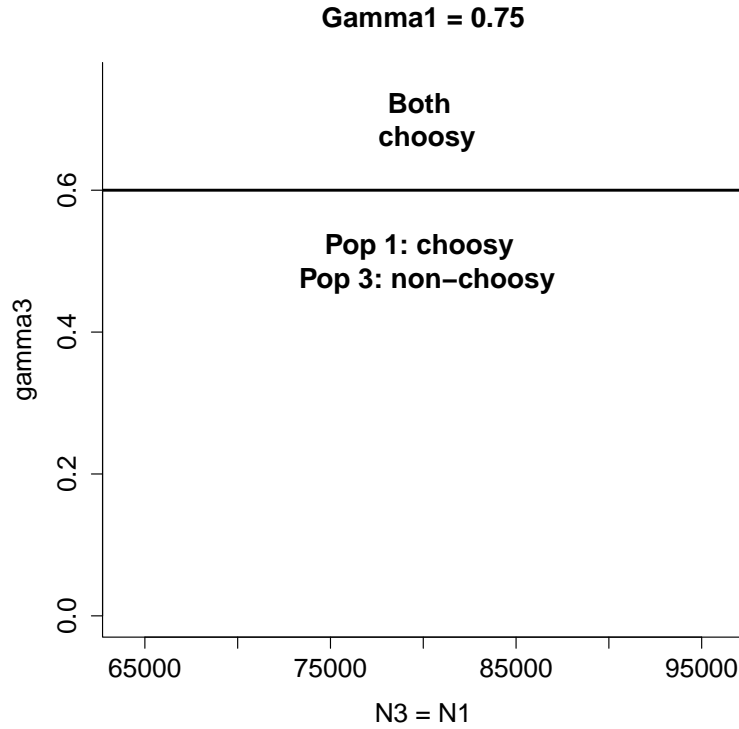


Figure 4.3: Mating behavior of populations 1 and 3 when γ differs between the two populations, and all others remain equal. γ_3 decreased below $\gamma_1 = 0.75$, while $K_1 = K_3 \equiv K$ varied. Other parameters were set to: $b = 20$, $s_1 = s_3 = 0.8$, $s_2 = 0.6$, $\sigma^2 = 0.04$, $\alpha_1 = \alpha_2 = \alpha_3 = 0.1$, $K_2 = (K_1 + K_3)/2$, $\gamma_2 = (\gamma_1 + \gamma_3)/2$.

stant $\gamma_2 = \sqrt{\gamma_1 \gamma_3} = 0.75$. We chose these conditions to assess whether our results depend on the mating patterns under equal fecundity costs ($\gamma_1 = \gamma_2 = \gamma_3$): both populations are non-choosy under the first condition, and choosy under the second.

With very different population sizes, the two populations exhibit the Hubbs pattern, consistent with our previous result (Figures 4.4A and 4.4B). This pattern occurs for a wide range of γ_x inequality. But even with large population size asymmetry, large γ_x asymmetry can revert the Hubbs pattern back into a convergent pattern (non-choosy in Figure 4.4A and choosy in Figure 4.4B). With even larger differences in γ_x , we then obtain Howard pattern (rare popula-

tion choosy, common population non-choosy). In both cases we considered, the Howard pattern only occurs when the ratio of γ values is larger than the ratio of population sizes.

We next investigated if asymmetry in encounter rate α_x can also reverse the effect of asymmetric population sizes. α_x proportionally changes the encounter rate with population x – an individual is more likely to encounter a partner from population x as α_x increases. Again, we found that differences in α_x can reverse a Hubbs pattern driven by population size differences, and with sufficient α_x asymmetry, the Howard pattern evolves in the model. Unlike the case of γ_x asymmetry, however, the one-to-one line occurs within the parameter region for convergent mating behaviors (dashed line in Figures 4.5A and 4.5B). Thus, asymmetry in α_x has the same effect as the asymmetry in population sizes. With the same ratio (but in opposite directions) asymmetries in α_x and K_x cancel out, giving equal encounter rates for populations 1 and 3.

Lastly, we considered the effect of asymmetry in s_x on the mating patterns. We set $s_1 = 0.8$, while s_3 changed from 0.3 to 0.8. We set $s_2 = 0.75s_3$ so that population 2 (hybrids) always have the lowest survival. s_x changes the population sizes, so differences in s_x translate to differences in population size. Changing s_x is therefore effectively equivalent to changing carrying capacity while holding other parameters constant (Figure 4.6).

4.5 Discussion

Divergent mating patterns where a hybridizing species pair evolve different mating strategies are observed widely across metazoans (Table 4.1), and differ-

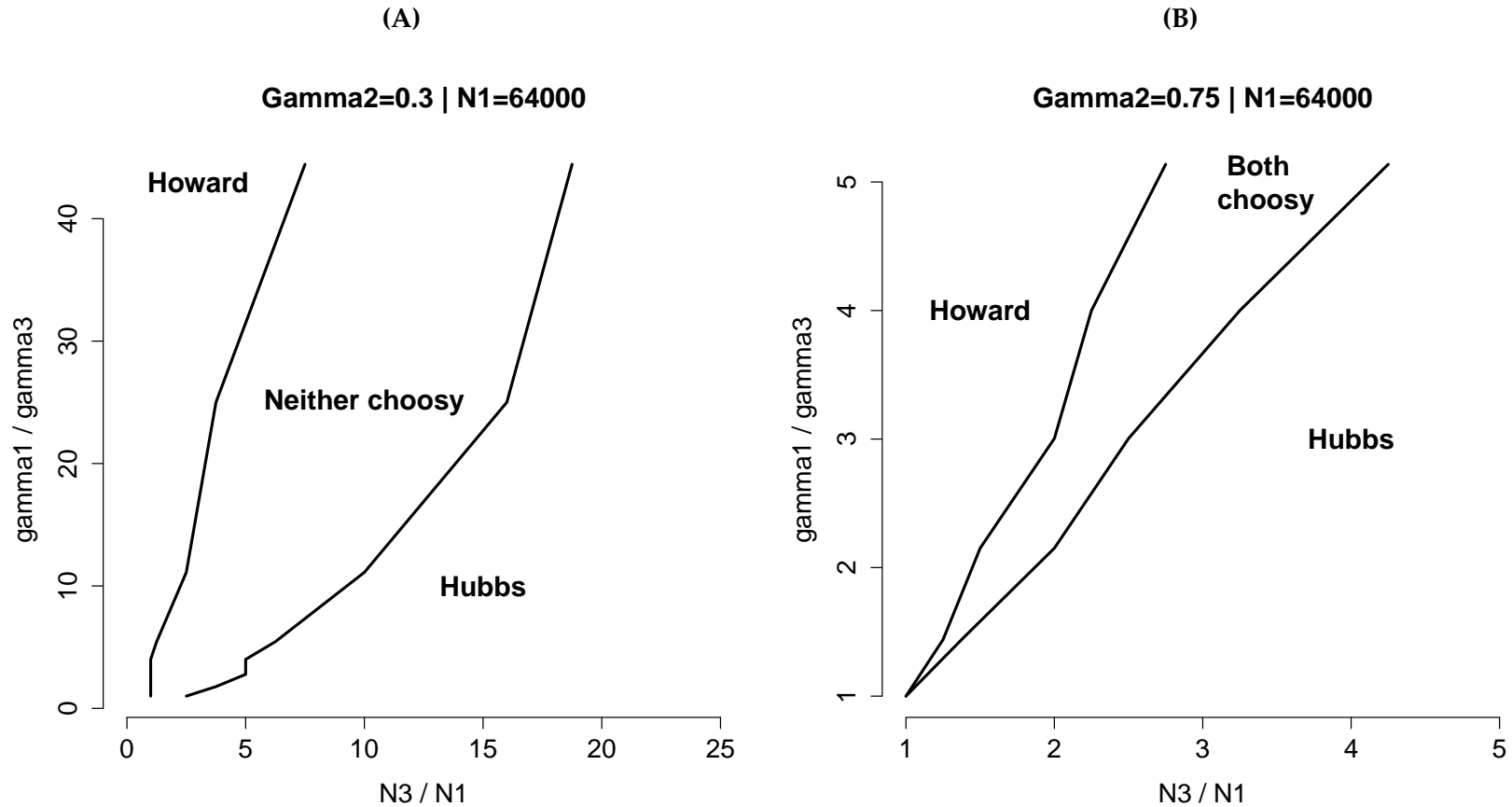


Figure 4.4: Mating behavior of populations 1 and 3 under asymmetric population sizes and asymmetric γ_x . “Hubbs” refers to the pattern where smaller population is non-choosy and larger population is choosy. “Howard” refers to the pattern where the smaller population is choosy and the larger population is non-choosy. K_3 increased above $K_1 = 8 \times 10^4$ while (A) γ_1 and γ_3 diverged around $\gamma_2 = \sqrt{\gamma_1 \gamma_3} = 0.3$ and (B) γ_1 and γ_3 diverged around $\gamma_2 = \sqrt{\gamma_1 \gamma_3} = 0.75$. Other parameters were set to: $b = 20$, $s_1 = s_3 = 0.8$, $s_2 = 0.6$, $\sigma^2 = 0.04$, $\alpha_1 = \alpha_2 = \alpha_3 = 0.1$, $K_2 = (K_1 + K_3)/2$.

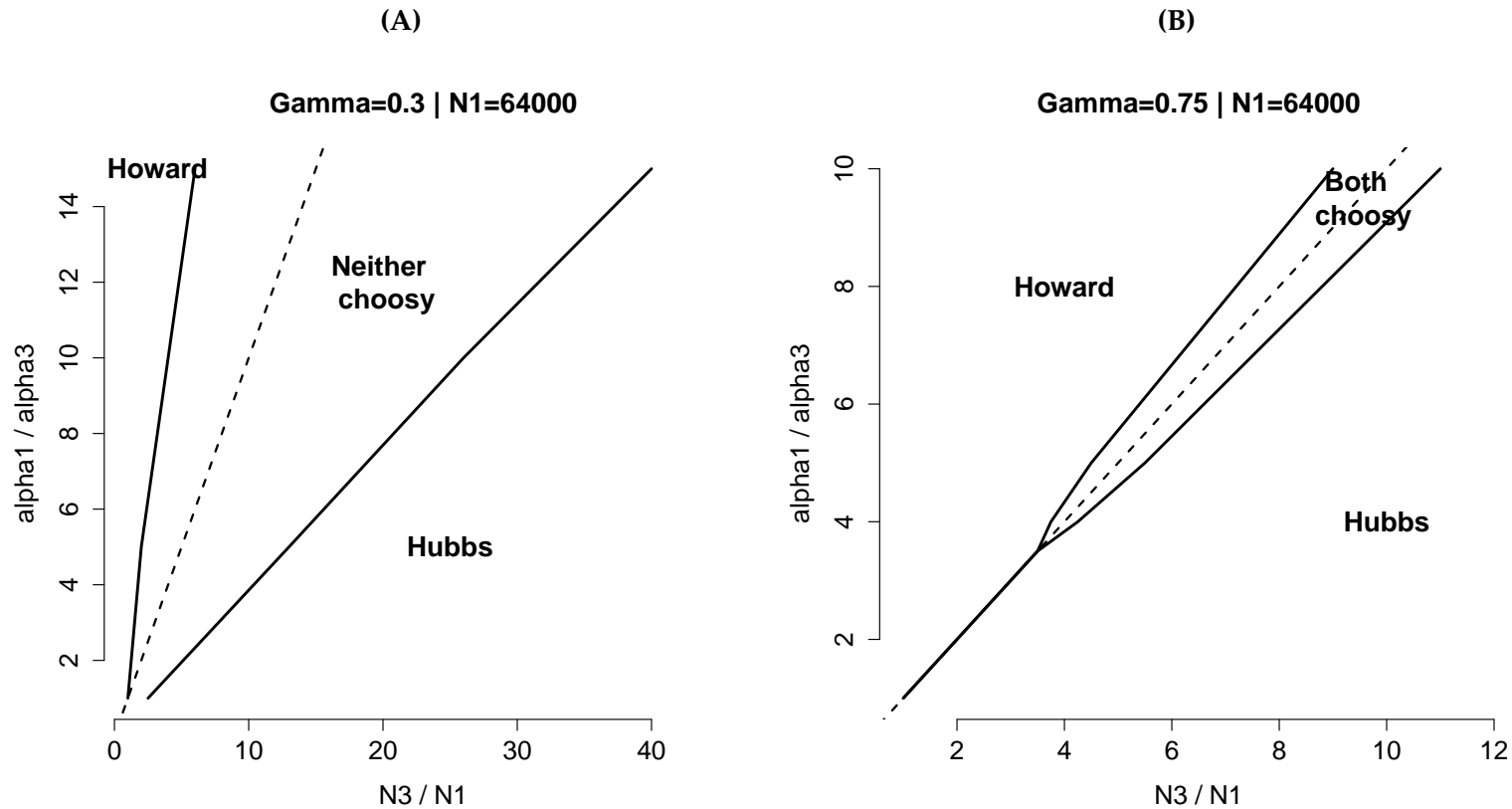


Figure 4.5: Mating behavior of populations 1 and 3 under asymmetric population sizes and asymmetric α_x . “Hubbs” refers to the pattern where smaller population is non-choosy and larger population is choosy. “Howard” refers to the pattern where smaller population is choosy and larger population is non-choosy. K_3 increased above $K_1 = 8 \times 10^4$ and α_3 decreased below $\alpha_1 = 0.1$ while **(A)** $\gamma_1 = \gamma_2 = \gamma_3 = 0.3$ and **(B)** $\gamma_1 = \gamma_2 = \gamma_3 = 0.75$. Other parameters were set to: $b = 20$, $s_1 = s_3 = 0.8$, $s_2 = 0.6$, $\sigma^2 = 0.04$, $\alpha_2 = (\alpha_1 + \alpha_3)/2$, $K_2 = (K_1 + K_3)/2$. Dashed line: one-to-one line.

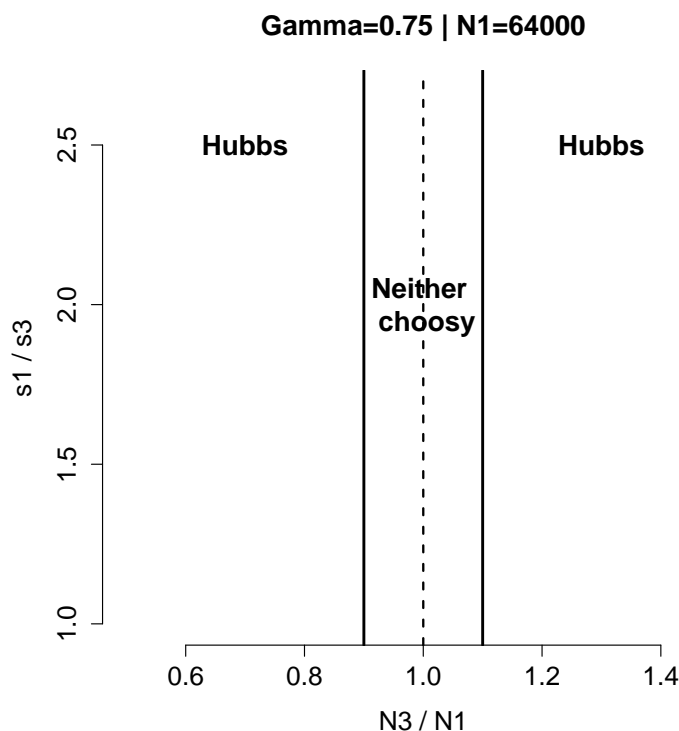


Figure 4.6: Mating behavior of populations 1 and 3 under asymmetric population sizes and asymmetric s_x . “Hubbs” refers to the pattern where smaller population is non-choosy and larger population is choosy. K_3 increased above $K_1 = 8 \times 10^4$ and s_3 decreased below $s_1 = 0.8$. Other parameters were set to: $b = 20$, $s_2 = 0.75s_3$, $\sigma^2 = 0.04$, $\alpha_1 = \alpha_2 = \alpha_3 = 0.1$, $K_2 = (K_1 + K_3)/2$, $\gamma_1 = \gamma_2 = \gamma_3 = 0.75$. Dashed line: $N_3/N_1 = 1$.

ent hypotheses have been developed to explain these patterns. Studies where the Howard pattern is observed (rare population more choosy) are used to support reinforcement theory (evolution of choosiness due to hybridization) [107, 111, 115, 116]. When the Hubbs pattern is observed, where the rare population is less choosy, it is interpreted as an adaptive strategy to maximize short-term mating success [108, 113]. We therefore have opposite predictions for how rare populations should evolve under hybridization. Yet, these two patterns have not previously been evaluated systematically, so the mechanisms underlying them are poorly resolved.

The Howard hypothesis was first stated in terms of the *rate* of evolution (due to different strengths of selection), instead of long-term evolution of divergent mating patterns [107, 115, 118, 119]. However, measuring the rate of evolution in mating behavior in the field is difficult. Consequently, recent studies have compared choosiness between populations with unequal population sizes, or unequal geographic ranges (as a proxy for population sizes), to test and support reinforcement theory [115, 116]. Here, we developed a simple model to test whether asymmetric population size alone could generate the Howard pattern, either in transient dynamics (smaller population evolving choosiness faster than larger population) or in steady-state of the system (smaller population becoming more choosy than larger population).

First, we showed that even under completely symmetric parameters, a cost for hybridization is not sufficient for reinforcement to occur. Depending on the value of γ (fecundity cost of hybridization), both populations can become either choosy or non-choosy – if the cost is low, hybridization is an adaptive strategy (Figure 4.1). Mating behavior in our model evolves under a trade-off between the cost of hybridization, and the opportunity cost of forgoing a mating (*i.e.* because the next potential partner during the available time is even less desirable). Studies on reinforcement should take encounter rate with conspecific and heterospecific individuals into consideration.

Second, we showed that asymmetry in population sizes without other asymmetries always leads to steady-states with the Hubbs pattern, and never to the Howard pattern, even though both hypotheses are based on asymmetry in population size. Furthermore, transient dynamics under reinforcement (when both populations evolve choosiness) also always show the Hubbs pattern, with the

larger population evolving choosiness faster than the smaller population (Figures 4.2A and 4.2B). As [144] emphasized, one important role of models in evolutionary biology is to provide a check on verbal arguments. Our model supports the verbal arguments leading to the Hubbs pattern, but not those leading to the Howard pattern, either as a transient state during the initial evolution of mating preferences, or as the long-term outcome of mating behavior evolution in the presence of unequal population sizes.

To obtain the Howard pattern, other asymmetries (Table 4.2) must be present. We used K_x (maximum vacant space) to control population sizes, but s_x (survivorship) and α_x (per capita encounter rate) essentially have the same effect: s_x changes the population size, while α_x makes the population size appear to be larger or smaller for a mate-seeking individual. Howard patterns obtained via asymmetries in K_x , α_x , and s_x (Figures 4.1, 4.5 and 4.6) therefore share the same mechanism. These three parameters work through encounter rates, where the population that encounters heterospecifics more often become less choosy. In nature, many animals have strategies that increase their encounter rates with conspecific partners. Spatial aggregation increases the visibility of conspecific partners, therefore increasing the effective encounter rate with conspecifics for that species. Pheromone dispersal and mating calls help individuals to find conspecific partners, even when the population size may be small. Asymmetries in these behaviors may be generating the Howard pattern that we observe in nature.

Can we obtain Howard pattern through mechanisms other than modifying the encounter rates? In our model, asymmetry in γ_x (cost of hybridization on fecundity) can also produce the Howard pattern (Figure 4.4). A rare population

with higher γ_x incurs additional cost from mating with encountered hybrids, so its choosiness evolves even when the choosing individuals often encounter hybrid potential partners. However, there is a trade-off: when an individual from a rare population is choosy, it risks encountering a heterospecific partner in the future and pay a higher cost in fecundity. With larger population size asymmetry, the ratio of γ_x values required to produce the Howard pattern is increasingly large.

We began our modeling with the expectation, based on Table 4.1, that there would be other processes or parameters besides population size, such that a small difference in one or more of these attributes would override a large difference in population size. That finding would have made it easy to understand why both the Hubbs and Howard patterns have often been observed. But our initial expectation proved to be incorrect. Overriding a large asymmetry in population size requires an equally large, or larger, asymmetry in something else in our model. We therefore hypothesize that such additional asymmetries can be found in cases where the Howard pattern is observed.

Our model may be extended to include other aspects of mating behavior. For example, mutual mate choice (where males are also choosy) is increasingly shown to be important in animal reproduction [145]. Suppose that the heterospecific male partners can reject the female individual. We expect females from smaller population to encounter heterospecific males more frequently than females from larger population. Females from smaller population would therefore experience more rejections, and therefore larger opportunity cost of mating. We hypothesize that mutual mate choice will pressure smaller population to relax choosiness.

Our model differs from previous models by incorporating the opportunity cost of choosiness. To capture the essence of the opportunity cost, we assumed that the individuals only have two chances to mate in each time step. As the number of chances increases, the opportunity cost of rejecting a hybrid partner decreases. With infinite number of chances, the opportunity cost will be zero and we expect our model to produce Howard pattern. Preliminary results from variants of our model with different mating rules show that opportunity cost is indeed the key to producing Hubbs pattern. For example, we created a variant of the model where each individual can encounter more than two potential partners over a time step, but each encounter comes with a cost. When the cost is zero, smaller population becomes choosy. However, with some encounter cost, smaller population becomes less choosy.

Our study highlights the importance of the trade-off between the opportunity cost of choosiness (missing a mating opportunity) and the cost of hybridization (lower reproductive success from a mating). Previous works on reinforcement largely ignored this trade-off, so the smaller population was expected to become more choosy under reinforcement. However, our study shows that the reverse is true when mating opportunities are limited. Therefore, a test for reinforcement where the smaller population becomes more choosy, or the smaller population evolves choosiness faster, should not be viewed as providing unambiguous support for reinforcement theory. Population sizes, encounter rates, opportunity costs of choosiness, and the costs of hybridization should all be evaluated to understand the adaptive strategies used by individuals in potentially hybridizing species.

4.6 Acknowledgements

We would like to especially thank our collaborator, Rick Harrison. Rick passed away unexpectedly before the completion of this study, while on sabbatical in Australia. His keen insights in speciation and hybridization, his vast knowledge on diverse biological systems, and his enthusiasm for science and people were instrumental in planning and developing this study.

APPENDIX A
SUPPLEMENTARY INFORMATION TO CHAPTER 2

A.1 Summary of analyses examining quality and potential biases in the NABA dataset.

Here we examine potential biases and quality issues common in citizen science datasets [8]. While there are some shortcomings, several lines of evidence and past studies (*e.g.* [31]) suggest that this is a reliable dataset and it is appropriate for our analyses. First, we compared our complete population indices with truncated indices that only included sampling dates that had consistent data cross all years. The truncated dataset constitutes a very small portion (20–25 %) of the original dataset, yet we see very high correlations between the two (Pearson’s r in Midwest: 0.88; Northeast: 0.94). Second, to address the potential for missing data early in the season, we plotted the yearly counts for the Midwest and Northeast to ensure that censuses captured a temporal increase in butterfly abundance in late spring. Third, we addressed the relationship between sampling effort and butterfly counts by transforming party hours to test for sampling effort biases common in citizen science datasets [8]. Fourth, we used Ripley’s K function [146] to assess whether the count data show a temporal bias of increased clustering over years. Finally, the potential for additional spatial biases in sampling are addressed in Sections 2.4 and 2.5.

Table A.1: A summary of the annual census data used in analyses. All data were compiled, normalized and smoothed from the raw data (see Section 2.3), except that of the last four columns beginning with Mexico.

YEAR	Spring South	Midwest	Northeast	Truncated Midwest	Truncated Northeast	Cape May	Peninsula Point	Fall South	Mexico ¹	Change in monarch population estimate (Mexico) ²	Average adoption of HT corn & soybean ³	Change in HT adoption ²
1993	NA	153.365	39.425	53.258	34.591	544.6	NA	NA	6.23	NA	0	0
1994	NA	226.537	59.704	210.537	39.124	839.8	NA	NA	7.81	1.58	0	0
1995	NA	35.737	43.021	34.37	35.147	248.5	NA	NA	12.61	4.8	0	0
1996	NA	102.151	37.713	61.293	32.97	503.6	104.411	NA	18.19	5.58	5	5
1997	NA	230.106	108.253	149.485	70.155	919.6	254.429	NA	5.77	-12.42	10.5	5.5
1998	NA	104.858	40.951	47.686	25.308	403.1	63.514	NA	5.56	-0.21	26.5	15.95
1999	NA	255.704	104.118	126.978	45.144	2849.2	287.665	NA	8.97	3.41	32	5.3
2000	NA	149.817	80.296	73.162	32.814	250.7	259.48	NA	3.83	-5.14	30.5	-1.4
2001	NA	307.803	90.546	141.428	34.372	658.4	421.751	NA	9.36	5.53	38	7.5
2002	NA	166.007	21.381	62.175	8.54	276.8	317.842	35	7.54	-1.82	43	5
2003	NA	193.017	41.897	103.476	17.272	392.3	466.94	110.833	11.12	3.58	48	5
2004	NA	58.672	16.049	33.361	9.238	74	92.053	28.25	2.19	-8.93	52.5	4.5
2005	44.629	163.33	58.997	89.566	20.206	538.2	401.245	56.734	5.91	3.72	56.5	4
2006	77.268	338.107	265.467	162.687	120.702	1743.4	56.64	133.614	6.87	0.96	62.5	6
2007	72.977	266.017	179.67	159.438	90.476	746	129.424	64.362	4.61	-2.26	71.5	9
2008	51.261	170.119	132.027	76.062	57.147	265.8	320.048	24.262	5.06	0.45	77.5	6
2009	75.296	185.16	88.072	84.44	43.095	281.2	177.383	183.774	1.92	-3.14	79.5	2
2010	29.595	306.761	95.789	156.473	51.278	1026.5	624.553	58.829	4.02	2.1	81.5	2
2011	34.3	140.353	80.143	76.412	35.492	681.73	108.428	171.66	2.89	-1.13	83	1.5
2012	20.861	169.584	178.336	89.023	114.551	1222.26	121.686	62.798	1.19	-1.7	83	0
2013	10.31	41.939	16.801	17.153	6.524	112.73	42.462	37.39	0.67	-0.52	89	6
2014	21.129	99.009	46.367	64.998	16.011	393.9	652.844	53.21	1.13	0.46	91.5	1.5

¹http://assets.worldwildlife.org/publications/768/files/original/REPORT_Monarch_Butterfly_colonies_Winter_2014.pdf?1422378439. For a YEAR N , the Mexico population corresponds to the butterflies overwintering from N to $N + 1$.

²the change given in year N represents the change from Year $N - 1$ to N .

³http://www.ers.usda.gov/media/185551/biotechcrops_d.html

A.1.1 Description of NABA dataset.

The North American Butterfly Association (NABA) has compiled butterfly counts from participating citizens across North America since 1975. The counts are taken from various locations throughout the year and the data includes the number of observed monarchs, the location (latitude and longitude), date, number of observers, number of parties (groups of observers), and the total hours spent.

The dataset goes back to 1975 initially as July 4th counts (led by the Xerces Society for Invertebrate Conservation, later acquired by NABA), but the number of sampling dates has been increasing every year, with samples taken more widely throughout the year. The number of counts gradually increased over the years and substantial number of counts were reported 1993–2014 (mean of 290 counts/year across the USA, see Figure A.1). Furthermore, these years correspond to the data available on the overwintering population in Mexico from the surveys by the WWF.

While the counts originally took place on July 4th, participants started to collect data more widely throughout the year. Figure A.2 shows the fraction of data points (each colored line represents a year) taken in each month. Northeast and Midwest are concentrated while South has wider sampling range. The two to three key breeding generations during the summer occur in the Midwest and Northeast regions. Although our earliest and latest NABA samples from these regions (across the 22 years in the dataset) were taken from March 27th and October 3rd, respectively, on average there are $\approx 74\%$ of counts in July, with fewer samples in June ($\approx 20\%$) and August ($\approx 5\%$). These months correspond to the

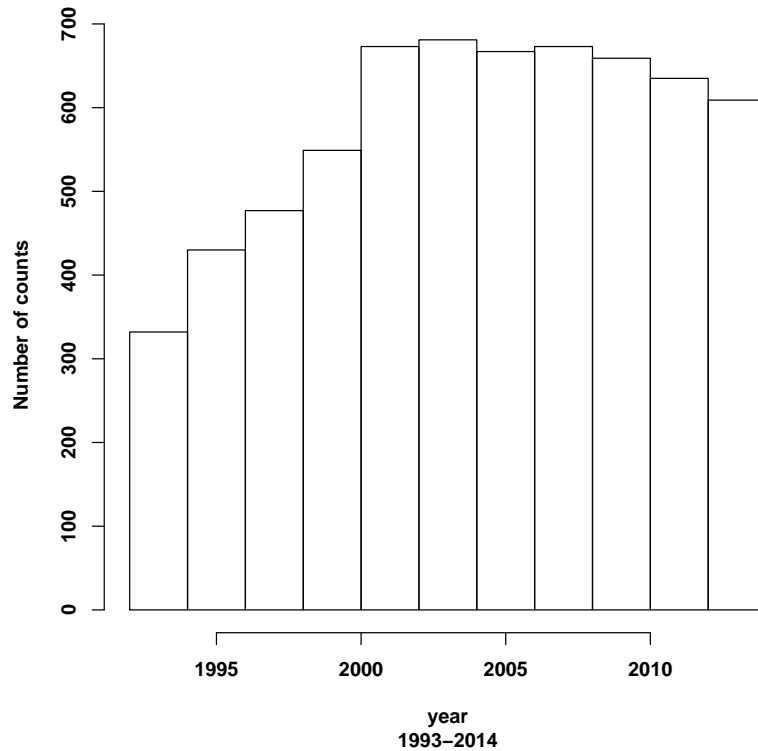


Figure A.1: Number of July 4th counts in NABA dataset across Midwest, Northeast, and South. The dataset goes back to 1975, but we used counts from 1993–2014 (mean of 290 counts).

peak abundance and breeding period of monarchs [147] (also see Figure 2.3B). We used March 27th to October 3rd to capture all the information available on the breeding populations. While these intervals are large, they again capture the regional dynamics (Figure 2.3B); a smaller subset of the dataset corresponding to the maximum of each peak (and with equal sampling effort across years) is highly correlated with the full dataset (see Appendix A.1.2 below).

It is important to note that intense sampling does not necessarily correspond to high butterfly counts. As a case in point, the mean relative population size index of the monarchs in the south is lower in the summer compared to spring and fall (Figure 2.3B), even though the number of samples are much higher in

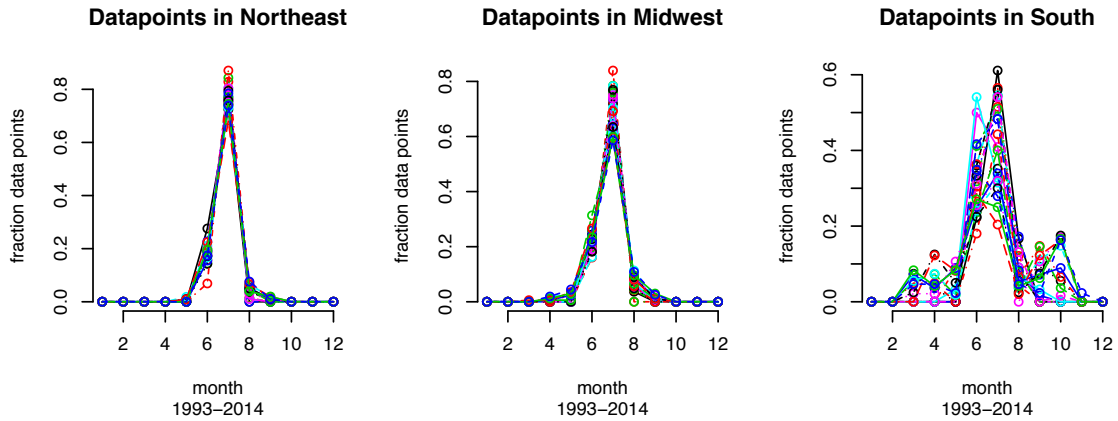


Figure A.2: Fraction of data points taken in each month, out of the total number of data points in a given year. Each colored line represents a year.

the summer than either season. Below we address potential issues with varying sampling intensity.

A.1.2 Moving average over large spatial and temporal scale:

Will varying intensity cause bias in moving average?

NABA data points are collected in various locations throughout the USA, with different years of coverage. Furthermore, we see varying sampling intensity within a year. Not surprisingly, we see no obvious population dynamics pattern at fine spatial and temporal scales in the dataset. In order to focus on the appropriate scale that reflects continental population dynamics, we use a moving average (*i.e.*, kernel estimation using uniform function) over 7-day windows. For each observed count within a region, let i be the day of year, and y_i the observed number of monarchs per party hour. Then, the averaged abundance

assigned to day j for the specified region is

$$\bar{y}_j = \frac{1}{n_j} \left(\sum_{i=j-3}^{j+3} y_i \right) \quad (\text{A.1})$$

where n_j is the number of counts that occurred during the 7-day window. If there are several counts on one day, they are both included in the sum. Conversely, a day without any counts within the 7-day window is assigned value 0.

Varying sampling intensity may bias our index, because clustered missing data results in 0, and therefore lowers the index compared to widely sampled years. For example, Figure A.3 shows the fraction of days in NE and MW where there was at least one data point within each 7-day window; the number of samples increases over time. This varying sampling intensity could bias our results, leading to non-decreasing population index over years. We do not believe this is the case for Spring South, where the population index is decreasing over time; any increase in sampling effort over time would counteract the observed decline. The concern lies in Midwest and Northeast, however, where we see a largely stable population index across years despite decreasing abundance in Mexico. We therefore focus on these two regions for the rest of Appendix A.1.

To assess this potential bias, we constructed a truncated dataset for each region where the averaged days consistently included a count, across all 22 years; that is, we focused on days where $n_j > 0$ across all years (See Figure A.4 for corresponding dates). We summed the indices from these days and compared them to the total Midwest and Northeast population indices derived by our methods. This reduced the dataset to samples taken from June 13th to Aug 1st. Importantly, this truncated index is not impacted by varying sampling inten-

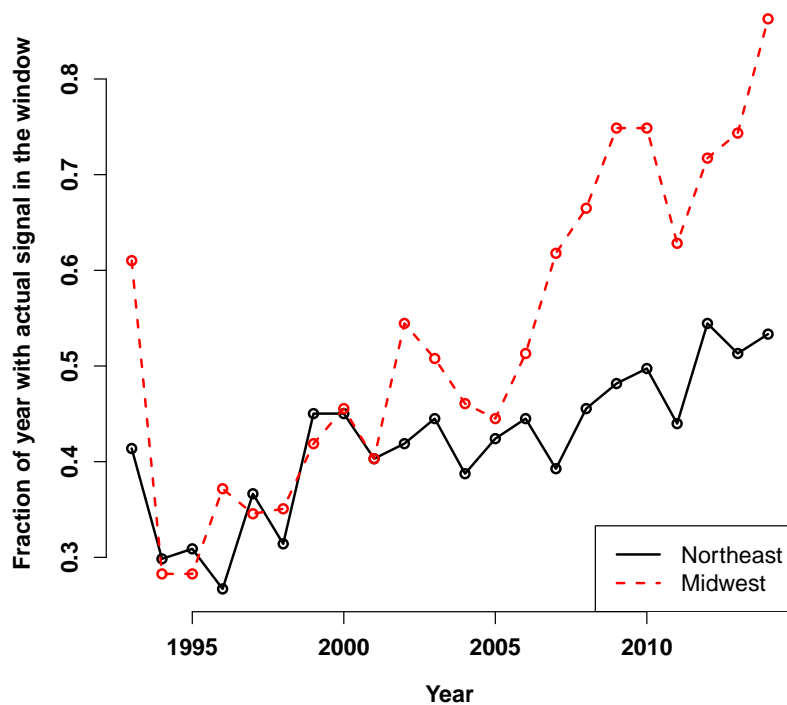


Figure A.3: Population index for a given day in a year is calculated by the average over a 7-day window centered around that day. For each year, we calculated the fraction of the year where there was at least one data point in the 7-day window. Northeast and Midwest used separate data, so the fractions were calculated separately.

sity across years because sampling intensity has been fixed (no days without counts). Our complete yearly index was highly correlated with this truncated index ($n = 22$, Midwest Pearson's $r = 0.88$, $p < 0.001$; Northeast Pearson's $r = 0.94$, $p < 0.001$; Figure A.5). Furthermore, analyses of linkages between regions and declines were qualitatively the same if we used the yearly index or the truncated index (data provided in Table A.1). We therefore conclude that varying sampling intensity across years is not affecting the population indices. Accordingly, to utilize the most available information, we include the complete index from March through October for the main analyses.

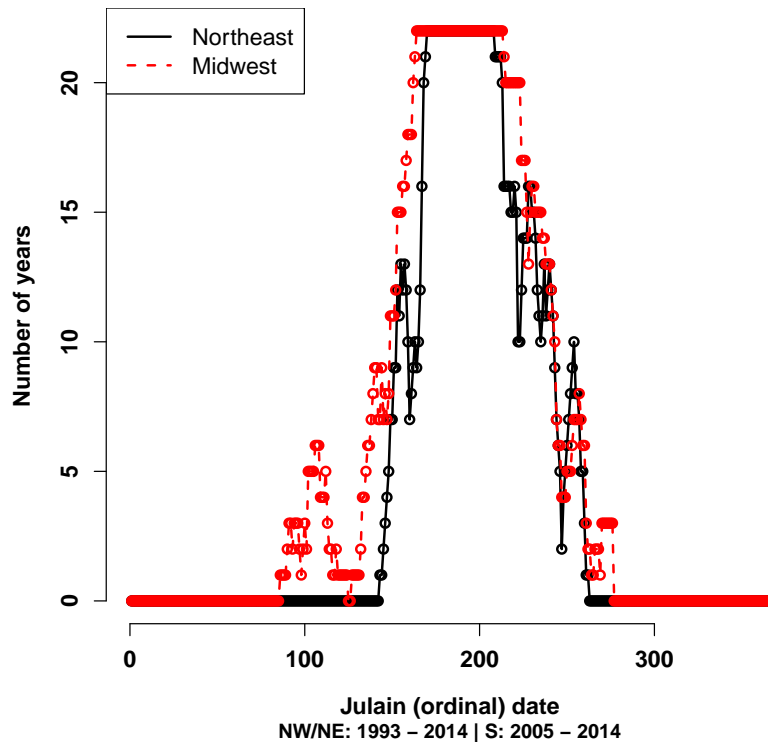


Figure A.4: The number of years with a count in the 7-day window for each date.

A.1.3 Census of early season butterflies

To address the potential for missing data early in the season, we plotted the yearly counts for the Midwest and Northeast to ensure that censuses captured a temporal increase in butterfly abundance in late spring. Namely, we were concerned that scarce sampling in some years could have missed some of the early migrating butterflies. In order to check that the incoming butterflies are all taken into account, we plotted the raw counts (*i.e.* before smoothing via moving average) for the Midwest and Northeast (Figure A.6). Throughout the panels, the seasonal data sets consistently begin with a low count (≈ 0 monarchs/h) early in the breeding season, and the values typically increase over time. This suggests

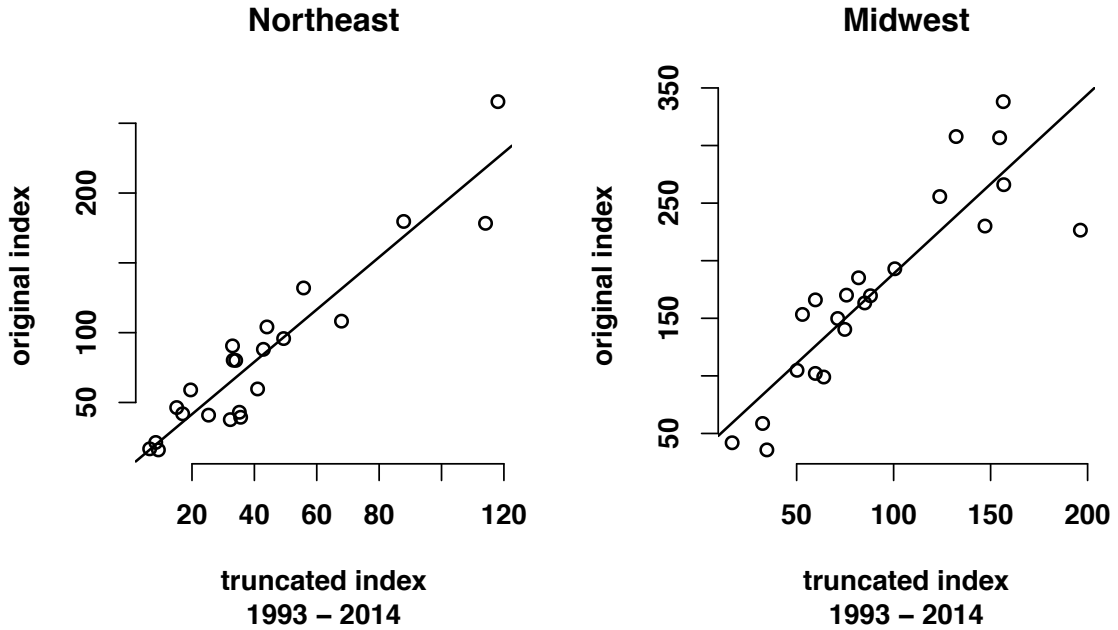


Figure A.5: Correlation between original population index (used in the main analyses) and the truncated population index for Northeast and Midwest. Truncated population index was constructed from a truncated dataset for each region, where the averaged days consistently included a count, across all 22 years (*i.e.* dates with the *Number of years* = 22 in Figure A.4).

that counts began each year early enough to capture the timing of monarch arrival (which is somewhat variable across years). Given the consistent sampling coverage within the time of high monarch abundance each year, we are confident that our indices capture both the migrants and the breeding populations in Midwest and Northeast.

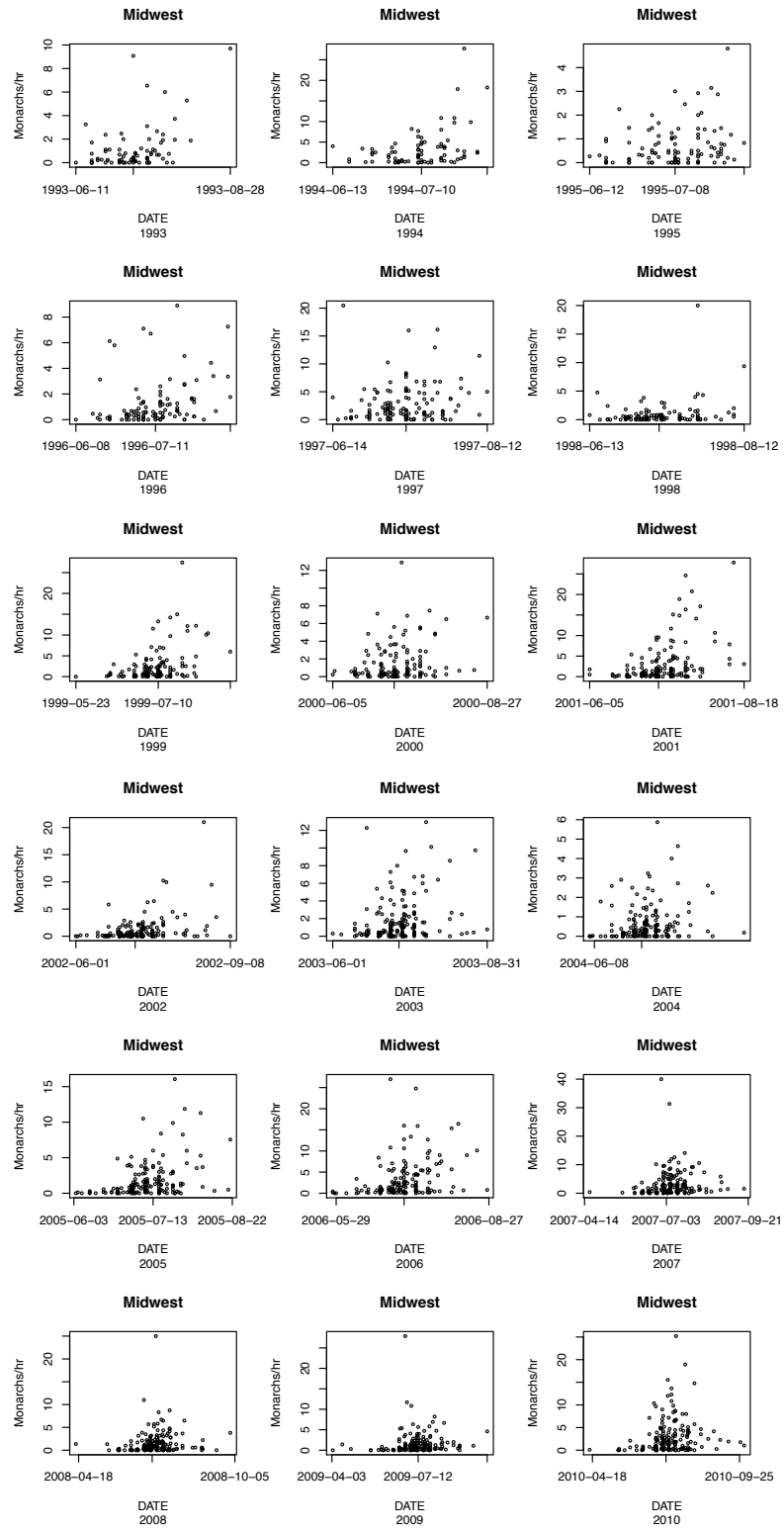
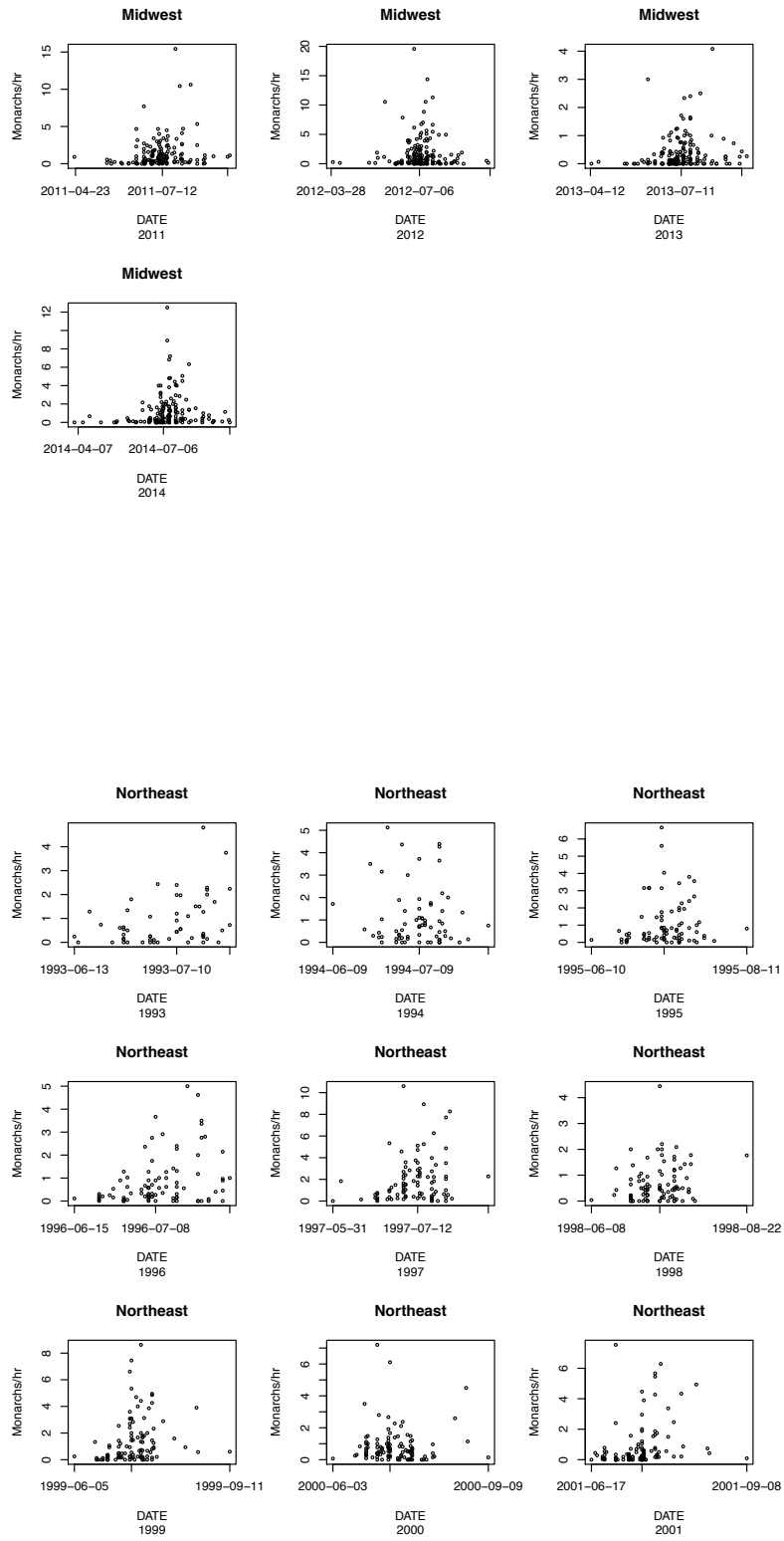
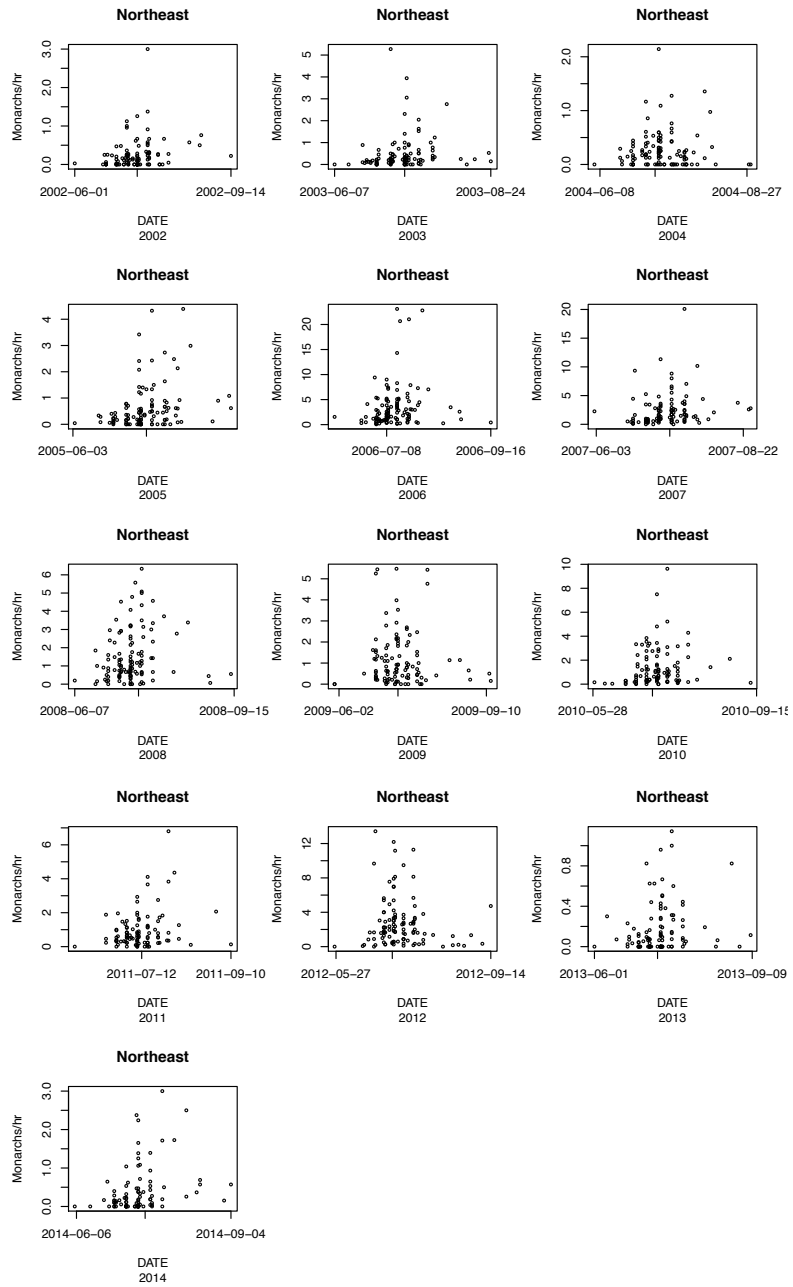


Figure A.6: Raw data counts (before smoothing via moving average) for the Midwest and Northeast, showing the first data point of the year for each region. Continues in next pages.





A.1.4 Are their biases in monarch censuses due to varying party hours?

A potential problem with citizen science datasets is variation in survey effort and its non-linear effect on counts [148]. As indicated in Section 2.3, each NABA count was normalized by dividing the number of observed monarchs by the party hours [16,32,149]. In some areas of citizen science analysis, as with Christmas bird counts, additional statistical methods have been used to account for potential spatial and temporal effort biases [8, 148]. For example, the number of organisms found may saturate with observation hours. These methods are used to correct for the saturating nature of count data with respect to hours spent. This bias would only appear when effort values are particularly high. Figure A.7 shows representative graphs (from year 1997 and 2012) of how the number of observed monarchs changes with party hours for the count in both Northeast and Midwest. Specifically, we focused on July (the most intensely sampled month) under the assumption that the population size is more or less the same within a region over a month. We do not see a saturating relationship between sampling effort and butterfly observations. Similar results hold for other years.

To further test our dataset, we transformed our party hours to see if it affected the analyses [148, 150]. We re-ran our analyses using counts standardized by the square root of party hours (a simple method of transformation suggested by [150]), and the patterns remain the same. Using $\sqrt{\text{effort}}$ and recalculating the annual indices, comparisons of the transformed to the original indices yielded R^2 values of 0.95 to 0.99 (with the intercepts not being significantly different from zero). Thus, given the linear relationship between effort

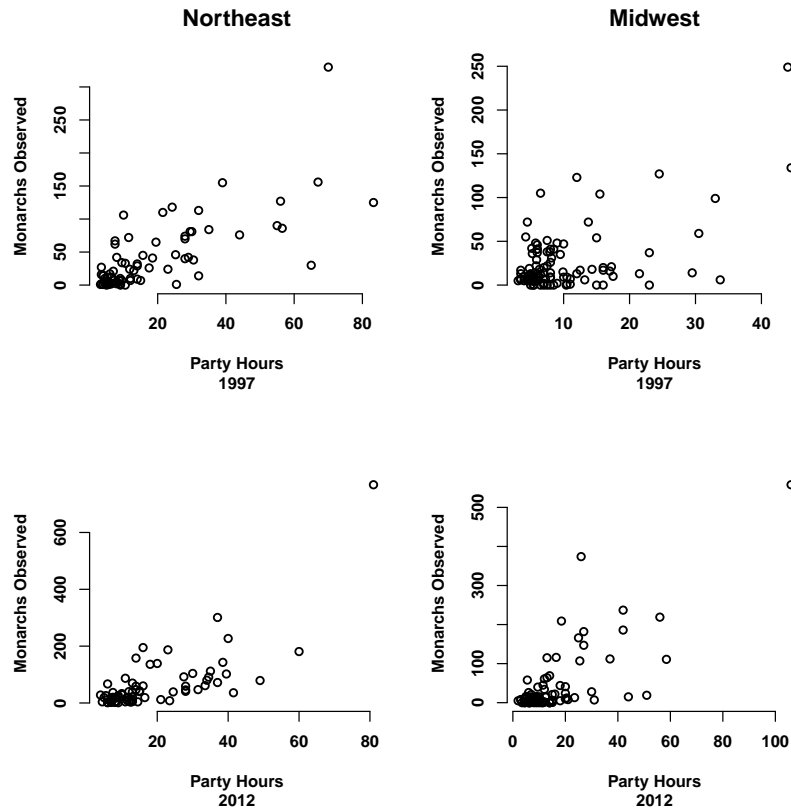


Figure A.7: Number of monarchs observed with varying party hours (sampling effort) in Northeast (left column) and Midwest (right column), from year 1997 (top row) and 2012 (bottom row).

and monarch counts, the lack of an effect of further transforming the data, and to align with previous analyses [16, 32, 149], we maintain using the count data standardized by party hours.

A.1.5 Do census points cluster more over the years?

If patches of suitable monarch habitat are disappearing (in particular, due to loss of milkweed), then it is conceivable that NABA citizen science counts in later years were done in the few remaining patches, leading to an upward bias

in population indices and masking a decline in the total regional population. To test for this possibility, we asked if NABA count locations show increasing spatial clustering in later years, which would occur if the counts are being done in a smaller number of locations. We used Ripley's K function [146], a standard measure of clustering in spatial statistics, to quantify the clustering of count locations in each year. Ripley's K function calculates the number of neighboring data points present within concentric circles around a focal sampling location, as the radius/distance increases. These values are averaged over all the sampling locations present in the data set for that year. We used Mercator projection (`mapproj` library in **R** [151]) of sampling locations (given as latitude and longitude in the NABA data set) and Ripley's isotropic correction estimate of K (`spatstat` library in **R** [152]).

The patterns are consistent across years in both Northeast and Midwest regions (Figure A.8, different colors and lines correspond to different years), and do not differ substantially across years. More importantly, we do not see any trends in the K function with respect to year (Figure A.9) at any spatial scale. This implies that the count locations do not cluster more over time. We conclude that geographic clustering of monarch sampling is not increasing over time, and is therefore not a source of temporal bias in the NABA dataset.

A.2 Statistical analyses to examine temporal change in the relationship between stages of the annual migratory cycle.

In the following series of analyses, we investigated the relationship between population size at one stage of the annual migratory cycle (DONOR region,

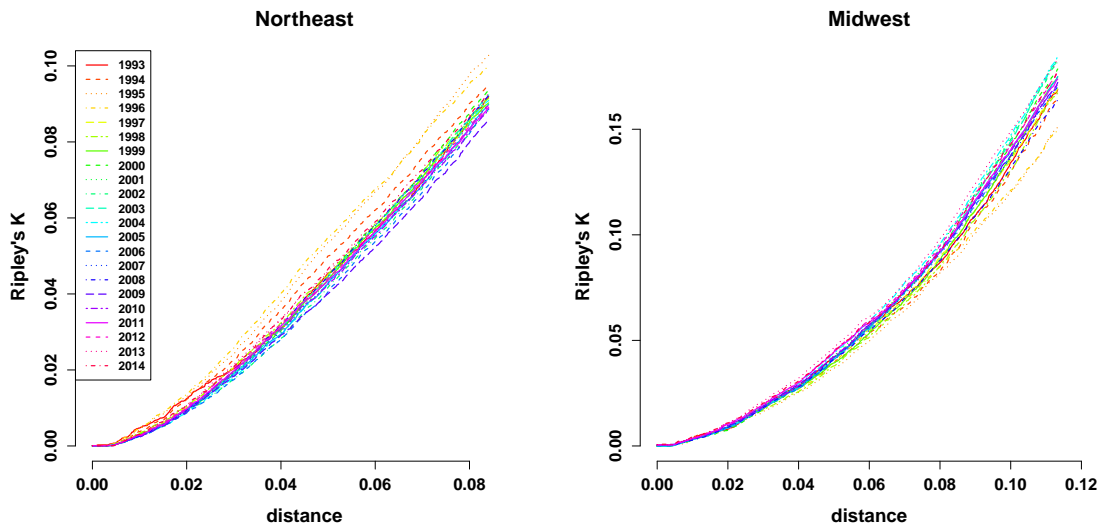


Figure A.8: Ripley's K function for the spatial locations of NABA population counts in each year. The different colors and lines correspond to different years.

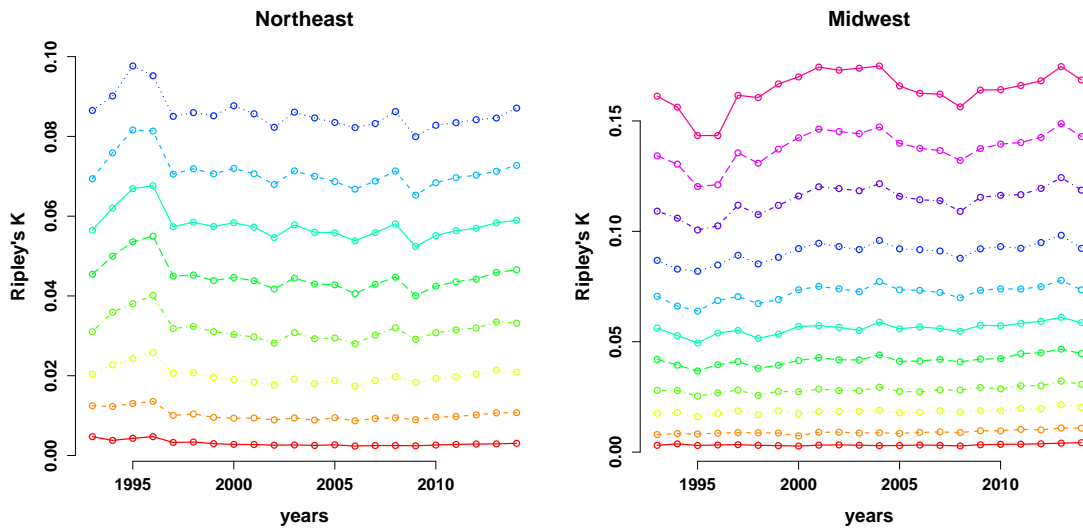


Figure A.9: Ripley's K function as a function of year for the Northeast and Midwest regions. The different colors and lines correspond to distances 0.01, 0.02, ..., 0.11 from bottom to top.

independent variable) and the next time step (RECIPIENT region, dependent variable). To address temporal change in these relationships, we considered YEAR and the DONOR \times YEAR interaction as additional covariates. YEAR was entered as a numerical covariate because we are interested in directional trends over time. Because the change in YEAR is small relative to its mean, DONOR and DONOR \times YEAR are strongly collinear. To remove this, we centered YEAR about its mean. We considered the following models:

- Model 1: RECIPIENT \sim DONOR + YEAR + DONOR \times YEAR
- Model 2: RECIPIENT \sim DONOR + DONOR \times YEAR
- Model 3: RECIPIENT \sim DONOR
- Model 4: RECIPIENT \sim DONOR \times YEAR
- Model 5: RECIPIENT \sim DONOR + YEAR
- Model 6: RECIPIENT \sim YEAR + DONOR \times YEAR
- Model 7: RECIPIENT \sim YEAR

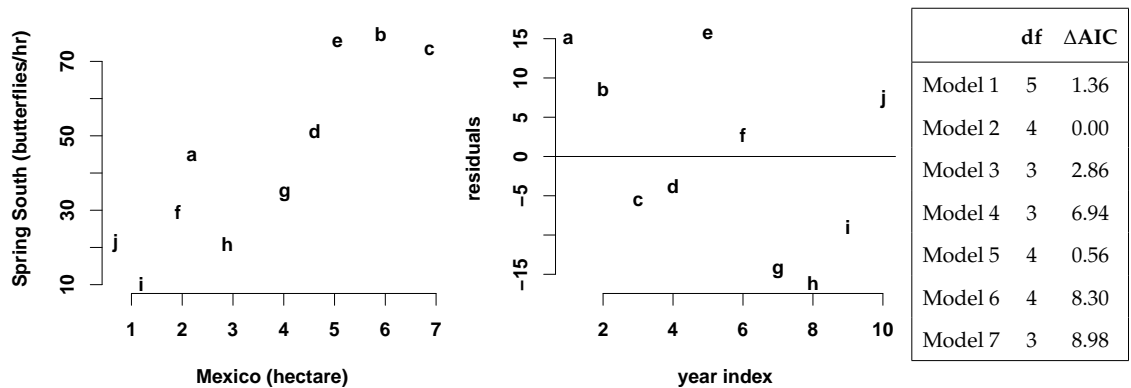
For each DONOR-RECIPIENT pair, we plot the relationship between regions or between region and year, with the letters on the plot indicating chronological order (a = first year of census, *etc.*). The table next to the graph shows the Δ AIC value for each model, relative to the lowest AIC value.

We performed stepwise model selection based on AIC values [96], and also *F*-tests to evaluate the statistical significance of terms by a comparison of nested models with and without the term. We performed both backward and forward selection to check for consistency between these approaches. In backward selection, we started with the full model (Model 1) and sequentially eliminated the

non-significant term (if any such exist) that resulted in the largest improvement in AIC, stopping when all terms are significant. In forward selection, we started with either DONOR (Model 3) or YEAR (Model 7), whichever had the stronger univariate correlation with the dependent variable, and sequentially added the term that gave the largest improvement in AIC, stopping when the added term was not statistically significant.

The table below each plot summarizes backward and forward model selection. The entries under **Model Comparison** in each row show the significance of that covariate, based on an F -test against a model with that term dropped (for Backward selection) or added (for Forward selection). The AIC of the modified model (with a term added or dropped) is also given. If an outlier was detected, the table reflects the analyses after it was removed.

A.2.1 Mexico to Spring South



	Model	AIC	Model comparison		
Backward			Mexico	YEAR	Mexico \times YEAR
1	Mexico + YEAR + Mexico \times YEAR	50.38	AIC=57.32, p=0.03	AIC=49.02, p=0.55	AIC=49.58, p=0.42
2	Mexico + Mexico \times YEAR	49.02	AIC=55.95, p=0.02		AIC=51.88, p=0.07
Forward					
3	Mexico	51.88		AIC=49.58, p=0.09	AIC=49.02, p=0.07
2	Mexico + Mexico \times YEAR	49.02		AIC=50.38, p=0.55	

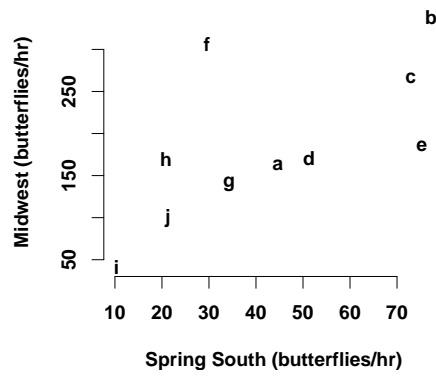
Backward and Forward model selection both lead to Model 2,

$$\text{Spring South} \sim \text{Mexico} + \text{Mexico} \times \text{YEAR} \quad (\text{A.2})$$

AIC favors the addition of Mexico \times YEAR (Model 2), but the F -test shows that this term is only marginal ($p = 0.07$) and the residuals from Model 3 (plotted above) do not show any visible pattern over time.

Conclusion: The overwintering populations in Mexico predict Spring South populations. There is marginal evidence for a small decrease in the slope of this relationship over time.

A.2.2 Spring South to Midwest



	df	Δ AIC
Model 1	5	3.32
Model 2	4	1.43
Model 3	3	0.00
Model 4	3	0.70
Model 5	4	1.35
Model 6	4	2.40
Model 7	3	0.54

	Model	AIC	Model comparison		
Backward			Spring South	YEAR	Spring South \times YEAR
1	Spring South + YEAR + Spring South \times YEAR	91.2	AIC=90.28, p=0.44	AIC=89.30, p=0.81	AIC=89.22, p=0.91
5	Spring South + YEAR	89.22	AIC=88.42, p=0.38	AIC=87.87, p=0.51	
3	<i>Spring South</i>	87.87	AIC=91.30, p=0.04		
Forward					
3	<i>Spring South</i>	87.87		AIC=89.22, p=0.51	AIC=89.30, p=0.54

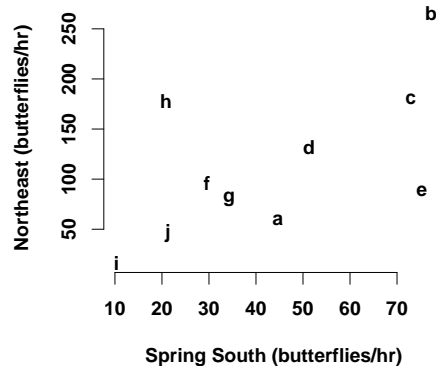
Forward selection, Backward selection, and AIC all lead to Model 3,

$$\text{Midwest} \sim \text{Spring South} \quad (\text{A.3})$$

with the donor region as the only significant predictor ($p < 0.05$).

Conclusion: Monarch populations in Spring South significantly predict those in the Midwest. There is no evidence for a temporal trend in this relationship.

A.2.3 Spring South to Northeast



	df	Δ AIC
Model 1	5	2.29
Model 2	4	1.35
Model 3	3	0.00
Model 4	3	0.24
Model 5	4	1.98
Model 6	4	1.70
Model 7	3	1.87

	Model	AIC	Model comparison		
Backward			Spring South	YEAR	Spring South \times YEAR
1	Spring South + YEAR + Spring South \times YEAR	87.03	AIC=86.44, $p=0.38$	AIC=86.09, $p=0.44$	AIC=86.72, $p=0.33$
2	Spring South + Spring South \times YEAR	86.09	AIC=84.98, $p=0.45$		AIC=84.74, $p=0.52$
3	<i>Spring South</i>	84.74	AIC=87.35, $p=0.06$		
Forward					
3	<i>Spring South</i>	84.74		AIC=86.72, $p=0.92$	AIC=86.09, $p=0.52$

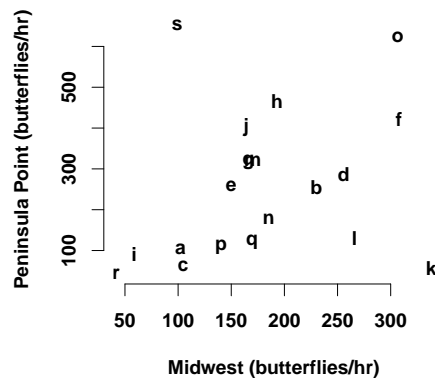
Forward selection, Backward selection, and AIC all lead to Model 3,

$$\text{Northeast} \sim \text{Spring South} \quad (\text{A.4})$$

with the donor region as the marginally significant predictor ($p = 0.06$).

Conclusion: Monarch populations in Spring South marginally predict that in the Northeast. There is no evidence for a temporal trend in this relationship.

A.2.4 Midwest to Peninsula Point



	df	Δ AIC
Model 1	5	3.87
Model 2	4	1.99
Model 3	3	0.00
Model 4	3	4.46
Model 5	4	1.93
Model 6	4	6.05
Model 7	3	4.37

	Model	AIC	Model comparison		
			Midwest	YEAR	Midwest \times YEAR
Backward					
1	Midwest + YEAR + Midwest \times YEAR	186.29	AIC=188.47, p=0.08	AIC=184.40, p=0.77	AIC=184.35, p=0.83
5	Midwest + YEAR	184.35	AIC=186.78, p=0.06	AIC=182.41, p=0.82	
3	<i>Midwest</i>	182.41	AIC=184.87, p<0.05		
Forward					
3	<i>Midwest</i>	182.41		AIC=184.35, p=0.82	AIC=184.40, p=0.91

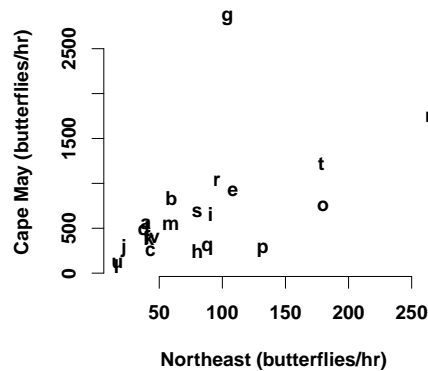
Forward selection, Backward selection, and AIC all lead to Model 3,

$$\text{Peninsula Point} \sim \text{Midwest} \quad (\text{A.5})$$

With an outlier (2014: Midwest = 98.8, Peninsula Point = 652.8; Studentized residual > 3.1) included, Midwest is not a significant predictor ($p = 0.26$). However with an outlier removed, Midwest becomes a significant predictor ($p < 0.05$). The model selection table reflects the analysis after the outlier was removed.

Conclusion: Without an outlier, Midwest monarch populations significantly predict fall migrants through Peninsula Point, and we do not see any signatures of change in the slope over time.

A.2.5 Northeast to Cape May



	df	Δ AIC
Model 1	5	2.55
Model 2	4	1.24
Model 3	3	0.00
Model 4	3	18.60
Model 5	4	0.62
Model 6	4	16.45
Model 7	3	21.21

	Model	AIC	Model comparison		
Backward			Northeast	YEAR	Northeast \times YEAR
1	Northeast + YEAR + Northeast \times YEAR	236.29	AIC=250.20, $p < 0.001$	AIC=234.98, $p = 0.46$	AIC=234.36, $p = 0.81$
5	Northeast + YEAR	234.36	AIC=254.96, $p < 0.0001$	AIC=233.74, $p = 0.28$	
3	<i>Northeast</i>	233.74	AIC=253.10, $p < 0.0001$		
Forward					
3	<i>Northeast</i>	233.74		AIC=234.36, $p = 0.28$	AIC=234.98, $p = 0.43$

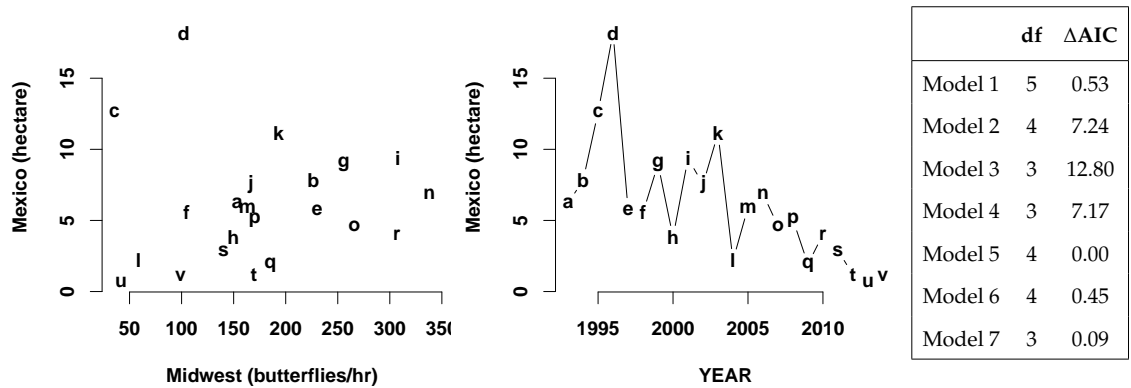
Without an outlier (1999: Northeast = 104.1, Cape May = 2849.2; Studentized residual = 8.420), Forward selection, Backward selection, and AIC all lead to Model 3,

$$\text{Cape May} \sim \text{Northeast} \quad (\text{A.6})$$

When the outlier is included, however, we see marginally significant effect ($p = 0.09$) of the interaction term (Model 2) with negative slope. The model selection table reflects the analysis after the outlier was removed.

Conclusion: Northeast monarch populations predict Cape May, and the weak evidence for a temporal trend was due to a single outlier.

A.2.6 Midwest to Mexico



	Model	AIC	Model comparison		
Backward			Midwest	YEAR	Midwest × YEAR
1	Midwest + YEAR + Midwest × YEAR	39.56	AIC=39.49, p=0.22	AIC=46.27, p<0.01	AIC=39.04, p=0.28
5	Midwest + YEAR	39.04	AIC=39.12, p=0.19	AIC=51.84, p<0.001	
7	YEAR	39.12		AIC=51.21, p<0.001	
Forward					
7	YEAR	39.12	AIC=39.04, p=0.19		AIC=39.49, p=0.24

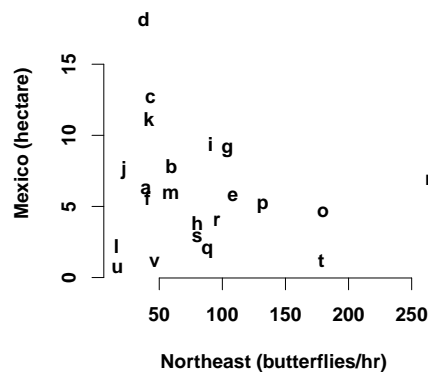
Forward and Backward model selection both lead to Model 7,

$$\text{Mexico} \sim \text{YEAR} \quad (\text{A.7})$$

AIC favors the addition of Midwest (Model 5), but this term is not significant ($p = 0.19$). We had the same result with and without an outlier (1996: Midwest = 102.15, Mexico = 18.19; Studentized residual = 3.93). The model selection table reflects the analysis after the outlier was removed.

Conclusion: YEAR is an important predictor of the Mexican overwintering population, and neither Midwest nor the interaction shows statistical significance.

A.2.7 Northeast to Mexico



	df	Δ AIC
Model 1	5	3.63
Model 2	4	7.93
Model 3	3	13.37
Model 4	3	6.75
Model 5	4	1.93
Model 6	4	1.64
Model 7	3	0.00

	Model	AIC	Model comparison		
			Northeast	YEAR	Northeast \times YEAR
Backward					
1	Northeast + YEAR + Northeast \times YEAR	56.05	AIC=54.06, p=0.91	AIC=60.35, p=0.03	AIC=54.35, p=0.62
6	YEAR + Northeast \times YEAR	54.06		AIC=59.16, p=0.01	AIC=52.42, p=0.58
7	YEAR	52.42		AIC=64.26, p<0.001	
Forward					
7	YEAR	52.42	AIC=54.35, p=0.81		AIC=54.06, p=0.58

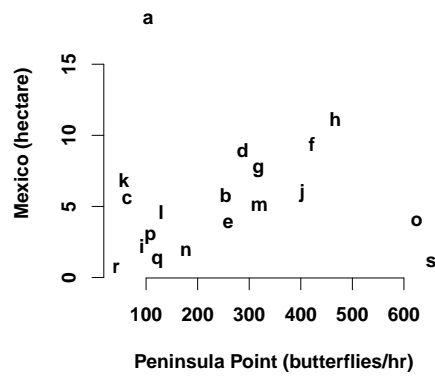
Forward selection, Backward selection, and AIC all lead to Model 7,

$$\text{Mexico} \sim \text{YEAR} \quad (\text{A.8})$$

where YEAR is the only significant predictor ($p < 0.001$).

Conclusion: YEAR is an important predictor of the Mexican overwintering population, and neither Northeast nor the interaction shows statistical significance.

A.2.8 Peninsula Point to Mexico



	df	Δ AIC
Model 1	5	1.49
Model 2	4	0.00
Model 3	3	16.48
Model 4	3	9.55
Model 5	4	5.06
Model 6	4	8.29
Model 7	3	6.70

	Model	AIC	Model comparison		
			Peninsula Point	YEAR	Peninsula Point \times YEAR
Backward					
1	Pen Point + YEAR + Pen Point \times YEAR	26.63	AIC=33.43, p=0.01	AIC=25.14, p=0.54	AIC=30.20, p=0.04
2	Pen Point + Pen Point \times YEAR	25.14	AIC=34.69, p<0.01		AIC=41.62, p<0.001
Forward					
3	Pen Point	41.62		AIC=30.2, p<0.001	AIC=25.14, p<0.001
2	Pen Point + Pen Point \times YEAR	25.14		AIC=26.63, p=0.54	

Including the outlier, Forward selection, Backward selection, and AIC all lead to Model 7,

$$\text{Mexico} \sim \text{YEAR} \quad (\text{A.9})$$

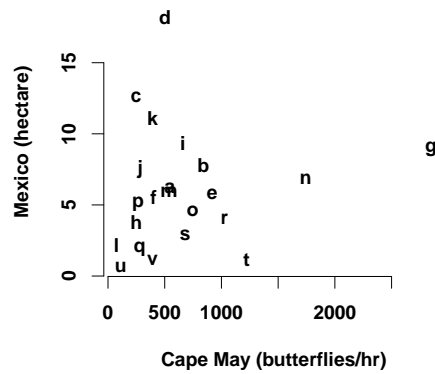
However when an outlier (1996: Peninsula Point = 104.4, Mexico = 18.19; Studentized residual = 4.41) is removed, Forward selection, Backward selection, and AIC all lead to Model 2,

$$\text{Mexico} \sim \text{Pen Point} + \text{Pen Point} \times \text{YEAR} \quad (\text{A.10})$$

with a negative coefficient for the interaction term ($p < 0.001$) and significant donor region ($p < 0.01$). The model selection table reflects the analysis after the outlier was removed.

Conclusion: With an outlier remove, Peninsula Point predicts Mexico and the relationship changes over time (*i.e.* the slope decreases over time). This effect cannot be explained by declining milkweed.

A.2.9 Cape May to Mexico



	df	ΔAIC
Model 1	5	3.34
Model 2	4	9.35
Model 3	3	13.50
Model 4	3	7.35
Model 5	4	1.75
Model 6	4	1.81
Model 7	3	0.00

	Model	AIC	Model comparison		
			Cape May	YEAR	Cape May × YEAR
Backward					
1	Cape May + YEAR + Cape May × YEAR	55.76	AIC=54.23, p=0.54	AIC=61.76, p=0.01	AIC=54.17, p=0.57
5	Cape May + YEAR	54.17	AIC=52.42, p=0.65	AIC=65.92, p<0.001	
7	YEAR	52.42		AIC=64.26, p<0.001	
Forward					
7	YEAR	52.42	AIC=54.17, p=0.65		AIC=54.23, p=0.69

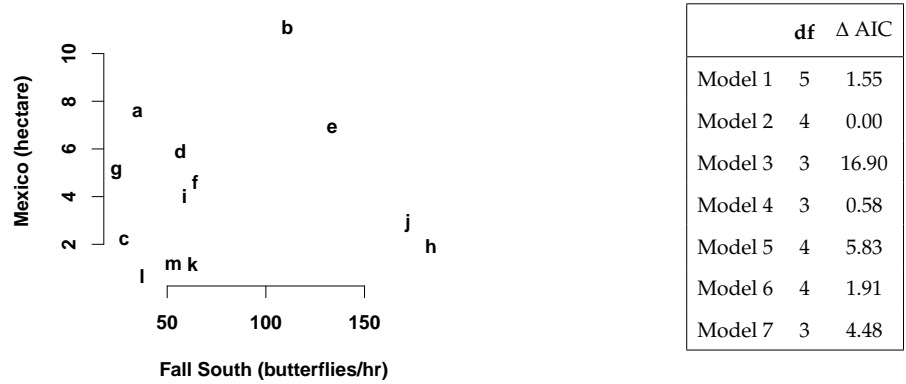
Forward selection, Backward selection, and AIC all lead to Model 7,

$$\text{Mexico} \sim \text{YEAR} \quad (\text{A.11})$$

where YEAR is the only significant predictor ($p < 0.001$).

Conclusion: YEAR is an important predictor of the Mexican overwintering population, and neither Cape May nor the interaction shows statistical significance.

A.2.10 Fall South to Mexico



	Model	AIC	Model comparison		
			Fall South	YEAR	Fall South × YEAR
Backward					
1	Fall South + YEAR + Fall South × YEAR	16.56	AIC=16.92, p=0.21	AIC=15.01, p=0.59	AIC=20.84, p<0.05
2	Fall South + Fall South × YEAR	15.01	AIC=15.59, p=0.17		AIC=31.90, p<0.001
4	Fall South × YEAR	15.59			AIC=29.99, p<0.001
Forward					
7	YEAR	19.49	AIC=20.84, p=0.49		AIC=16.92, p=0.07
6	YEAR + Fall South × YEAR	16.92	AIC=16.56, p=0.21		

AIC leads to Model 2, but backward selection shows that Fall South is not significant under the F -test. Forward selection shows that the interaction term is marginally significant even when YEAR is included in the model. Taken together, we infer that

$$\text{Mexico} \sim \text{Fall South} \times \text{YEAR} \quad (\text{A.12})$$

is the best model.

Conclusion: Interaction term is an important predictor of the Mexican overwintering population, and neither Fall South nor YEAR shows statistical significance.

APPENDIX B
SUPPLEMENTARY INFORMATION TO CHAPTER 3

B.1 Experimental materials and methods

B.1.1 Cloning and assessing the stability of pCM62-GFP- *Acetobacter tropicalis*

Genes were amplified by PCR and cloned using enzymes from New England Biolabs as per the manufacturer's recommendations. All products were amplified using Phusion polymerase, cut with restriction enzymes as indicated below, and ligated with T4 DNA ligase to the plasmid pCM62 [153] (prepared by cutting with the same enzymes as product to be cloned) such that the Plac promoter would drive expression of the cloned gene. GFP gene was amplified from pMQ80 template [154] with forward [5'-GCTTGCATGCCTGCAGACTAGTC-3'] and reverse [5'-TAAAAAGCTTCAAGCCGTCAATTGTCTGATTCGTTACC-3'] primers, with an annealing temperature of 59 °C, extension time of 1 min, and product cloned with PstI and HindIII. Ligated products were introduced into *Acetobacter tropicalis* by conjugation as described [155]. Briefly, bacteria were cultured overnight in potato medium and cells from 0.5 ml of culture harvested by centrifugation. Cells of donor and recipient were washed separately in sterile growth medium twice, re-suspended in a final volume of 50 µl potato medium, then mixed together and transferred to a fresh potato medium plate. After incubation at 30 °C for 16 h, cells were harvested and plated onto YPG medium (0.5 % yeast extract, 0.5 % peptone, 1 % glycerol, 1.5 % agar) containing 0.2 %

acetic acid and 20 mg l^{-1} chlortetracycline. Colonies that appeared after 48 h of incubation were sub-cultured on potato medium supplemented with 20 mg l^{-1} chlortetracycline.

We assessed the stability of pCM62-GFP in *A. tropicalis* by 2 different methods. First, we assessed the *in vitro* stability of GFP expression in the absence of antibiotic selection. If the plasmid were unstable, the bacteria would lose GFP expression as the tetracycline resistance is unnecessary in the absence of antibiotic selection. *A. tropicalis* with pCM62-GFP were serially passaged in MRS without tetracycline. Microbial cultures underwent daily 1:1000 dilution over 5 d. At the end of 5 d, we manually counted the number of *A. tropicalis* under fluorescent microscope, with and without fluorescence. Across samples, $(90.44 \pm 0.07)\%$ of *A. tropicalis* cells ($n = 5$ independent serial passages) expressed fluorescence, indicating that the bacteria retain pCM62-GFP *in vitro*.

Second, we assessed the *in vivo* stability of *A. tropicalis* in retaining pCM62 plasmid. Axenic flies were mono-associated with pCM62-GFP-*A. tropicalis* for 15 d, and fly homogenates were plated on MRS media with and without tetracycline. Number of colonies were compared between the two plates to assess the retention of pCM62-GFP. If the bacteria lose the plasmid, then they lose the tetracycline resistance. We therefore expect to see more bacteria on the plates without tetracycline if the plasmid were unstable. We obtained equal number of colonies on plates with and without tetracycline (Figure B.1), indicating that the bacteria retain pCM62-GFP *in vivo*. Taken together, these results indicate that the bacteria retain the plasmid even in association with the *Drosophila* host, and GFP is stably present even in the absence of antibiotic selection.

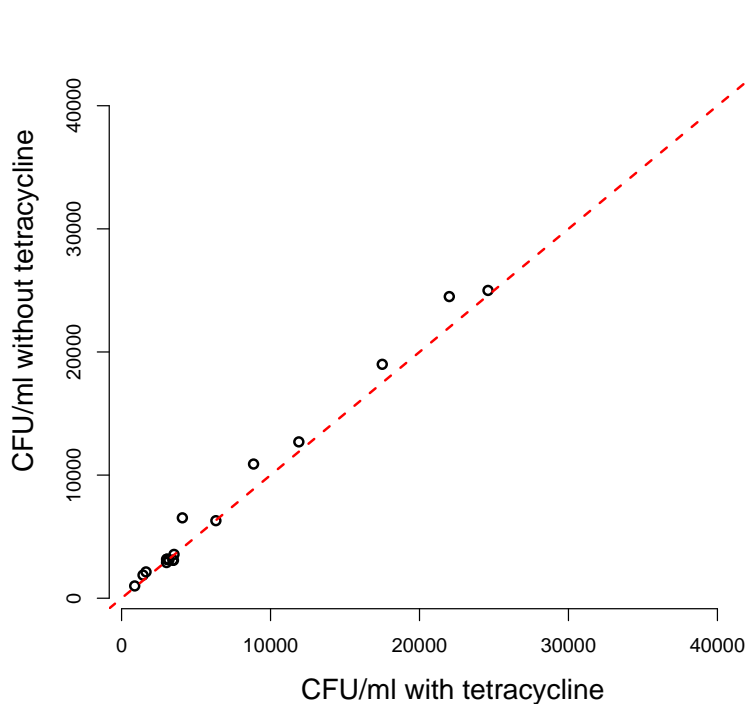


Figure B.1: Density of *A. tropicalis* colonies (CFU/ml) from fly homogenates plated on mMRS media with and without tetracycline. Axenic flies were mono-associated with pCM62-GFP-*A. tropicalis* for 15 d to assess the *in vivo* stability of pCM62 plasmid. Red dashed line: 1-to-1 line.

B.1.2 Assessing the quality of the automated counting method

The number of particles (microsphere and bacteria) recovered from feces and in inoculum were quantified using the open-source image analysis software CellProfiler [106] and supplemented by manual counting. CellProfiler allows automated counting by discriminating particles based on size, shape, and color. Parameters for particle detections were determined by comparing automated and manual counts over several images. Parameters were chosen such that the particles were identified appropriately and matched visual inspection. To determine the quality of the automated counts, we randomly chose 10 additional images

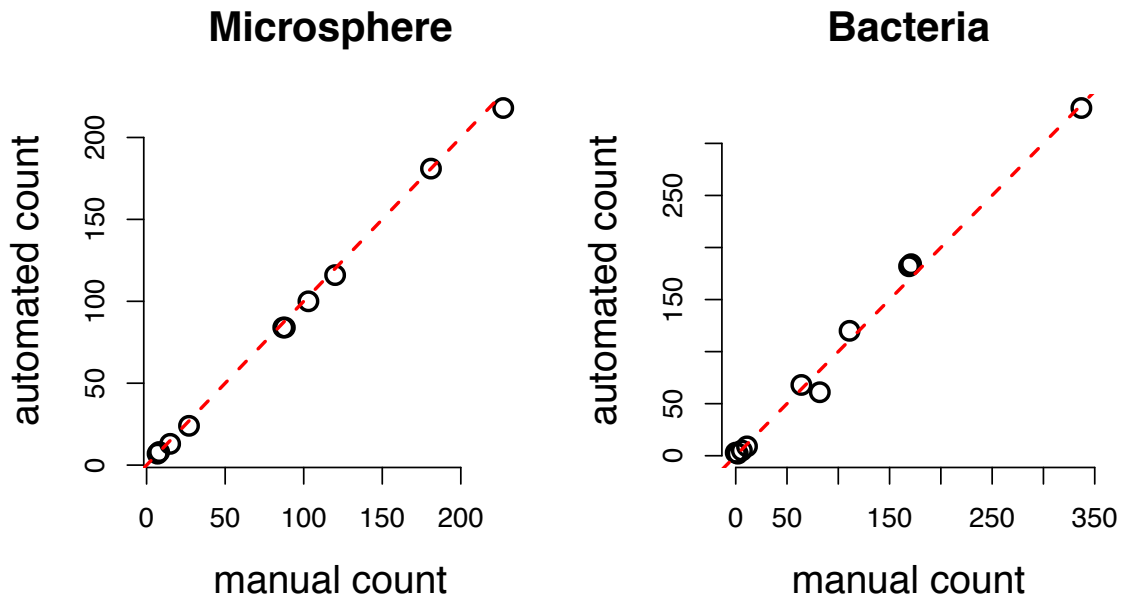


Figure B.2: Consistency between manual and automated counts of microspheres and bacteria. Ten microscopy images were chosen at random and their number of microsphere and bacteria were counted manually and automatically (using CellProfiler). Red dashed line: 1-to-1 line.

and quantified the particle abundance by both methods. We saw consistency between the two methods, for both microspheres and GFP-labeled *A. tropicalis* (Figure B.2).

B.1.3 Estimating proportions of *A. tropicalis* retained by, egested out of, and lost in the fly

Ingested bacteria only have three mutually exclusive fates: 1. Intact bacteria are egested out; 2. Intact bacteria are retained in the host over the experiment; or 3. Bacteria are lost due to lysis. To clarify our calculations, we will walk through the procedure using data values from one of the three replicate experiments in *Microbial Fate Experiment* (first row of Axenic fly treatment, Table 3.1). We

calculate proportion of bacteria egested in both *Egestion Time Experiment* and *Microbial Fate Experiment*.

1. The first step is to quantify the number of cells ingested by the fly relative to the number of ingested microspheres. Assuming that flies ingested cells and microspheres indiscriminately, this ratio equals the ratio of cells to microspheres in the inoculum, which was measured in each replicate experiment (0.289 cells/microsphere in this example).

$$\begin{aligned} \frac{\# \text{ cells ingested}}{\# \text{ microspheres ingested}} &= \frac{\# \text{ cells in inoculum}}{\# \text{ microspheres in inoculum}} \\ &= 0.289 \frac{\text{cells ingested}}{\text{microspheres ingested}} \end{aligned} \quad (\text{B.1})$$

2. The second step is to quantify the number of cells egested by the fly over 5 h relative to the number of egested microspheres. Assuming that cells and microspheres were recovered indiscriminately from the feces, this ratio equals the number of cells recovered from fly feces relative to the number of microspheres recovered over 5 h.

$$\begin{aligned} \frac{\# \text{ cells egested}}{\# \text{ microspheres egested}} &= \frac{\# \text{ cells recovered from feces}}{\# \text{ microspheres recovered from feces}} \\ &= \frac{3129.421 \text{ cells/fly}}{95\,647.944 \text{ microspheres/fly}} \\ &= 0.0327 \frac{\text{cells}}{\text{microsphere}} \end{aligned} \quad (\text{B.2})$$

3. The third step is to calculate the proportion of bacteria egested. Because microspheres were scarce in our 5–24 h and 24–48 h samples, we assume that the total number of microspheres egested over 5 h equals the total

number of microspheres ingested.

$$\begin{aligned} \text{Proportion of bacteria egested} &= \frac{\# \text{ cells egested}}{\# \text{ cells ingested}} \\ &= \frac{(\# \text{ cells egested})/(\# \text{ microspheres ingested})}{(\# \text{ cells ingested})/(\# \text{ microspheres ingested})} \\ &= \frac{(\# \text{ cells egested})/(\# \text{ microspheres egested})}{(\# \text{ cells ingested})/(\# \text{ microspheres ingested})} \quad (\text{B.3}) \\ &= \frac{0.0327 \text{ cells/microsphere}}{0.289 \text{ cells/microsphere}} \\ &= 0.113 \end{aligned}$$

4. To calculate proportion of bacteria retained in the fly in *Microbial Fate Experiment*, we compare the numbers of bacteria ingested and retained. The number of bacteria ingested is calculated from the number of microspheres ingested, using Equation (B.1). We assume that the number of microspheres ingested equals the number egested over 5 h, because microspheres were scarce in our 5–24 h and 24–48 h samples. Microspheres in feces were counted under a microscope. However, microscopy may only account for a fraction of egested microspheres, as some egested particles are lost under our protocols before microscopy (*e.g.* in the process of washing the vials and pelleting the feces by centrifuge). We therefore need to consider the proportion of particles recovered from feces. In Appendix B.1.4 below, we derive this proportion for each replicate experiment. Using the proportion of particles recovered (0.034 for this example),

we calculate the number of microspheres egested:

$$\begin{aligned}
 \frac{\# \text{ microspheres ingested}}{\text{fly}} &= \frac{\# \text{ microspheres egested}}{\text{fly}} \\
 &= \frac{\# \text{ microspheres recovered from feces/fly}}{\text{Proportion of particles recovered}} \\
 &= \frac{95\,647.944 \text{ microspheres/fly}}{0.034} \\
 &= 2\,813\,175 \frac{\text{microspheres ingested}}{\text{fly}}
 \end{aligned} \tag{B.4}$$

Equation (B.1) then gives us the number of bacteria ingested (813 007.5 cell/fly in this example).

5. Next we estimate the number of cells retained intact in the host. At the end of 5 h, we homogenized the *Passaged* flies and used a spiral plater to estimate the number of *A. tropicalis* CFU per fly. In Appendix B.1.5 below, we derive the conversion factor from number of CFU's (spiral plater) to the number of cells scored by fluorescence microscopy (1 CFU/ml = 2.83 cells/ml). Using this conversion factor,

$$\begin{aligned}
 \frac{\# \text{ cells retained}}{\text{fly}} &= \frac{\# \text{ CFU retained}}{\text{fly}} \times \text{Conversion factor} \\
 &= 25\,011.8 \frac{\text{CFU}}{\text{fly}} \times 2.83 \frac{\text{cells}}{\text{CFU}} \\
 &= 70\,783.39 \frac{\text{cells retained}}{\text{fly}}
 \end{aligned} \tag{B.5}$$

Then using the numbers of cells retained and ingested, we have

$$\begin{aligned}
 \text{Proportion of bacteria retained} &= \frac{\# \text{ cells retained}}{\# \text{ cells ingested}} \\
 &= \frac{70\,783.39 \text{ cells/fly}}{813\,007.5 \text{ cells/fly}} \\
 &= 0.087
 \end{aligned} \tag{B.6}$$

6. Lastly, we calculate the proportion of ingested *A. tropicalis* that are lysed by the end of the experiment.

Proportion of bacteria lysed

$$\begin{aligned}
 &= 1 - (\text{Proportion of bacteria egested}) - (\text{Proportion of bacteria retained}) \\
 &= 1 - 0.113 - 0.087 \\
 &= 0.8
 \end{aligned}
 \tag{B.7}$$

We performed the same calculations for all samples and the results are shown in Table 3.1. Across both Axenic and Gnotobiotic samples, we observed statistically significant proportions of bacteria egested, retained, and lysed (*t*-test against null hypothesis that mean = 0. Mean \pm s.e.m. = 0.25 ± 0.10 , $p = 0.048$; 0.09 ± 0.02 , $p = 0.005$; and 0.66 ± 0.11 , $p = 0.002$, respectively). Importantly, proportions of bacteria egested are similar between *Egestion Time Experiment* and *Microbial Fate Experiment* (LA: mean \pm s.e.m. = 0.25 ± 0.12 and 0.18 ± 0.08 , respectively. LG: 0.30 ± 0.18 and 0.53 ± 0.11 , respectively), implying consistency between the experiments.

In these calculations, we ignored the possibility of bacteria reproduction in the host. If reproduction is present, then actual proportion of bacteria lysed would be higher than our calculated estimate. Suppose that there is some reproduction, z , in the host. Then the actual proportion of bacteria lysed is:

Proportion of bacteria lysed

$$\begin{aligned}
 &= \frac{(\# \text{ cells ingested} + z) - (\# \text{ cells egested}) - (\# \text{ cells retained})}{(\# \text{ cells ingested} + z)} \\
 &= \frac{a + z}{b + z}
 \end{aligned}
 \tag{B.8}$$

where $a = \# \text{ cells lysed}$ and $b = \# \text{ cells ingested}$, with $a \leq b$. Equation (B.8) is an increasing function of z . Our estimated proportion of bacteria lysed, therefore, is a conservative estimate of the actual proportion. Conversely, some egested and retained cells would have been cells produced in the host. The actual proportions of egested and retained bacteria would then be lower than our estimated proportions.

Finally, what happens to our calculated proportions of bacteria egested, retained, and lysed if some of the microspheres were retained by the host? For example, suppose that 50 % of ingested microspheres were retained in the fly gut, and only 50 % of ingested microspheres were egested. Then in Equation (B.3) for the proportion of bacteria egested, we would have

$$\begin{aligned}
 \text{Proportion of bacteria egested} &= \frac{\# \text{ cells egested}}{\# \text{ cells ingested}} \\
 &= \frac{(\# \text{ cells egested})/(\# \text{ microspheres ingested})}{(\# \text{ cells ingested})/(\# \text{ microspheres ingested})} \\
 &= \frac{(\# \text{ cells egested})/(2 \times \# \text{ **microspheres egested**})}{(\# \text{ cells ingested})/(\# \text{ microspheres ingested})} \quad (\text{B.9}) \\
 &= \frac{0.0327 \text{ cells/microsphere}}{2 \times 0.289 \text{ cells/microsphere}} \\
 &= 0.057
 \end{aligned}$$

The value in Table 3.1 for the proportion of bacteria egested would then be too high by a factor of 2.

The proportion of bacteria retained was also calculated using the number of microspheres egested to estimate the number of bacteria ingested, in Equation (B.4) and Equation (B.1). If half the microspheres were retained rather than egested, the estimated number of bacteria ingested would be low by a factor of 2. Then instead of Equation (B.6) for the proportion of bacteria retained, we

would have

$$\begin{aligned}\text{Proportion of bacteria retained} &= \frac{\# \text{ cells retained}}{\# \text{ cells ingested}} \\ &= \frac{70\,783.39 \text{ cells/fly}}{2 \times 813\,007.5 \text{ cells/fly}} \quad (\text{B.10}) \\ &= 0.044\end{aligned}$$

The value in Table 3.1 for the proportion of bacteria retained also would be too high by a factor of 2.

Therefore, if not all ingested microspheres are egested, the actual values of the proportions of bacteria egested and retained would be lower than the values in Table 3.1, and the values of the proportion of bacteria lysed would be higher. However, this has no effect on our qualitative conclusion: some of the ingested bacteria are egested and retained intact, while many are lysed in the host.

B.1.4 Calculating the proportion of particles recovered in *Microbial Fate Experiment*

Here we derive the proportion of particles recovered that was used to generate Table 3.1, as explained in Appendix B.1.3. To clarify the calculation, we will walk through the procedure using data values from the first replicate experiment (first row in Axenic fly treatment, Table 3.1) of the *Microbial Fate Experiment*.

The proportion of particles recovered was estimated from the *Microbial Fate Experiment* data on Low density axenic (LA) flies. We assume that proportion of particles recovered is a characteristic of each replicate experiment (*i.e.* a result

of how vials were washed, how feces were centrifuged, *etc.* on each date). The derived proportion of particles recovered for a replicate experiment was therefore applied to both Axenic and Gnotobiotic flies on that date, to calculate the number of microspheres and bacteria ingested from the number of microspheres recovered from feces (Equation (B.4)).

The first step is to calculate the number of cells ingested using the CFU counts in the *Immediate* (1 h) sample. In Appendix B.1.5 below, we derive the conversion factor to calculate the number of cells under fluorescent microscope from the CFU on spiral plater (1 CFU/ml = 2.83 bacteria cells/ml). We use this conversion factor to calculate the number of *A. tropicalis* cells ingested by the fly from the number of CFU ingested.

$$\begin{aligned}
 \frac{\# \text{ cells ingested}}{\text{fly}} &= \frac{\# \text{ CFU ingested}}{\text{fly}} \times \text{Conversion factor} \\
 &= 270\,808 \frac{\text{CFU}}{\text{ml}} \times 2.83 \frac{\text{cells}}{\text{CFU}} \\
 &= 766\,386.6 \frac{\text{cells ingested}}{\text{ml}}
 \end{aligned}
 \tag{B.11}$$

We measured the bacteria cells : microsphere ratio in the inoculum used in each replicate experiment. Assuming that the flies ingested microsphere and bacteria indiscriminately, we use this ratio to calculate the number of microspheres ingested by a fly from the number of cells ingested.

$$\begin{aligned}
 &\frac{\# \text{ microspheres ingested}}{\text{fly}} \\
 &= \frac{\# \text{ cells ingested/fly}}{\# \text{ cells in inoculum/\# microspheres in inoculum}} \\
 &= \frac{766\,386.6 \text{ cells/fly}}{0.289 \text{ cells/microspheres}} \\
 &= 2\,651\,857 \frac{\text{microspheres ingested}}{\text{fly}}
 \end{aligned}
 \tag{B.12}$$

This is the number of microspheres ingested by a fly in Axenic *Immediate* sample. We assume that a fly in Axenic *Passaged* sample also ingested the same number of microspheres. Furthermore, because microspheres were scarce in our 5–24 h and 24–48 h samples, we assume that all ingested microspheres were egested by 5 h.

We counted the number of microspheres recovered in hourly samples from the *Passaged* flies, and summing these over 5 h gives the total number of microspheres recovered from the feces (*e.g.* 91 194.54 microspheres/fly). We calculate the proportion of particles recovered for a replicate experiment using the number of microspheres recovered and egested.

$$\begin{aligned}
 & \text{Proportion of particles recovered} \\
 &= \frac{\# \text{ microspheres recovered from feces}}{\# \text{ microspheres egested}} \\
 &= \frac{\# \text{ microspheres recovered from feces}}{\# \text{ microspheres ingested}} \quad (\text{B.13}) \\
 &= \frac{91\,194.54 \text{ microspheres/fly}}{2\,651\,857 \text{ microspheres/fly}} \\
 &= 0.034
 \end{aligned}$$

Applying the same calculation to all three replicate experiment of the *Microbial Fate Experiment* gave estimated proportions of particles recovered of 0.034, 0.012 and 0.023.

Note that we calculate proportion of particles recovered using numbers of microspheres recovered from feces (relative to the estimated number of microspheres egested). In the experiments, both microspheres and bacteria were homogeneously distributed on the experimental food, and fecal samples were collected indiscriminately. We therefore assume that the proportion of particles

recovered is the same for bacteria as it is for microspheres.

As noted above, we also assume that the same proportion of particles recovered applies to all samples within a replicate experiment, including both Axenic and Gnotobiotic flies. To test this assumption and validate the estimates of proportion of particles recovered, we re-calculate the proportion of bacteria egested using the proportion of particles recovered, and compare the results to the values in Table 3.1. The values in Table 3.1 did not use the proportion of particles recovered (Equation (B.3)). Therefore, if this alternative calculation (AC) leads to similar values as Table 3.1, then we conclude that our estimate for the proportion of particles recovered is sound. To test our assumption that the proportion of particles recovered (calculated using Axenic flies) also applies to Gnotobiotic flies, we re-calculate the proportion of bacteria egested using the Gnotobiotic flies. To clarify AC, we will walk through its calculation using data values from the second replicate experiment (first row in Gnotobiotic fly treatment, Table 3.1).

In AC, we assume that each fly in *Passaged* samples (including Gnotobiotic flies) ingested the same number of bacteria as Axenic *Immediate* flies. The flies in the *Immediate* sample from our example ingested 108 888 CFU/fly. We convert the number of CFU ingested to the number of *A. tropicalis* cells ingested by a fly using the conversion factor.

$$\begin{aligned}
 \frac{\# \text{ cells ingested}}{\text{fly}} &= \frac{\# \text{ CFU ingested}}{\text{fly}} \times \text{Conversion factor} \\
 &= 108\,888 \frac{\text{microbial CFU}}{\text{fly}} \times 2.83 \frac{\text{cells}}{\text{CFU}} \\
 &= 308\,153 \frac{\text{cells ingested}}{\text{fly}}
 \end{aligned}
 \tag{B.14}$$

Next, we calculate the number of cells egested from the number of cells recovered in feces.

$$\begin{aligned}
 \frac{\# \text{ cells egested}}{\text{fly}} &= \frac{\# \text{ cells recovered from feces/fly}}{\text{Proportion of particles recovered}} \\
 &= \frac{2588 \text{ cells/fly}}{0.012} \\
 &= 215\,667 \frac{\text{cells egested}}{\text{fly}}
 \end{aligned} \tag{B.15}$$

The proportion of bacteria egested using numbers of cells egested (Equation (B.15)) and ingested (Equation (B.14)) under AC is

$$\begin{aligned}
 \text{Proportion of bacteria egested} &= \frac{\# \text{ cells egested}}{\# \text{ cells ingested}} \\
 &= \frac{215\,667 \text{ cells/fly}}{308\,153 \text{ cells/fly}} \\
 &= 0.7
 \end{aligned} \tag{B.16}$$

Calculating the proportion of bacteria egested with (AC) and without (Equation (B.3)) the proportion of particles recovered led to similar values (mean \pm s.e.m. = 0.45 ± 0.26 and 0.53 ± 0.11 , respectively) across Gnotobiotic samples. We conclude that our calculation of the proportion of particles recovered is sound.

B.1.5 Conversion factor between microscopy (cells/ml) and spiral plater (CFU/ml) bacterial counts

Here we derive the conversion factor between microscopy and spiral plater that was used in Appendix B.1.3 and Appendix B.1.4. Quantification of retained *A. tropicalis* involves two different methods to count the number of bacteria: fecal samples under fluorescent microscopy (measured in cells/ml) and fly ho-

mogenate samples on spiral plater (measured in CFU/ml). The two approaches have different ranges for measurable microbial densities. We must calculate the conversion factor between the two methods so that measurements by the two methods can both be used. We calculated the conversion factor by the following. We grew a culture of GFP-labeled *A. tropicalis* overnight, and re-suspended the culture in PBS. We serially diluted the culture, such that some dilutions are within the measurable range for the spiral plater, whereas others are within the measurable range for microscopy. For each serial dilution, we regressed microscopy or spiral plater measurements against the dilution factor of the sample to obtain a slope between measurements and dilution. We thus obtained paired slopes (β for spiral plater against dilution factor and α for microscopy against dilution factor) for each sample:

$$\begin{aligned}
 \text{Spiral plater:} \quad & \left[\text{Number} \frac{\text{CFU}}{\text{ml}} \right] = \beta[\text{dilution factor}] \\
 \text{Microscopy:} \quad & \left[\text{Number} \frac{\text{cells}}{\text{ml}} \right] = \alpha[\text{dilution factor}] \\
 & = \left(\frac{\alpha}{\beta} \right) \left[\text{Number} \frac{\text{CFU}}{\text{ml}} \right]
 \end{aligned} \tag{B.17}$$

We repeated this for 4 samples, obtaining 4 values of α and β . We regressed (through the origin) the slope from microscopy against the slope from spiral plater, to get a conversion factor across all samples (equivalent to α/β). The estimated conversion factor between two units is 1 CFU/ml = 2.83 bacteria cells/ml (simple linear regression: Standard error = 0.35, adjusted $R^2 = 0.94$, $p = 0.004$). Alternatively, we regressed (through the origin) the slope from spiral plater against the slope from microscopy (equivalent to β/α) and then took its inverse to calculate α/β . We obtained 1 CFU/ml = 2.96 bacteria cells/ml. The two meth-

ods result in similar conversion factor. Since we convert the number of CFU to the number of cells, we use 1 CFU/ml = 2.83 bacteria cells/ml for the paper.

B.1.6 Summary of calculations for Table 3.1

Here we summarize compactly how the quantities estimated in Appendices B.1.3 to B.1.5 were used to get the numbers in Table 3.1. Terms in the calculations are in one of three typefaces to distinguish whether they were directly observed or indirectly inferred. Each typeface describes the following:

- Normal type: Data collected by directly observing samples (*e.g.* feces from Axenic *Passaged* flies, inoculum used in a replicate experiment).
- *Italic type*: Inferred from calculation using data on same fly type only.
- **Bold face type**: Inferred from calculation using, in whole or part, data from another fly type.

1. Proportion of particles recovered (Appendix B.1.4)

$$0.034 = \frac{\# \text{ microspheres recovered from feces (Axenic } \textit{Passaged} \text{ fly)}}{\# \textit{ microspheres ingested}}$$

$$\# \textit{ microspheres ingested} = \# \textit{ cells ingested} \times \frac{\# \text{ microspheres in inoculum}}{\# \text{ cells in inoculum}}$$

$$\# \textit{ cells ingested} = \# \text{ CFU ingested (Axenic } \textit{Immediate} \text{ fly)} \times \text{Conversion factor}$$

Proportion of particles recovered is calculated using samples from same fly type: Axenic *Passaged* and Axenic *Immediate* samples. Once the propor-

tion is calculated, however, the same proportion is also applied to Gnotobiotic *Passaged* flies in the same replicate experiment.

2. Proportion of bacteria egested (Appendix B.1.3)

$$0.10 = \frac{(\# \text{ cells egested})/(\# \text{ microspheres egested})}{(\# \text{ cells ingested})/(\# \text{ microspheres ingested})}$$

$$\frac{\# \text{ cells egested}}{\# \text{ microspheres egested}} = \frac{\# \text{ cells recovered}}{\# \text{ microspheres recovered}}$$

$$\frac{\# \text{ cells ingested}}{\# \text{ microspheres ingested}} = \frac{\# \text{ cells in inoculum}}{\# \text{ microspheres in inoculum}}$$

3. Proportion of bacteria retained (Appendix B.1.3)

$$0.03 = \frac{\# \text{ intact cells in } \textit{Passaged} \text{ fly}}{\# \text{ cells ingested}}$$

$$\# \text{ intact cells in } \textit{Passaged} \text{ fly} = \# \text{ CFU's in } \textit{Passaged} \text{ fly} \times \text{Conversion factor}$$

$$\# \text{ cells ingested} = \# \text{ microspheres ingested} \times \frac{\# \text{ cells in inoculum}}{\# \text{ microspheres in inoculum}}$$

$$\# \text{ microspheres ingested}$$

$$= \frac{\# \text{ microspheres recovered from feces (Axenic and Gnotobiotic } \textit{Passaged} \text{ flies)}}{\text{Proportion of particles recovered (Axenic } \textit{Immediate} \text{ and } \textit{Passaged} \text{ flies)}}$$

Calculating the proportion of bacteria retained involves the number of cells ingested. As above, we use the proportion of particles recovered to calculate the number of cells ingested. Proportion of particles recovered is calculated from data on Axenic flies. We assume that the proportion of particles recovered is the same within a replicate experiment for both Axenic and Gnotobiotic fecal samples. Therefore, calculating the proportion of bacteria retained for Axenic flies would only involve data from the

same fly type. The calculation for Gnotobiotic flies, however, would involve data from another fly type.

4. Proportion of bacteria lysed (Appendix B.1.3)

$$0.87 = 1 - \text{Proportion of bacteria egested} - \text{Proportion of bacteria retained}$$

The proportion of bacteria retained in *Axenic Passaged* samples would only involve data from the same fly type, whereas the proportion of bacteria retained in *Gnotobiotic Passaged* samples would involve data from another fly type.

B.2 Derivation of theoretical egestion time statistics from models

Here, we derive egestion time statistics in simple models that allow us to infer ecological processes affecting microbial population dynamics in the host. While it is difficult to directly measure population dynamics *in situ* (*i.e.* track population size of the microorganisms directly in the host gut over time), we show that ecological processes can be inferred by observing some statistical properties of the egestion time.

We first define some of the relevant terms:

- **Compartment** refers to a microbial population in a region along the gut with more or less the same characterization. For example, separating bacteria into populations in foregut, midgut, and hindgut corresponds to a

system with 3 compartments.

- **Egestion time** refers to the time that a particle (*i.e.* a microorganism or a microsphere) is egested from the last compartment. Here, we treat it as a random variable.
- **Apparent death** refers to a microorganism disappearing from a compartment, instead of getting egested. Because egestion time is recorded only when a microorganism successfully exits the host, a “dead” microorganism does not have an egestion time. Apparent death could be caused by actual death (*e.g.* due to aging, immunity), or could be due to retention of a microorganism by the host (*e.g.* long-term adhesion to the host gut).

Appendix B.2.1 and Appendix B.2.2 are for mathematically-inclined readers. Appendix B.2.1 derives the formulae for the mean and the variance of the egestion time, and intuition behind our results is further confirmed in Appendix B.2.2. In Appendix B.2.3, we use data from *Egestion Time Experiment* (Section 3.5.4) to test our models. The biological implications of all the theoretical work is presented in Appendix B.2.3 and Appendix B.2.3. In summary, any ecological processes contributing to apparent death leads to shorter mean and variance of the egestion time. Egestion time statistics and proportion of microorganisms recovered together allow us to infer within-host population dynamics from fecal time series data.

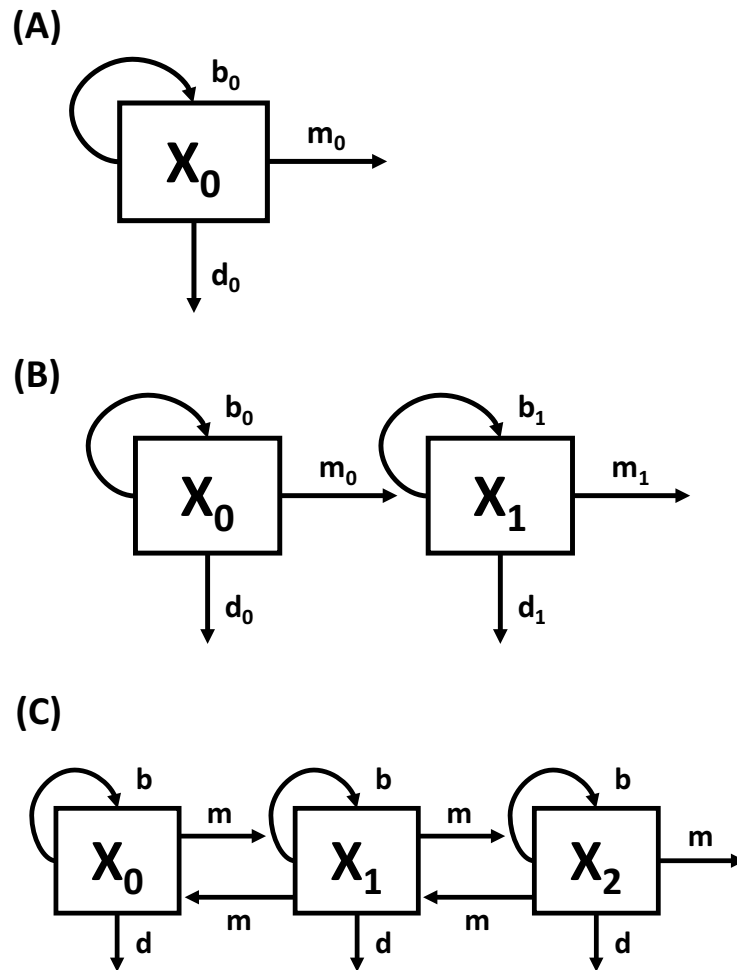


Figure B.3: (A) One and (B) two compartments models with unidirectional emigration. (C) Three compartments model with bi-directional emigration.

B.2.1 Compartment models

One compartment model

We start with the simplest model, assuming a single, well-mixed, homogenous gut. Assume that there are some initial number of microorganism N in the gut, the net population growth rate per microorganism is $r_0 = b_0 - d_0$, and the emigration rate per microorganism is m_0 (Figure B.3A). $X_0(t)$ represents the number

of microorganism in the gut at time t , so $X_0(t = 0) = N$. Further assume that $r_0 < m_0$, so $r_0 - m_0 < 0$. Otherwise, $X_0(t)$ increases to $+\infty$, contrary to our observation (see Figures 3.1 and 3.3B). Note that if $b_0 = 0$ but $d_0 > 0$ (*i.e.* no birth, but some microorganisms die or are retained), then $r_0 < 0$ and our assumption holds. Under these assumptions, gut microbial population size changes as:

$$\frac{dX_0}{dt} = (r_0 - m_0)X_0 \quad (\text{B.18})$$

The solution to this system is $X_0(t) = Ne^{(r_0 - m_0)t}$. With the emigration rate m_0 and the microbial population size $X_0(t)$, the number of microorganisms egested at time t is $m_0X_0(t)$ and the total number of microorganisms egested over time is $\int_0^\infty m_0X_0(t)dt$. Then, the proportion of microorganisms egested at time t relative to the total microorganisms egested is $p(t) = \frac{m_0X_0(t)}{\int_0^\infty m_0X_0(t)dt}$. Let \hat{t}_0 be an egestion time of a microorganism, so $E[\hat{t}_0]$ and $Var[\hat{t}_0]$ are the mean and variance of the egestion time, respectively. For convenience, define $q_0 = r_0 - m_0 < 0$. Then,

$$\begin{aligned} E[\hat{t}_0] &= \int_0^\infty tp(t)dt = \int_0^\infty t \frac{m_0X_0}{\int_0^\infty m_0X_0dt} dt \\ &= \frac{\int_0^\infty tX_0dt}{\int_0^\infty X_0dt} = \frac{\int_0^\infty te^{q_0t} dt}{\int_0^\infty e^{q_0t} dt} = \frac{1/(r_0 - m_0)^2}{-1/(r_0 - m_0)} \\ &= \frac{1}{m_0 - r_0} \end{aligned} \quad (\text{B.19})$$

$$\begin{aligned} Var[\hat{t}_0] &= E[\hat{t}_0^2] - E[\hat{t}_0]^2 = \int_0^\infty t^2 p(t)dt - \left(\frac{1}{m_0 - r_0}\right)^2 \\ &= \frac{\int_0^\infty t^2 e^{q_0t} dt}{\int_0^\infty e^{q_0t} dt} - \frac{1}{q_0^2} = \frac{-2/q_0^3}{-1/q_0} - \frac{1}{q_0^2} = \frac{2}{q_0^2} - \frac{1}{q_0^2} \\ &= \frac{1}{(m_0 - r_0)^2} \end{aligned} \quad (\text{B.20})$$

In particular, $E[\hat{t}_0] = \frac{1}{m_0}$ and $Var[\hat{t}_0] = \frac{1}{m_0^2}$ when $r_0 = 0$.

Two compartments model

A more realistic model would have at least two compartments. For example, food is first stored in fly crop, and slowly enters the gut over time. Given the different anatomical and physiological environments in these two compartments, microorganisms may encounter different immune responses and niche availability. In our experiment, flies were starved for 4 h to clear out the gut. We then fed the flies for an hour, so the ingested bacteria is more dense in fly anterior than the posterior.

Assume there are some initial number of bacteria N in the source compartment (*e.g.* crop, food in the environment) and the microorganisms flow into the egesting compartment (*e.g.* gut) over time (Figure B.3B). The net population growth rate per microorganism in compartment i is $r_i = b_i - d_i$, where $i = 0$ or 1 corresponds to the source and egesting compartment, respectively. Similarly, the emigration rate per microorganism is m_i and $X_i(t)$ is the number of microorganism at time t . Assume that $r_i < m_i$, so $q_i = r_i - m_i < 0$ for all i . Under these assumptions, gut microbial population sizes change as:

$$\begin{aligned}\frac{dX_0}{dt} &= q_0 X_0 \\ \frac{dX_1}{dt} &= m_0 X_0 + q_1 X_1\end{aligned}\tag{B.21}$$

The solution to this system is $X_0(t) = Ne^{q_0 t}$ and $X_1(t) = \frac{m_0 N}{q_0 - q_1}(e^{q_0 t} - e^{q_1 t})$ assuming $q_0 \neq q_1$ (the final result will be the same even if $q_0 = q_1$). Let \hat{t}_1 be the egestion time from the egesting compartment, so $E[\hat{t}_1]$ and $Var[\hat{t}_1]$ are the mean and

variance of the egestion time, respectively. Then,

$$\begin{aligned}
E[\hat{t}_1] &= \int_0^\infty t p(t) dt = \frac{\int_0^\infty t X_1 dt}{\int_0^\infty X_1 dt} = \frac{\int_0^\infty t(e^{q_0 t} - e^{q_1 t}) dt}{\int_0^\infty e^{q_0 t} - e^{q_1 t} dt} \\
&= \frac{q_1^2 - q_0^2}{q_0^2 q_1^2} \frac{q_1 q_0}{q_0 - q_1} = \frac{-q_1 - q_0}{q_1 q_0} \\
&= -\frac{1}{q_0} - \frac{1}{q_1}
\end{aligned} \tag{B.22}$$

$$\begin{aligned}
Var[\hat{t}_1] &= E[\hat{t}_1^2] - E[\hat{t}_1]^2 = \int_0^\infty t^2 p(t) dt - \left(\frac{1}{q_0} + \frac{1}{q_1}\right)^2 \\
&= \frac{\int_0^\infty t^2 (e^{q_0 t} - e^{q_1 t}) dt}{\int_0^\infty e^{q_0 t} - e^{q_1 t} dt} - \left(\frac{1}{q_0} + \frac{1}{q_1}\right)^2 = \frac{2}{q_0^2 q_1^2} \frac{q_0^3 - q_1^3}{q_0 - q_1} - \left(\frac{1}{q_0} + \frac{1}{q_1}\right)^2 \\
&= \frac{2(q_0^2 + q_0 q_1 + q_1^2)}{q_0^2 q_1^2} - \frac{(q_0 + q_1)^2}{q_0^2 q_1^2} \\
&= \frac{1}{q_0^2} + \frac{1}{q_1^2}
\end{aligned} \tag{B.23}$$

Note that $E[\hat{t}_1] > 0$ and specifically, $E[\hat{t}_1] = \frac{1}{m_0} + \frac{1}{m_1}$ and $Var[\hat{t}_1] = \frac{1}{m_0^2} + \frac{1}{m_1^2}$ when $r_0 = r_1 = 0$.

$n + 1$ compartments model

Let us generalize the models above, by having many compartments between the source and the egesting compartments (Figure 3.4A). For example, microorganisms may go through different environments in the crop, foregut, midgut, and hindgut. The net population growth rate per microorganism in compartment i is $r_i = b_i - d_i$ and the emigration rate per microorganism is m_i , where $i = 0, 1, 2, \dots, n$. Define $q_i = r_i - m_i$. Under these assumptions, gut microbial

population sizes change as:

$$\begin{aligned}
\frac{dX_0}{dt} &= q_0 X_0 \\
\frac{dX_1}{dt} &= m_0 X_0 + q_1 X_1 \\
\frac{dX_2}{dt} &= m_1 X_1 + q_2 X_2 \\
&\vdots \\
\frac{dX_n}{dt} &= m_{n-1} X_{n-1} + q_n X_n
\end{aligned} \tag{B.24}$$

Theorem 1. Let $E[\hat{t}_i]$ and $Var[\hat{t}_i]$ be the mean and variance of a random variable \hat{t}_i , an egestion time from compartment X_i . Assume that $X_0(0) = N$ but $X_k(0) = 0$ for all $k = 1, 2, \dots, n$, and $r_i < m_i$ so that $q_i = r_i - m_i < 0$ for all $i = 0, 1, 2, \dots, n$. Then,

$$\begin{aligned}
E[\hat{t}_i] &= \begin{cases} -\frac{1}{q_0} & \text{if } i = 0 \\ E[\hat{t}_{i-1}] - \frac{1}{q_i} & \text{if } i > 0 \end{cases} \\
Var[\hat{t}_i] &= \begin{cases} \frac{1}{q_0^2} & \text{if } i = 0 \\ Var[\hat{t}_{i-1}] + \frac{1}{q_i^2} & \text{if } i > 0 \end{cases}
\end{aligned} \tag{B.25}$$

Therefore, $E[\hat{t}_n] = \sum_{i=0}^n \frac{1}{m_i - r_i}$ and $Var[\hat{t}_n] = \sum_{i=0}^n \frac{1}{(m_i - r_i)^2}$ for any $n = 0, 1, 2, \dots$

Proof. 1. From Equations (B.19) and (B.22), $E[\hat{t}_0] = \frac{1}{m_0 - r_0} = -\frac{1}{q_0}$ and $E[\hat{t}_1] = -\frac{1}{q_0} - \frac{1}{q_1} = E[\hat{t}_0] - \frac{1}{q_1}$. From Equations (B.20) and (B.23), $Var[\hat{t}_0] = \frac{1}{q_0^2}$ and $Var[\hat{t}_1] = \frac{1}{q_0^2} + \frac{1}{q_1^2} = Var[\hat{t}_0] + \frac{1}{q_1^2}$. So, the theorem holds for $i = 0, 1$.

2. By hypothesis, $X_k(0) = 0$ for all $k = 1, 2, \dots, n$. So for an arbitrary $n > 0$, the solution for $\frac{dX_n}{dt}$ is $X_n(t) = \int_0^t m_{n-1} X_{n-1}(s) e^{q_n(t-s)} ds$. Then,

$$E[\hat{t}_n] = \frac{\int_0^\infty t X_n(t) dt}{\int_0^\infty X_n(t) dt} = \frac{\int_{t=0}^\infty \int_{s=0}^t t X_{n-1}(s) e^{q_n(t-s)} ds dt}{\int_{t=0}^\infty \int_{s=0}^t X_{n-1}(s) e^{q_n(t-s)} ds dt} \tag{B.26}$$

Switch the order of integration and pull out some terms:

$$E[\hat{t}_n] = \frac{\int_{s=0}^{\infty} X_{n-1}(s)e^{-q_n s} \int_{t=s}^{\infty} t e^{q_n t} dt ds}{\int_{s=0}^{\infty} X_{n-1}(s)e^{-q_n s} \int_{t=s}^{\infty} e^{q_n t} dt ds} \quad (\text{B.27})$$

Calculate the inner integrals in the numerator and the denominator first:

$$\begin{aligned} E[\hat{t}_n] &= \frac{\int_{s=0}^{\infty} X_{n-1}(s)e^{-q_n s} (1/q_n^2 - s/q_n) e^{q_n s} ds}{\int_{s=0}^{\infty} X_{n-1}(s)e^{-q_n s} (-e^{q_n s}/q_n) ds} = \frac{\int_{s=0}^{\infty} X_{n-1}(s)(1/q_n^2 - s/q_n) ds}{(-1/q_n) \int_{s=0}^{\infty} X_{n-1}(s) ds} \\ &= \frac{\frac{1}{q_n^2} \int_0^{\infty} X_{n-1}(s) ds - \frac{1}{q_n} \int_0^{\infty} s X_{n-1}(s) ds}{-\frac{1}{q_n} \int_0^{\infty} X_{n-1}(s) ds} = \frac{\int_0^{\infty} s X_{n-1}(s) ds}{\int_0^{\infty} X_{n-1}(s) ds} - \frac{1}{q_n} \\ &= E[\hat{t}_{n-1}] - \frac{1}{q_n} \end{aligned} \quad (\text{B.28})$$

because $\frac{\int_0^{\infty} s X_{n-1}(s) ds}{\int_0^{\infty} X_{n-1}(s) ds} = E[\hat{t}_{n-1}]$.

Next,

$$\begin{aligned} \text{Var}[\hat{t}_n] &= E[\hat{t}_n^2] - E[\hat{t}_n]^2 = \frac{\int_0^{\infty} t^2 X_n dt}{\int_0^{\infty} X_n dt} - E[\hat{t}_n]^2 \\ &= \frac{\int_{t=0}^{\infty} \int_{s=0}^t t^2 X_{n-1}(s) e^{q_n(t-s)} ds dt}{\int_{t=0}^{\infty} \int_{s=0}^t X_{n-1}(s) e^{q_n(t-s)} ds dt} - E[\hat{t}_n]^2 \end{aligned} \quad (\text{B.29})$$

Switch the order of integration, and pull out some terms. Also note that we calculated the denominator while deriving $E[\hat{t}_n]$ in Equations (B.26) to (B.28):

$$\text{Var}[\hat{t}_n] = \frac{\int_{s=0}^{\infty} X_{n-1}(s)e^{-q_n s} \int_{t=s}^{\infty} t^2 e^{q_n t} dt ds}{(-1/q_n) \int_{s=0}^{\infty} X_{n-1}(s) ds} - E[\hat{t}_n]^2 \quad (\text{B.30})$$

Calculate the inner integrals in the numerator first:

$$\begin{aligned}
\text{Var}[\hat{t}_n] &= \frac{\int_{s=0}^{\infty} X_{n-1}(s) e^{-q_n s} (-e^{q_n s} (s^2/q_n - 2s/q_n^2 + 2/q_n^3)) ds}{(-1/q_n) \int_{s=0}^{\infty} X_{n-1}(s) ds} - E[\hat{t}_n]^2 \\
&= \frac{-\frac{1}{q_n} \int_0^{\infty} s^2 X_{n-1}(s) ds + \frac{2}{q_n^2} \int_0^{\infty} s X_{n-1}(s) ds - \frac{2}{q_n^3} \int_0^{\infty} X_{n-1}(s) ds}{\frac{-1}{q_n} \int_{s=0}^{\infty} X_{n-1}(s) ds} - E[\hat{t}_n]^2 \\
&= \frac{\int_0^{\infty} s^2 X_{n-1}(s) ds}{\int_0^{\infty} X_{n-1}(s) ds} - \frac{2}{q_n} \frac{\int_0^{\infty} s X_{n-1}(s) ds}{\int_0^{\infty} X_{n-1}(s) ds} + \frac{2}{q_n^2} - E[\hat{t}_n]^2
\end{aligned} \tag{B.31}$$

Note that $\frac{\int_0^{\infty} s^2 X_{n-1}(s) ds}{\int_0^{\infty} X_{n-1}(s) ds} = E[\hat{t}_{n-1}^2]$ and $\frac{\int_0^{\infty} s X_{n-1}(s) ds}{\int_0^{\infty} X_{n-1}(s) ds} = E[\hat{t}_{n-1}]$:

$$\text{Var}[\hat{t}_n] = E[\hat{t}_{n-1}^2] - \frac{2}{q_n} E[\hat{t}_{n-1}] + \frac{2}{q_n^2} - E[\hat{t}_n]^2 \tag{B.32}$$

Finally, using $E[\hat{t}_n] = E[\hat{t}_{n-1}] - \frac{1}{q_n}$ derived in Equation (B.28):

$$\begin{aligned}
\text{Var}[\hat{t}_n] &= E[\hat{t}_{n-1}^2] - \frac{2}{q_n} E[\hat{t}_{n-1}] + \frac{2}{q_n^2} - \left(E[\hat{t}_{n-1}] - \frac{1}{q_n} \right)^2 \\
&= E[\hat{t}_{n-1}^2] - E[\hat{t}_{n-1}]^2 - \frac{2}{q_n} E[\hat{t}_{n-1}] + \frac{2}{q_n} E[\hat{t}_{n-1}] + \frac{2}{q_n^2} - \frac{1}{q_n^2} \\
&= \text{Var}[\hat{t}_{n-1}] + \frac{1}{q_n^2}
\end{aligned} \tag{B.33}$$

by noticing that $E[\hat{t}_{n-1}^2] - E[\hat{t}_{n-1}]^2 = \text{Var}[\hat{t}_{n-1}]$

3. By induction, $E[\hat{t}_0] = -\frac{1}{q_0}$ and $E[\hat{t}_i] = E[\hat{t}_{i-1}] - \frac{1}{q_i}$ for all $i = 1, 2, \dots$. Similarly,

$\text{Var}[\hat{t}_0] = \frac{1}{q_0^2}$ and $\text{Var}[\hat{t}_i] = \text{Var}[\hat{t}_{i-1}] + \frac{1}{q_i^2}$ for all $i = 1, 2, \dots$. It follows that

$E[\hat{t}_n] = \sum_{i=0}^n -\frac{1}{q_i} = \sum_{i=0}^n \frac{1}{m_i - r_i}$ and $\text{Var}[\hat{t}_n] = \sum_{i=0}^n \frac{1}{q_i^2} = \sum_{i=0}^n \frac{1}{(m_i - r_i)^2}$ for all $n =$

$0, 1, 2, 3, \dots$

□

In particular, $E[\hat{t}_n] = \sum_{i=0}^n \frac{1}{m_i}$ and $\text{Var}[\hat{t}_n] = \sum_{i=0}^n \frac{1}{m_i^2}$ if $r_i = 0$ for all $i = 0, 1, 2, \dots$

Numerical exploration of bi-directional migration

The biological intuition behind our results above is simple and straightforward: as death/retention rate in the host increases (*i.e.* $r = b-d$ decreases), microorganisms that are observed to egest are biased towards earlier egestion time. Longer egestion time means that a microorganism must endure higher probability of death/retention, and therefore lowers the probability of it being detected in an experiment. Furthermore, as this detection bias gets stronger, we expect less variance. The same logic applies to higher emigration rate (*i.e.* higher m).

However, does the same intuition work when we relax our model assumptions? For example, we assumed that the microorganism can only flow unidirectionally through the compartments. While this is often a valid assumption, it may not always be the case (*e.g.* regurgitation of food from the crop). We now relax this assumption and consider an extreme case: a microorganism has an equal probability of migrating to the posterior compartment as well as the anterior compartment (Figure B.3C). Specifically, we simulated the following model:

$$\begin{aligned}\frac{dX_0}{dt} &= (r - m)X_0 + mX_1 \\ \frac{dX_1}{dt} &= (r - 2m)X_1 + mX_0 + mX_2 \\ \frac{dX_2}{dt} &= (r - 2m)X_2 + mX_1\end{aligned}\tag{B.34}$$

Even under this assumption, we observed that decreasing r always leads to decreasing mean egestion time. Bidirectional emigration therefore does not change the qualitative effect of r on the mean egestion time. We also observed a pattern in variance consistent with our previous analyses. (Figure B.4). Sim-

ilarly, we observed that increasing m always leads to decreasing mean egestion time. Bidirectional emigration therefore does not change the qualitative effect of m on the mean egestion time. Again, we observed a pattern in variance consistent with our previous analyses. (Figure B.4).

Importantly, we observed that the distributions of the egestion time in our simulations are **stochastically ordered**; that is, the cumulative distribution curve of a larger r (smaller m) always lie on or under the curve of a smaller r (larger m). Stochastic ordering is consistent with our intuition, as any ecological process biasing the distribution towards earlier egestion time would lead to stochastically smaller distribution. In Appendix B.2.2, we analyze larger class of models to show that our result in stochastic ordering does not hinge on our specific model structure.

B.2.2 Structural model

Our results from Appendix B.2.1 imply that, all else being equal, apparent death of the microorganisms leads to stochastically smaller distribution. In this section, we test whether apparent death alone could lead to stochastic ordering, without hinging on specific model structure. To do so, we drop the assumption of compartments and ignore the specific movement pattern of the microorganisms within the gut. Instead, we focus on the distribution of microorganisms egested over time with and without apparent death. The basic idea is as follows. We track the microorganisms as they move through the gut. We “mark” them as dead when they die, but we let them continue to move as if they were still alive, and count them when they exit. We then have two different distributions stem-

ming from the exact same egestion pattern: a distribution of microorganisms with apparent death (only unmarked microorganisms) and without apparent death (both marked and unmarked microorganisms). We compare these two distributions to understand the effect of apparent death.

We use the function $f(t)$ to represent the number of microorganisms egested at time t if apparent death were absent. We use the function $f(t)g(t)$ to describe the number of unmarked microorganisms egested if apparent death were present. The function $g(t)$ is survival rate. It decreases monotonically with time, because the longer a microorganism stays in the host, more likely it would be marked as dead. The assumption that $g' \leq 0$ is natural for a mortality-only situations, because it just says that the longer a microorganism spends in the host, the more likely it is to be marked dead. Our model below is actually more general than mortality-only situations, and Theorem 2 is true even if $g(t)$ is the net result of reproduction and mortality. In fact, a microorganism can even have positive net reproduction rate in the gut, as long as total amount of f over time eventually goes to 0.

In terms of Appendix B.2.1, f is the number of microorganisms we obtain if we set $r_i = 0$ for all compartments i . Conversely, fg is the number of microorganisms we obtain if we have $r_i = b_i - d_i < 0$ for any compartment i . Without specifying the exact functions, we ask if qualitative assumptions below are sufficient to generate a bias in mean egestion time. See Figure B.5 for some examples of f and g satisfying the assumptions below.

Theorem 2. *Let $f(t)$ be the number of microorganisms egested at time t , and $g(t)$ be the survival rate of the microorganisms egested at time t . Assume that f and g are both Lebesgue integrable and continuously differentiable, $f, g \geq 0$ for all t , f is bounded and*

$g'(t) \leq 0$ for all t . Let t_0 and t_1 be the egestion time random variable for the microorganisms without and with apparent death, respectively. Then,

$$P(t_0 \leq a) \equiv \int_0^a \frac{f(t)}{\int_0^\infty f(x)dx} dt \leq \int_0^a \frac{f(t)g(t)}{\int_0^\infty f(x)g(x)dx} dt \equiv P(t_1 \leq a) \quad (\text{B.35})$$

for all $a \geq 0$, i.e. t_0 is **stochastically greater** (written \geq_{st}) than t_1 .

Proof. First, note that both denominators are positive constants in the inequality above:

$$\begin{aligned} \int_0^a \frac{f(t)}{\int_0^\infty f(x)dx} dt \leq \int_0^a \frac{f(t)g(t)}{\int_0^\infty f(x)g(x)dx} dt &\iff \frac{\int_0^a f(t)dt}{\int_0^\infty f(t)dt} \leq \frac{\int_0^a f(t)g(t)dt}{\int_0^\infty f(t)g(t)dt} \\ &\iff \int_0^a f(t)dt \int_0^\infty f(t)g(t)dt \leq \int_0^a f(t)g(t)dt \int_0^\infty f(t)dt \end{aligned} \quad (\text{B.36})$$

Second, for a fixed a , let $H_a(x) \equiv \int_0^a f(t)dt \int_0^x f(t)g(t)dt$ and $J_a(x) \equiv \int_0^a f(t)g(t)dt \int_0^x f(t)dt$:

$$\begin{aligned} \int_0^a f(t)dt \int_0^\infty f(t)g(t)dt &\leq \int_0^a f(t)g(t)dt \int_0^\infty f(t)dt \\ &\iff \lim_{x \rightarrow \infty} H_a(x) \leq \lim_{x \rightarrow \infty} J_a(x) \iff \lim_{x \rightarrow \infty} \int_0^x H'_a(y)dy \leq \lim_{x \rightarrow \infty} \int_0^x J'_a(y)dy \\ &\iff \lim_{x \rightarrow \infty} \left[\int_0^a H'_a(y)dy + \int_a^x H'_a(y)dy \right] \leq \lim_{x \rightarrow \infty} \left[\int_0^a J'_a(y)dy + \int_a^x J'_a(y)dy \right] \end{aligned} \quad (\text{B.37})$$

Third, note that $H_a(a) = J_a(a)$:

$$\begin{aligned} \lim_{x \rightarrow \infty} \left[\int_0^a H'_a(y)dy + \int_a^x H'_a(y)dy \right] &\leq \lim_{x \rightarrow \infty} \left[\int_0^a J'_a(y)dy + \int_a^x J'_a(y)dy \right] \\ &\iff \lim_{x \rightarrow \infty} \int_a^x H'_a(y)dy \leq \lim_{x \rightarrow \infty} \int_a^x J'_a(y)dy \end{aligned} \quad (\text{B.38})$$

To prove the inequality in Equation (B.38) for all a , we shall consider the

derivatives of H_a and J_a with respect to x .

$$\begin{aligned} H'_a(x) &= \left[\int_0^a f(t) dt \right] f(x)g(x) \\ J'_a(x) &= \left[\int_0^a f(t)g(t) dt \right] f(x) \end{aligned} \quad (\text{B.39})$$

By hypothesis, $g' \leq 0$ which implies that $\int_0^a f(t)g(t) dt \geq \left[\int_0^a f(t) dt \right] g(a)$. So,

$$\begin{aligned} H'_a(y) &= \left[\int_0^a f(t) dt \right] f(y)g(y) \\ &\leq \left[\int_0^a f(t) dt \right] f(y)g(a) \leq \left[\int_0^a f(t)g(t) dt \right] f(y) = J'_a(y) \end{aligned} \quad (\text{B.40})$$

for $y \geq a$. Finally, H'_a and J'_a are positive and integrable, so $H'_a \leq J'_a$ for $y \geq a$ implies

$$\int_a^x H'_a(y) dy \leq \int_a^x J'_a(y) dy \implies \lim_{x \rightarrow \infty} \int_a^x H'_a(y) dy \leq \lim_{x \rightarrow \infty} \int_a^x J'_a(y) dy \quad (\text{B.41})$$

which holds for any chosen $a \geq 0$. □

Theorem 2 leads us immediately to some useful statistical properties:

- $t_0 \geq_{st} t_1$ implies that $E[u(t_0)] \geq E[u(t_1)]$ for any non-decreasing function u .
In particular, $E[t_0] \geq E[t_1]$.
- Suppose $E[t_0] = E[t_1]$. Then, $Var[t_0] \geq Var[t_1]$.
- Suppose we want to compare mutant with wild-type microorganisms, where we have a common baseline death rate $k(t)$ for both but time-dependent benefit $g(t)$ for mutant. Suppose $k(t)$ is continuously differentiable. Then, we can replace $f(t)$ with $\hat{f}(t) = f(t)k(t)$ and Theorem 2 holds.

Conjecture 1. *Under the assumptions in Theorem 2, $Var[t_1] \leq Var[t_0]$.*

B.2.3 Supporting theory with empirical data and inferring biological process from theoretical results

To apply our theory to our experiments, we first validate our theory by testing some of its key predictions using our experimental results. We then describe how we use our theoretical results to understand the processes occurring in the host.

Testing theory with experimental and simulated data

For the model in Figure 3.4A, we derived the mean egestion time as $\sum_{i=0}^n 1/(m_i - r_i)$ and the variance of the egestion time as $\sum_{i=0}^n 1/(m_i - r_i)^2$, where m_i and r_i refer to emigration rate and net reproductive rate at the i^{th} compartment. For simplicity, let $k_i = 1/(m_i - r_i)$. The mean egestion time is then $\sum_{i=0}^n k_i$ and the variance of the egestion time is $\sum_{i=0}^n k_i^2$. These formulae lead to two key predictions. We test these predictions on microsphere and microbial egestion time data from our *Egestion Time Experiment* (Section 3.5.4) and simulated data. Simulated data were generated for 1000 samples, each with 5 compartments. For each simulated sample, we drew $\{k_i\}$ from continuous uniform distribution with domain $[0, 1]$. We then calculated the mean and the variance from $\{k_i\}$ according to the formulae.

First, suppose that we have two samples, A and B. Suppose sample A has higher k_i in some compartments than in sample B, but the same k_i in the other compartments. Then, the mean (variance) of the egestion time of sample A is larger than the mean (variance) of the egestion time of sample B. Therefore, we predict positive correlation between the mean and the variance of the egestion

time. To test this prediction, we performed correlation test between mean and the variance of the egestion time using Spearman's rank correlation. Both simulated and experimental data showed positive correlation (Simulated: Spearman's $\rho = 0.96$, $p < 2.2 \times 10^{-16}$; Microsphere: Spearman's $\rho = 0.57$, $p = 8 \times 10^{-5}$; Bacteria: Spearman's $\rho = 0.75$, $p = 5.7 \times 10^{-8}$; Figure B.6, top row)

Second, our formulae show that

$$\frac{\text{Variance}}{\text{Mean}^2} = \frac{\sum_{i=0}^n k_i^2}{(\sum_{i=0}^n k_i)^2} = \frac{\sum_{i=0}^n k_i^2}{\sum_{i=0}^n k_i^2 + 2 \sum_{i \neq j} k_i k_j} \leq 1 \quad (\text{B.42})$$

Equation (B.42) implies that the coefficient of variation (C.V.) = $\sqrt{\text{Var}/\text{Mean}^2} \leq 1$. To test this prediction, we performed Student's t -test against the null hypothesis of $\mu = 1$. Both simulated and experimental data showed that the mean of C.V. values are significantly less than 1 (Simulated: mean C.V. = 0.52, $p < 2.2 \times 10^{-16}$; Microsphere: mean C.V. = 0.49, $p < 2.2 \times 10^{-16}$; Bacteria: mean C.V. = 0.41, $p < 2.2 \times 10^{-16}$; Figure B.6, bottom row).

To ensure that our simulated dataset were not dependent on the number of compartments or the domain of $\{k_i\}$, we also generated 1000 samples where the number of compartments was randomly generated from discrete uniform distribution with domain $[1, 50]$, and $\{k_i\}$ were drawn from continuous uniform distribution with domain $[0, 100]$. Our conclusions remained the same with this dataset.

Taken together, the data from our experiment support our theory. Next, we use our theory to further analyze our data.

Biological implications and inferring within-host population dynamics

Our theoretical results lead to important biological implications:

- The intuition behind our results is the following: as apparent death rate in the host increases (i.e. lower r), microorganisms that are egested intact are biased towards earlier egestion time whereas dead/retained microorganisms are not observed to egest. This bias towards earlier egestion time translates into lower mean of the egestion time. Furthermore, as the bias gets stronger, we expect less variance. The same logic applies to higher emigration rate (i.e. higher m).
- Even under a very general model, we showed that the qualitative results do not change; any ecological processes contributing to apparent death leads to shorter mean egestion time. Mean egestion time therefore is useful in inferring demographic processes.
- We do not need to measure the number of microorganisms ingested by the host; the time-series of the microorganisms egested is sufficient for calculating statistics of the egestion time distribution. Our approach could therefore be applied to pre-existing datasets, where the number of egested microorganisms was tracked over time.

While the number of ingested microorganisms is unnecessary to calculate egestion time statistics, it nevertheless provides additional information on the microbial demographic processes. Below, we categorize different demographic patterns of the microorganisms in the host, by leveraging both the proportion of microorganisms egested (relative to the number ingested) and the egestion time statistics.

Table B.1: Hypothetical microsphere and microbial populations used in numerical examples, with their set of r_i parameters and the resulting proportion of particles egested (%), mean (μ), and variance (σ^2) of the egestion time. For all five populations, $m_0 = 5, m_1 = m_2 = m_3 = m_4 = 1$.

Population	r_0	r_1	r_2	r_3	r_4	%	μ	σ^2
Microsphere	0	0	0	0	0	100	4.2	4.04
A	0	0	0	0	0	100	4.2	4.04
B	-5	0	0	0	0	50	4.1	4.01
C	-0.18	-0.18	-0.18	-0.18	-0.18	50	3.6	2.91
D	-5	-5	-5	-5	-5	0.04	0.8	0.12

Demographic interpretation of comparisons within treatments or between treatments using proportion of microorganisms egested and egestion time statistics.

In Figure 3.4B we identified four possible patterns in the fecal data resulting from different demographic processes in the host. Here we use numerical examples to illustrate this classification scheme. Table Table B.1 gives parameter values describing four hypothetical microbial populations and a hypothetical microsphere “population” used in these examples. All five of these populations had the same set of m_i values, but differed in the set of r_i values. Microspheres had the same set of m_i parameter values as the microbial population (*i.e.* $m_0 = 5, m_1 = m_2 = m_3 = m_4 = 1$), but had $r_i = 0$ for all i (no birth or mortality). We use Theorem 1 (*i.e.* mean egestion time = $\sum_{i=0}^n 1/(m_i - r_i)$ and variance of the egestion time = $\sum_{i=0}^n 1/(m_i - r_i)^2$), together with the proportion of particles (bacteria or microspheres) egested, to characterize how population dynamics are affected by the within-host processes.

Example 1: Equal proportions egested, and equal mean and variance of the egestion time.

Consider population A and microsphere in Table B.1. Throughout the gut, population A has $r_i = 0$ for all i and therefore has the same population dynamics as the microspheres. Consequently, the proportion of particles egested, the mean, and the variance of the egestion time are equal between microspheres and population A.

⇒ In general, if two types of particle have no demographic differences, we expect an equal proportion of particles egested, and equal mean and variance of the egestion times.

Example 2: Lower proportion egested, and lower mean and variance of the egestion time.

Consider population A and population D in Table B.1. Population D has large mortality and retention occurring across multiple compartments ($r_i = -5$ for all i), resulting in only 0.04 % of bacteria being egested in feces. Reduced population size in the gut affects the egestion time distribution, resulting in smaller mean and variance of the egestion time for population D than for population A.

⇒ In general, if one particle type has additional mortality and retention compared to another particle type, occurring gradually throughout gut passage, we expect a lower proportion egested and lower mean and variance of the egestion time.

Example 3: Lower proportion of particles egested but equal mean and variance of the egestion time.

Consider population B and the microspheres in Table B.1. In population B, mortality and retention happen quickly and intensely in one compartment, but not in others. The fraction of particles egested is lower for the bacteria, by a factor of 2. In contrast, the mean and variance of egestion time are both very similar to those for the microspheres.

⇒ *In general, if mortality or retention occur rapidly, the proportion of particles egested can be low even when the effect on the egestion time distribution is very small.*

Example 4: Equal proportion of particles egested but lower mean and variance of the egestion time.

Consider population B and population C in Table B.1. In population B, mortality and retention happen quickly and intensely in one compartment. In population C, mortality and retention happen gradually but persistently across the gut. Here, the mean egestion time for population B is 4.1, and the mean egestion time for population C is 3.6. Similarly, the variance of the egestion time for population B is 4.01, and the variance of the egestion time for population C is 2.91. Despite these differences, the fractions of bacteria that survive to be egested in feces are equal (both populations 50 %).

⇒ *In general, gradual but persistent mortality and retention can result in a similar proportion of particles egested as quick and intense mortality and retention, but the effect on the egestion time distribution is large. We expect similar proportion of particles egested between the two, but large difference in the egestion time statistics.*

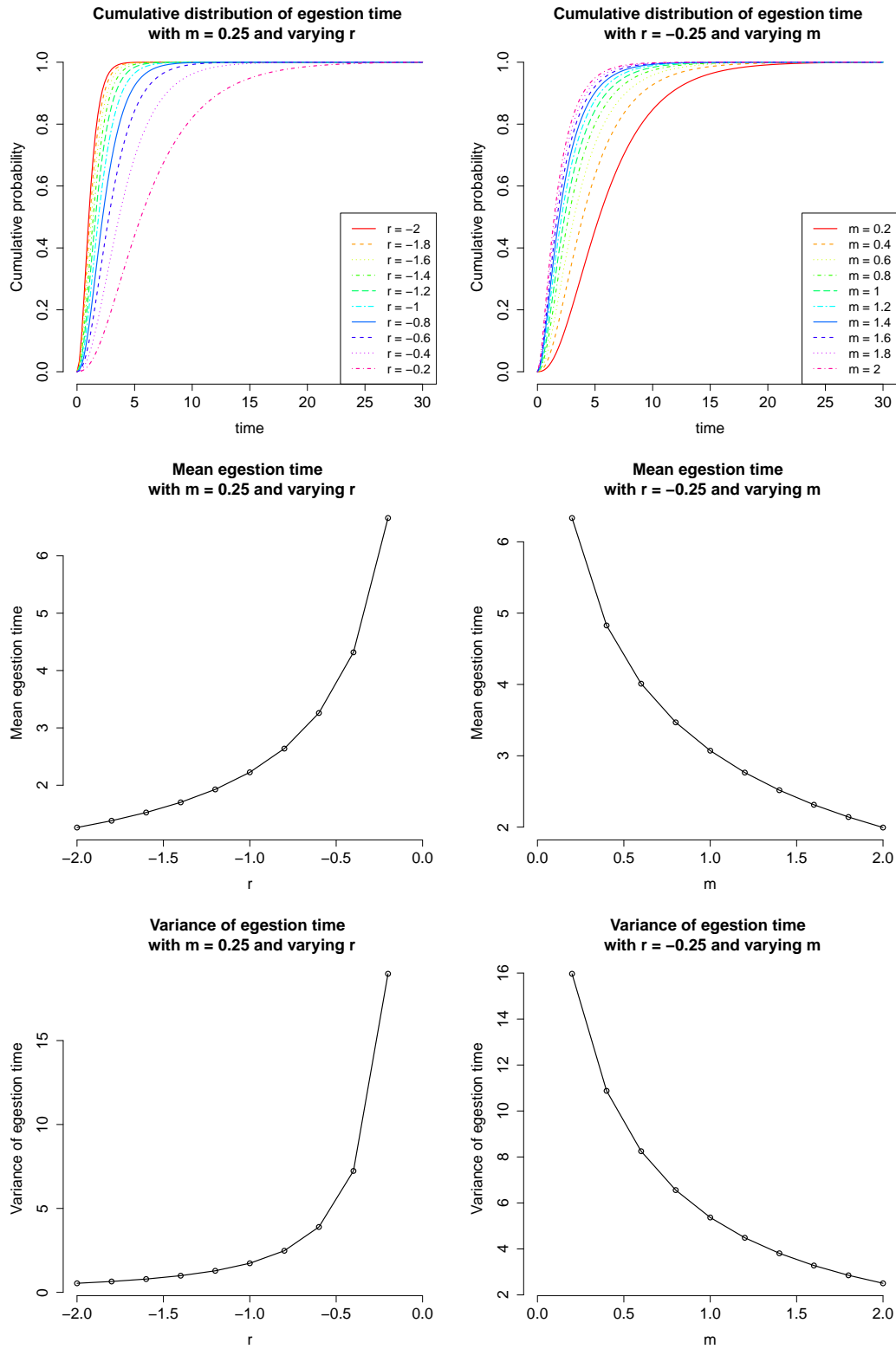


Figure B.4: Cumulative distribution function (top row), mean (middle row), and variance (bottom row) of the bacteria egestion time with varying parameters calculated by simulating Equation (B.34)

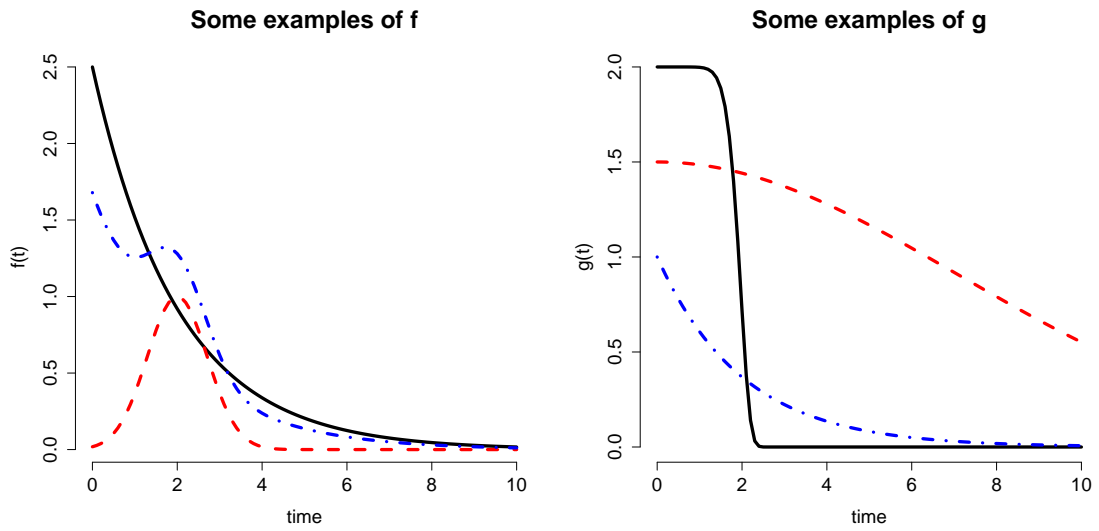


Figure B.5: Some examples of possible functional forms for f and g . Note that many other parameter values as well as vastly different functional forms satisfy the assumptions of Theorem 2.

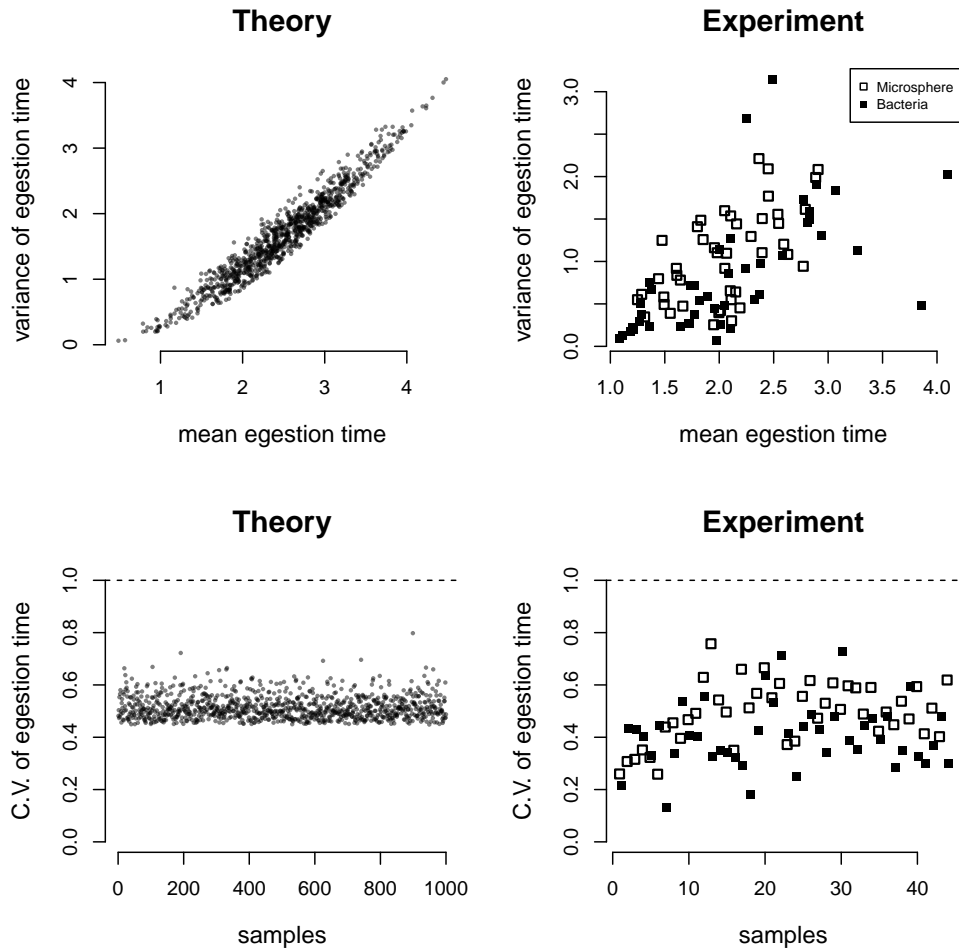


Figure B.6: Egestion time statistics from a simulation based on our theory (“Theory”, left column) and microsphere (white square) and bacteria (black square) in our experiments (“Experiment”, right column). Top row: Theory predicts a positive correlation between the variance and the mean of the egestion time. Bottom row: Theory predicts coefficient of variation (C.V.) ≤ 1 (dashed line).

SUPPLEMENTARY INFORMATION TO CHAPTER 4

C.1 Mating rate μ

In Section 4.3.1, we detailed the mating rule that an individual follows. In brief, an individual gets two chances to mate, but can mate once over a time step. $m(z)$ is the probability that an individual mates with a hybrid partner on her first chance, but she never mates with a heterospecific partner. An individual always mates with a partner on her second chance. Hybrid individual mates with everyone. Under these rules, we summarize the mating rate between $\{x, z\}$ individual and $\{x'', z''\}$ partners as:

$$\begin{aligned}
& \text{Mating with } \{x'', z''\} \text{ on first chance} + \text{Mating with } \{x'', z''\} \text{ on second chance} \\
&= \text{Probability of encountering and mating with } \{x'', z''\} \\
&\quad + (\text{Probability of encountering but not mating with } \{x'', z''\} \\
&\quad \quad \times \text{Probability of encountering } \{x'', z''\}) \\
&\quad + (\text{Probability of encountering but not mating with others} \\
&\quad \quad \times \text{Probability of encountering } \{x'', z''\})
\end{aligned} \tag{C.1}$$

With probability density of encountering $\{x'', z''\}$ partner (Equation (4.10)) and probability of mating with a hybrid (Equation (4.11)), we calculate the mating rate using Equation (C.1). Over each timestep, the probability μ_{ij} that an individual from population j with traits $\{y, z\}$ mates with a partner from popu-

lation i with trait in $[y'', y'' + h]$ and $[z'', z'' + h]$ is:

$$\begin{aligned}
\mu_{11} &= \alpha_1 E(n_1(z'', t)) \left[1 + \alpha_3 \int E(n_3(u, t)) du + E(0) + (1 - m(z)) \alpha_2 \int E(n_2(u, t)) du \right] \\
\mu_{21} &= \alpha_2 E(n_2(z'', t)) \left[\alpha_3 \int E(n_3(u, t)) du + E(0) + m(z) + (1 - m(z)) \alpha_2 \int E(n_2(u, t)) du \right] \\
\mu_{31} &= \alpha_3 E(n_3(z'', t)) \left[\alpha_3 \int E(n_3(u, t)) du + E(0) + (1 - m(z)) \alpha_2 \int E(n_2(u, t)) du \right] \\
\mu_{12} &= \alpha_1 E(n_1(z'', t)) [1 + E(0)] \\
\mu_{22} &= \alpha_2 E(n_2(z'', t)) [1 + E(0)] \\
\mu_{32} &= \alpha_3 E(n_3(z'', t)) [1 + E(0)] \\
\mu_{13} &= \alpha_1 E(n_1(z'', t)) \left[\alpha_1 \int E(n_1(u, t)) du + E(0) + (1 - m(z)) \alpha_2 \int E(n_2(u, t)) du \right] \\
\mu_{23} &= \alpha_2 E(n_2(z'', t)) \left[\alpha_1 \int E(n_1(u, t)) du + E(0) + m(z) + (1 - m(z)) \alpha_2 \int E(n_2(u, t)) du \right] \\
\mu_{33} &= \alpha_3 E(n_3(z'', t)) \left[1 + \alpha_3 \int E(n_1(u, t)) du + E(0) + (1 - m(z)) \alpha_2 \int E(n_2(u, t)) du \right]
\end{aligned} \tag{C.2}$$

BIBLIOGRAPHY

- [1] Levin, S. A. 1992. The problem of pattern and scale in ecology: the Robert H. MacArthur award lecture. *Ecology* 73:1943–1967.
- [2] Gould, S. J. 2002. *The Structure of Evolutionary Theory*. Harvard University Press.
- [3] Yoshida, T., L. E. Jones, S. P. Ellner, G. F. Fussmann, and N. G. Hairston. 2003. Rapid evolution drives ecological dynamics in a predator-prey system. *Nature* 424:303–306.
- [4] Murdoch, W. W., B. E. Kendall, R. M. Nisbet, C. J. Briggs, E. McCauley, and R. Bolser. 2002. Single-species models for many-species food webs. *Nature* 417:541–543.
- [5] Levins, R. 1968. *Evolution in Changing Environments: Some Theoretical Explorations*. Monographs in population biology. Princeton University Press.
- [6] Hiltunen, T., N. G. Hairston, G. Hooker, L. E. Jones, and S. P. Ellner. 2014. A newly discovered role of evolution in previously published consumer-resource dynamics. *Ecology Letters* 17:915–923.
- [7] Rosenblueth, A. and N. Wiener. 1945. The role of models in science. *Philosophy of Science* 12:316–321.
- [8] Dickinson, J. L., B. Zuckerberg, and D. N. Bonter. 2010. Citizen science as an ecological research tool: challenges and benefits. *Annual Review of Ecology, Evolution, and Systematics* 41:149–172.
- [9] Inamine, H., S. P. Ellner, J. P. Springer, and A. A. Agrawal. 2016. Linking the continental migratory cycle of the monarch butterfly to understand its population decline. *Oikos* 125:1081–1091.
- [10] Wilcove, D. S. and M. Wikelski. 2008. Going, going, gone: Is animal migration disappearing? *PLoS Biology* 6:e188.
- [11] Gustafsson, K. M., A. A. Agrawal, B. V. Lewenstein, and S. A. Wolf. 2015. The monarch butterfly through time and space: the social construction of an icon. *Bioscience* 65:612–622.

- [12] Garcia-Serrano, E., L. J. Reyes, and B. X. M. Alvarez. 2004. Locations and area occupied by monarch butterflies overwintering in Mexico from 1993-2002. In K. S. Oberhauser and M. J. Solensky, eds., *The Monarch Butterfly*, pp. 129–134. Ithaca, NY.
- [13] Rendón-Salinas, E., A. Fajarsdo-Arroyo, and G. Tavera-Alonso. 2014. Forest surface occupied by monarch butterfly hibernation colonies in December 2014. Tech. rep.
- [14] Swengel, A. B. 1995. Population fluctuations of the monarch (*Danaus plexippus*) in the 4th of July Butterfly Count 1977-1994. *American Midland Naturalist* 134:205–214.
- [15] Brower, L. P., O. R. TAYLOR, E. H. WILLIAMS, D. A. SLAYBACK, R. R. Zubieta, and M. I. Ramírez. 2011. Decline of monarch butterflies overwintering in Mexico: is the migratory phenomenon at risk? *Insect Conservation and Diversity* 5:95–100.
- [16] Ries, L., D. J. Taron, E. Rendón-Salinas, and K. S. Oberhauser. 2015. Connecting Eastern monarch population dynamics across their migratory cycle. In K. S. Oberhauser, K. R. Nail, and S. Altizer, eds., *Monarchs in a Changing World*. Cornell University Press, Ithaca, NY.
- [17] Badgett, G. and A. K. Davis. 2015. Population trends of monarchs at a Northern monitoring site: analyses of 19 years of fall migration counts at Peninsula Point, MI. *Annals of the Entomological Society of America* 108:700–706.
- [18] Davis, A. K. 2011. Are migratory monarchs really declining in Eastern North America? Examining evidence from two fall census programs. *Insect Conservation and Diversity* 5:101–105.
- [19] Crouse, D. T., L. B. Crowder, and H. Caswell. 1987. A stage-based population model for loggerhead sea turtles and implications for conservation. *Ecology* 68:1412–1423.
- [20] Flockhart, D. T. T., L. I. Wassenaar, T. G. Martin, K. A. Hobson, M. B. Wunder, and D. R. Norris. 2013. Tracking multi-generational colonization of the breeding grounds by monarch butterflies in Eastern North America. *Proceedings of the Royal Society B: Biological Sciences* 280:20131087.
- [21] Malcolm, S. B. 1993. Conservation of monarch butterfly migration in North America: An endangered phenomenon. In S. B. Malcolm and M. P.

Zalucki, eds., *Biology and Conservation of the Monarch Butterfly*, pp. 357–361. Natural History Museum of Los Angeles County.

- [22] Slayback, D. A. and L. P. Brower. 2007. Further aerial surveys confirm the extreme localization of overwintering monarch butterfly colonies in Mexico. *American Entomologist* 53:146–149.
- [23] Bradley, C. A. and S. Altizer. 2005. Parasites hinder monarch butterfly flight: implications for disease spread in migratory hosts. *Ecology Letters* 8:290–300.
- [24] Brower, L. P., L. S. Fink, and P. Walford. 2006. Fueling the fall migration of the monarch butterfly. *American Zoologist* 46:1123–1142.
- [25] Oberhauser, K. S. and A. T. Peterson. 2003. Modeling current and future potential wintering distributions of Eastern North American monarch butterflies. *Proceedings of the National Academy of Sciences of the United States of America* 100:14063–14068.
- [26] Oberhauser, K. S., M. D. Prysby, H. R. Mattila, D. E. Stanley-Horn, M. K. Sears, G. Dively, E. Olson, J. M. Pleasants, W. Lam, and R. L. Hellmich. 2001. Temporal and spatial overlap between monarch larvae and corn pollen. *Proceedings of the National Academy of Sciences of the United States of America* 98:11913–11918.
- [27] Pleasants, J. M. and K. S. Oberhauser. 2012. Milkweed loss in agricultural fields because of herbicide use: effect on the monarch butterfly population. *Insect Conservation and Diversity* 6:135–144.
- [28] Stenoien, C., K. R. Nail, and K. S. Oberhauser. 2015. Habitat productivity and temporal patterns of monarch butterfly egg densities in the Eastern United States. *Annals of the Entomological Society of America* 108:670–679.
- [29] Zalucki, M. P. and J. H. Lammers. 2010. Dispersal and egg shortfall in monarch butterflies: what happens when the matrix is cleaned up? *Ecological Entomology* 35:84–91.
- [30] Flockhart, D. T. T., J.-B. Pichancourt, D. R. Norris, and T. G. Martin. 2015. Unravelling the annual cycle in a migratory animal: breeding-season habitat loss drives population declines of monarch butterflies. *The Journal of Animal Ecology* 84:155–165.

- [31] Ries, L., D. J. Taron, and E. Rendón-Salinas. 2015. The disconnect between summer and winter monarch trends for the Eastern migratory population: possible links to differing drivers. *Annals of the Entomological Society of America* 108:691–699.
- [32] Koenig, W. D. 2006. Spatial synchrony of monarch butterflies. *American Midland Naturalist* 155:39–49.
- [33] Brower, L. P., L. S. Fink, R. J. Kiphart, V. Pocius, R. R. Zubieta, and M. I. Ramírez. 2015. Effect of the 2010–2011 drought on the lipid content of monarchs migrating through Texas to overwintering sites in Mexico. In K. S. Oberhauser, K. R. Nail, and S. Altizer, eds., *Monarchs in a Changing World*, pp. 117–129. Cornell University Press, Ithaca, NY.
- [34] Pleasants, J. M., E. H. WILLIAMS, L. P. Brower, K. S. Oberhauser, and O. R. TAYLOR. 2016. Conclusion of no decline in summer monarch population not supported. *Annals of the Entomological Society of America* 109:169–171.
- [35] Brown, R. G. 2004. *Smoothing, forecasting and prediction of discrete time series*. Dover Publications.
- [36] Walton, R. K. and L. P. Brower. 1996. Monitoring the fall migration of the monarch butterfly *Danaus plexippus* L. (Nymphalidae: Danainae) in Eastern North America: 1991-1994. *Journal of the Lepidopterists Society* pp. 1–20.
- [37] Meitner, C. J., L. P. Brower, and A. K. Davis. 2004. Migration patterns and environmental effects on stopover of monarch butterflies (Lepidoptera, Nymphalidae) at Peninsula Point, Michigan. *Environmental Entomology* 33:249–256.
- [38] R Core Team. 2017. *R: A Language and Environment for Statistical Computing*. R Foundation for Statistical Computing, Vienna, Austria.
- [39] Lund, R. E. 1975. Tables for an approximate test for outliers in linear models. *Technometrics* 17:473–476.
- [40] Davis, A. K. and L. A. Dyer. 2015. Long-term trends in Eastern North American monarch butterflies: a collection of studies focusing on spring, summer, and fall dynamics. *Annals of the Entomological Society of America* 108:661–663.
- [41] Dyer, L. A. and M. L. Forister. 2016. Wherefore and whither the modeler:

Understanding the population dynamics of monarchs will require integrative and quantitative techniques. *Annals of the Entomological Society of America* 109:172–175.

- [42] Crewe, T. L. and J. D. McCracken. 2015. Long-term trends in the number of monarch butterflies (Lepidoptera: Nymphalidae) counted on fall migration at Long Point, Ontario, Canada (1995-2014). *Annals of the Entomological Society of America* 108:707–717.
- [43] Nail, K. R., C. Stenoien, and K. S. Oberhauser. 2015. Immature monarch survival: effects of site characteristics, density, and time. *Annals of the Entomological Society of America* 108:680–690.
- [44] Hobson, K. A. 2008. Applying isotopic methods to tracking animal movements. In K. A. Hobson and L. I. Wassenaar, eds., *Tracking animal migration with stable isotopes*. Academic Press, Amsterdam.
- [45] Wassenaar, L. I. and A. Hobson. 1998. Natal origins of migratory monarch butterflies at wintering colonies in Mexico: new isotopic evidence. *Proceedings of the National Academy of Sciences of the United States of America* 95:15436–15439.
- [46] Brindza, L., L. P. Brower, and A. K. Davis. 2008. Comparative success of monarch butterfly migration to overwintering sites in Mexico from inland and coastal sites in Virginia. *Journal of the Lepidopterists Society* 62:189–200.
- [47] Steffy, G. 2015. Trends observed in fall migrant monarch butterflies (Lepidoptera: Nymphalidae) east of the Appalachian Mountains at an inland stopover in southern Pennsylvania over an eighteen year period. *Annals of the Entomological Society of America* 108:718–728.
- [48] Zipkin, E. F., L. Ries, R. Reeves, J. Regetz, and K. S. Oberhauser. 2012. Tracking climate impacts on the migratory monarch butterfly. *Global Change Biology* 18:3039–3049.
- [49] Krischik, V., M. Rogers, G. Gupta, and A. Varshney. 2015. Soil-applied imidacloprid translocates to ornamental flowers and reduces survival of adult *Coleomegilla maculata*, *Harmonia axyridis*, and *Hippodamia convergens* lady beetles, and larval *Danaus plexippus* and *Vanessa cardui* butterflies. *PloS One* 10:e0119133.
- [50] Vidal, O., J. López-García, and E. Rendón-Salinas. 2014. Trends in deforestation and forest degradation after a decade of monitoring in the

Monarch Butterfly Biosphere Reserve in Mexico. *Conservation Biology* 28:177–186.

- [51] Alonso-Mejía, A., E. Rendón-Salinas, E. Montesinos-Patiño, and L. P. Brower. 1997. Use of lipid reserves by monarch butterflies overwintering in Mexico: implications for conservation. *Ecological Applications* 7:934–947.
- [52] Montenegro, H., V. N. Solferini, L. B. Klaczko, and G. D. D. Hurst. 2005. Male-killing *Spiroplasma* naturally infecting *Drosophila melanogaster*. *Insect molecular biology* 14:281–287.
- [53] McKenna, D. D. and K. M. McKenna. 2001. Mortality of Lepidoptera along roadways in central Illinois. *Journal of the Lepidopterists Society* 55:63–68.
- [54] Guerra, P. A., R. J. Gegear, and S. M. Reppert. 2014. A magnetic compass aids monarch butterfly migration. *Nature communications* 5:4164.
- [55] Batalden, R. V. and K. S. Oberhauser. 2015. Potential changes in eastern North American monarch migration in response to an introduced milkweed, *Asclepias curassavica*. In K. S. Oberhauser, ed., *Monarchs in a Changing World*. Cornell University Press, Ithaca, NY.
- [56] Casagrande, R. A., F. S. Chew, and R. G. van Driesche. 2014. Ecological traps and weed biological control. In *Proceedings of the XIV International Symposium on Biological Control of Weeds, Kruger National Park, South Africa, 2-7 March 2014.*, pp. 105–111.
- [57] Davis, A. K. and E. Rendón-Salinas. 2010. Are female monarch butterflies declining in eastern North America? Evidence of a 30-year change in sex ratios at Mexican overwintering sites. *Biology Letters* 6:45–47.
- [58] Howard, E. and A. K. Davis. 2015. Investigating long-term changes in the spring migration of monarch butterflies (Lepidoptera: Nymphalidae) using 18 years of data from Journey North, a citizen science program. *Annals of the Entomological Society of America* 108:664–669.
- [59] Berenbaum, M. 2015. Road worrier. *American Entomologist* 61:5–8.
- [60] Rubinoff, D. 2015. Monarch butterfly doesn't need so much help. *The Washington Post* .

- [61] Shapiro, A. 2015. What you should know about monarchs (the Davis version). *The Davis Enterprise* .
- [62] Wagner, D., T. Gilligan, and J. Shuey. 2014. The committee's thoughts on the "Petition to protect the Monarch Butterfly (*Danaus plexippus plexippus*) under the Endangered Species Act". *News of The Lepidopterists Society* 56:190–191.
- [63] Espeset, A. E., J. G. Harrison, A. M. Shapiro, C. C. Nice, J. H. Thorne, D. P. Waetjen, J. A. Fordyce, and M. L. Forister. 2016. Understanding a migratory species in a changing world: climatic effects and demographic declines in the western monarch revealed by four decades of intensive monitoring. *Oecologia* 181:819–830.
- [64] McFall-Ngai, M., M. G. Hadfield, T. C. G. Bosch, H. V. Carey, T. Domazet-Lošo, A. E. Douglas, N. Dubilier, G. Eberl, T. Fukami, S. F. Gilbert, U. Hentschel, N. King, S. Kjelleberg, A. H. Knoll, N. Kremer, S. K. Mazmanian, J. L. Metcalf, K. Neelson, N. E. Pierce, J. F. Rawls, A. Reid, E. G. Ruby, M. Rumpho, J. G. Sanders, D. Tautz, and J. J. Wernegreen. 2013. Animals in a bacterial world, a new imperative for the life sciences. *Proceedings of the National Academy of Sciences of the United States of America* 110:3229–3236.
- [65] Hooper, L. V. and J. I. Gordon. 2001. Commensal host-bacterial relationships in the gut. *Science* 292:1115–1118.
- [66] Ezenwa, V. O., N. M. Gerardo, D. W. Inouye, M. Medina, and J. B. Xavier. 2012. Animal behavior and the microbiome. *Science* 338:198–199.
- [67] Bauer, K. C., K. E. Huus, and B. B. Finlay. 2016. Microbes and the mind: emerging hallmarks of the gut microbiota-brain axis. *Cellular Microbiology* 18:632–644.
- [68] Rooks, M. G. and W. S. Garrett. 2016. Gut microbiota, metabolites and host immunity. *Nature Reviews Immunology* 16:341–352.
- [69] Flint, H. J., K. P. Scott, P. Louis, and S. H. Duncan. 2012. The role of the gut microbiota in nutrition and health. *Nature Reviews Gastroenterology & Hepatology* 9:577–589.
- [70] Buchon, N., N. Silverman, and S. Cherry. 2014. Immunity in *Drosophila melanogaster* – from microbial recognition to whole-organism physiology. *Nature Reviews Immunology* 14:796–810.

- [71] Dethlefsen, L., M. McFall-Ngai, and D. A. Relman. 2007. An ecological and evolutionary perspective on human–microbe mutualism and disease. *Nature* 449:811–818.
- [72] Slack, E., S. Hapfelmeier, B. Stecher, Y. Velykoredko, M. Stoel, M. A. E. Lawson, M. B. Geuking, B. Beutler, T. F. Tedder, W.-D. Hardt, P. Bercik, E. F. Verdu, K. D. McCoy, and A. J. Macpherson. 2009. Innate and adaptive immunity cooperate flexibly to maintain host-microbiota mutualism. *Science* 325:617–620.
- [73] Costello, E. K., K. Stagaman, L. Dethlefsen, B. J. M. Bohannan, and D. A. Relman. 2012. The application of ecological theory toward an understanding of the human microbiome. *Science* 336:1255–1262.
- [74] Foster, K. R., J. Schluter, K. Z. Coyte, and S. Rakoff-Nahoum. 2017. The evolution of the host microbiome as an ecosystem on a leash. *Nature Publishing Group* 548:43–51.
- [75] Adair, K. L. and A. E. Douglas. 2017. Making a microbiome: the many determinants of host-associated microbial community composition. *Current Opinion in Microbiology* 35:23–29.
- [76] Prosser, J. I., B. J. M. Bohannan, T. P. Curtis, R. J. Ellis, M. K. Firestone, R. P. Freckleton, J. L. Green, L. E. Green, K. Killham, J. J. Lennon, A. M. Osborn, M. Solan, C. J. van der Gast, and J. P. W. Young. 2007. The role of ecological theory in microbial ecology. *Nature Reviews Microbiology* 5:384–392.
- [77] Obadia, B., Z. T. Güvener, V. Zhang, J. A. Ceja-Navarro, E. L. Brodie, W. W. Ja, and W. B. Ludington. 2017. Probabilistic invasion underlies natural gut microbiome stability. *Current Biology* 27:1999–2006.e8.
- [78] Faust, K., L. Lahti, D. Gonze, W. M. de Vos, and J. Raes. 2015. Metagenomics meets time series analysis: unraveling microbial community dynamics. *Current Opinion in Microbiology* 25:56–66.
- [79] Stein, R. R., V. Bucci, N. C. Toussaint, C. G. Buffie, G. Räscher, E. G. Pamer, C. Sander, and J. B. Xavier. 2013. Ecological modeling from time-series inference: insight into dynamics and stability of intestinal microbiota. *PLoS Computational Biology* 9:e1003388.
- [80] Fink, C., F. Staubach, S. Kuenzel, J. F. Baines, and T. Roeder. 2013. Noninvasive analysis of microbiome dynamics in the fruit fly *Drosophila melanogaster*. *Applied and Environmental Microbiology* 79:6984–6988.

- [81] Koenig, J. E., A. Spor, N. Scalfone, A. D. Fricker, J. Stombaugh, R. Knight, L. T. Angenent, and R. E. Ley. 2011. Succession of microbial consortia in the developing infant gut microbiome. *Proceedings of the National Academy of Sciences of the United States of America* 108:4578–4585.
- [82] Hoy, Y. E., E. M. Bik, T. D. Lawley, S. P. Holmes, D. M. Monack, J. A. Theriot, and D. A. Relman. 2015. Variation in taxonomic composition of the fecal microbiota in an inbred mouse strain across individuals and time. *PLoS One* 10:e0142825.
- [83] Jemielita, M., M. J. Taormina, A. R. Burns, J. S. Hampton, A. S. Rolig, K. Guillemin, and R. Parthasarathy. 2014. Spatial and temporal features of the growth of a bacterial species colonizing the zebrafish gut. *mBio* 5:e01751–14.
- [84] Vega, N. M. and J. Gore. 2017. Stochastic assembly produces heterogeneous communities in the *Caenorhabditis elegans* intestine. *PLoS Biology* 15:e2000633.
- [85] Erkosar, B., G. Storelli, A. Defaye, and F. Leulier. 2013. Host-intestinal microbiota mutualism: “learning on the fly”. *Cell Host & Microbe* 13:8–14.
- [86] Broderick, N. A. and B. Lemaitre. 2014. Gut-associated microbes of *Drosophila melanogaster*. *Gut Microbes* 3:307–321.
- [87] Wong, A. C.-N., J. M. Chaston, and A. E. Douglas. 2013. The inconstant gut microbiota of *Drosophila* species revealed by 16S rRNA gene analysis. *The ISME Journal* 7:1922–1932.
- [88] Wong, A. C.-N., Y. Luo, X. Jing, S. Franzenburg, A. Bost, and A. E. Douglas. 2015. The host as the driver of the microbiota in the gut and external environment of *Drosophila melanogaster*. *Applied and Environmental Microbiology* 81:6232–6240.
- [89] Chandler, J. A., J. Morgan Lang, S. Bhatnagar, J. A. Eisen, and A. Kopp. 2011. Bacterial communities of diverse *Drosophila* species: ecological context of a host–microbe model system. *PLoS genetics* 7:e1002272.
- [90] Broderick, N. A., N. Buchon, and B. Lemaitre. 2014. Microbiota-induced changes in *Drosophila melanogaster* host gene expression and gut morphology. *mBio* 5:e01117–14.

- [91] Staubach, F., J. F. Baines, S. Künzel, E. M. Bik, and D. A. Petrov. 2013. Host species and environmental effects on bacterial communities associated with *Drosophila* in the laboratory and in the natural environment. *PloS One* 8:e70749.
- [92] Blum, J. E., C. N. Fischer, J. Miles, and J. Handelsman. 2013. Frequent replenishment sustains the beneficial microbiome of *Drosophila melanogaster*. *mBio* 4:e00860–13.
- [93] Sang, J. H. 1956. The quantitative nutritional requirements of *Drosophila melanogaster*. *Journal of Experimental Biology* 33:45–72.
- [94] Newell, P. D. and A. E. Douglas. 2014. Interspecies interactions determine the impact of the gut microbiota on nutrient allocation in *Drosophila melanogaster*. *Applied and Environmental Microbiology* 80:788–796.
- [95] Chaston, J. M., P. D. Newell, and A. E. Douglas. 2014. Metagenome-wide association of microbial determinants of host phenotype in *Drosophila melanogaster*. *mBio* 5:e01631–14.
- [96] Johnson, J. B. and K. S. Omland. 2004. Model selection in ecology and evolution. *Trends in Ecology and Evolution* 19:101–108.
- [97] Akaike, H. 1998. Information theory and an extension of the maximum likelihood principle. In E. Parzen, K. Tanabe, and G. Kitagawa, eds., *Selected Papers of Hirotugu Akaike*, pp. 199–213. Springer New York, New York, NY.
- [98] Levy, R. and E. Borenstein. 2013. Metabolic modeling of species interaction in the human microbiome elucidates community-level assembly rules. *Proceedings of the National Academy of Sciences of the United States of America* 110:12804–12809.
- [99] Lemaitre, B. and I. Miguel-Aliaga. 2013. The digestive tract of *Drosophila melanogaster*. *Annual Review of Genetics* 47:377–404.
- [100] Overend, G., Y. Luo, L. Henderson, A. E. Douglas, S. A. Davies, and J. A. T. Dow. 2016. Molecular mechanism and functional significance of acid generation in the *Drosophila* midgut. *Scientific reports* 6:27242.
- [101] Buchon, N., N. A. Broderick, M. Poidevin, S. Pradervand, and B. Lemaitre.

2009. *Drosophila* intestinal response to bacterial infection: activation of host defense and stem cell proliferation. *Cell Host & Microbe* 5:200–211.
- [102] Buchon, N., D. Osman, F. P. A. David, H. Y. Fang, J.-P. Boquete, B. Deplancke, and B. Lemaitre. 2013. Morphological and molecular characterization of adult midgut compartmentalization in *Drosophila*. *Cell reports* 3:1725–1738.
- [103] Garcia, J. R. and N. M. Gerardo. 2014. The symbiont side of symbiosis: do microbes really benefit? *Frontiers in Microbiology* 5:510.
- [104] Hanski, I. 1991. Single-species metapopulation dynamics: concepts, models and observations. *Biological Journal of the Linnean Society* 42:17–38.
- [105] Buchon, N., N. A. Broderick, S. Chakrabarti, and B. Lemaitre. 2009. Invasive and indigenous microbiota impact intestinal stem cell activity through multiple pathways in *Drosophila*. *Genes & Development* 23:2333–2344.
- [106] Carpenter, A. E., T. R. Jones, M. R. Lamprecht, C. Clarke, I. H. Kang, O. Friman, D. A. Guertin, J. H. Chang, R. A. Lindquist, J. Moffat, P. Golland, and D. M. Sabatini. 2006. CellProfiler: image analysis software for identifying and quantifying cell phenotypes. *Genome Biology* 7:R100.
- [107] Howard, D. J. 1993. Reinforcement: origin, dynamics, and fate of an evolutionary hypothesis . In R. G. Harrison, ed., *Hybrid Zones and the Evolutionary Process*, pp. 46–69.
- [108] Hubbs, C. L. 1955. Hybridization between fish species in nature. *Systematic zoology* 4:1–20.
- [109] Barton, N. H. and G. M. Hewitt. 1989. Adaptation, speciation and hybrid zones. *Nature* 341:497–503.
- [110] Servedio, M. R. and M. A. Noor. 2003. The role of reinforcement in speciation: theory and data. *Annual Review of Ecology, Evolution, and Systematics* pp. 339–364.
- [111] Coyne, J. A. and H. A. Orr. 2004. *Speciation*. Sinauer.
- [112] Hopkins, R. and M. D. Rausher. 2012. Pollinator-mediated selection on flower color allele drives reinforcement. *Science* 335:1090–1092.

- [113] Wirtz, P. 1999. Mother species-father species: unidirectional hybridization in animals with female choice. *Animal Behaviour* 58:1–12.
- [114] Price, T. D. 2007. *Speciation in Birds*. Roberts and Company, Greenwood Village, Colorado.
- [115] Noor, M. A. 1995. Speciation driven by natural selection in *Drosophila*. *Nature* 375:674–675.
- [116] Yukilevich, R. 2012. Asymmetrical patterns of speciation uniquely support reinforcement in *Drosophila*. *Evolution* 66:1430–1446.
- [117] Matute, D. R. 2010. Reinforcement of gametic isolation in *Drosophila*. *PLoS Biology* 8:e1000341.
- [118] Benedix, J. H. and D. J. Howard. 1991. Calling song displacement in a zone of overlap and hybridization. *Evolution* 45:1751–1759.
- [119] Sawyer, S. and D. L. Hartl. 1981. On the evolution of behavioral reproductive isolation: the Wallace effect. *Theoretical Population Biology* 19:261–273.
- [120] Wilson, D. S. and A. Hedrick. 1982. Speciation and the economics of mate choice. *Evolutionary Theory* 6:15–24.
- [121] Real, L. 1990. Search theory and mate choice. I. Models of single-sex discrimination. *American Naturalist* 136:376–404.
- [122] Servedio, M. R. and M. Kirkpatrick. 1997. The effects of gene flow on reinforcement. *Evolution* 51:1764–1772.
- [123] Nosil, P., B. J. Crespi, and C. P. Sandoval. 2003. Reproductive isolation driven by the combined effects of ecological adaptation and reinforcement. *Proceedings of the Royal Society B: Biological Sciences* 270:1911–1918.
- [124] Nosil, P. 2012. Degree of sympatry affects reinforcement in *Drosophila*. *Evolution* 67:868–872.
- [125] Bordenstein, S. R., M. D. Drapeau, and J. H. Werren. 2000. Intraspecific variation in sexual isolation in the jewel wasp *Nasonia*. *Evolution* 54:567–573.

- [126] Izzo, A. S. and D. A. Gray. 2011. Heterospecific courtship and sequential mate choice in sister species of field crickets. *Animal Behaviour* 81:259–264.
- [127] Taylor, D. J. and P. D. Hebert. 1993. Habitat-dependent hybrid parentage and differential introgression between neighboringly sympatric *Daphnia* species. *Proceedings of the National Academy of Sciences of the United States of America* 90:7079–7083.
- [128] Ribi, G. and S. Oertli. 2000. Frequency of interspecific matings and of hybrid offspring in sympatric populations of *Viviparus ater* and *V. contectus* (Mollusca: Prosobranchia). *Biological Journal of the Linnean Society* 71:133–143.
- [129] Willis, P. M., M. J. Ryan, and G. G. Rosenthal. 2011. Encounter rates with conspecific males influence female mate choice in a naturally hybridizing fish. *Behavioral Ecology* 22:1234–1240.
- [130] Dowling, T. E., G. R. Smith, and W. M. Brown. 1989. Reproductive isolation and introgression between *Notropis cornutus* and *Notropis chrysocephalus* (Family Cyprinidae): comparison of morphology, allozymes, and mitochondrial DNA. *Evolution* 43:620–634.
- [131] Avise, J. C. and N. C. Saunders. 1984. Hybridization and introgression among species of sunfish (*Lepomis*): analysis by mitochondrial DNA and allozyme markers. *Genetics* 108:237–255.
- [132] Avise, J. C., P. C. Pierce, and M. J. Van Den Avyle. 1997. Cytonuclear introgressive swamping and species turnover of bass after an introduction. *Journal of Heredity* 88:14–20.
- [133] Hoskin, C. J., M. Higgie, K. R. McDonald, and C. Moritz. 2005. Reinforcement drives rapid allopatric speciation. *Nature* 437:1353–1356.
- [134] Malmos, K. B., B. K. Sullivan, and T. Lamb. 2001. Calling behavior and directional hybridization between two toads (*Bufo microscaphus* x *B. woodhousii*) in Arizona. *Evolution* 55:626–630.
- [135] Karl, S. A., B. W. Bowen, and J. C. Avise. 1995. Hybridization among the ancient mariners: characterization of marine turtle hybrids with molecular genetic assays. *Journal of Heredity* 86:262–268.
- [136] Helbig, A. J., M. Salomon, S. Bensch, and I. Seibold. 2001. Male-biased

gene flow across an avian hybrid zone: evidence from mitochondrial and microsatellite DNA. *Journal of Evolutionary Biology* 14:277–287.

- [137] Grant, P. R. and B. R. Grant. 1997. Hybridization, sexual imprinting, and mate choice. *American Naturalist* 149:1–28.
- [138] Thulin, C.-G. and H. Tegelström. 2002. Biased geographical distribution of mitochondrial DNA that passed the species barrier from mountain hares to brown hares (genus *Lepus*): an effect of genetic incompatibility and mating behaviour? *Journal of Zoology* 258:299–306.
- [139] Lancaster, M. L., S. D. Goldsworthy, and P. Sunnucks. 2010. Two behavioural traits promote fine-scale species segregation and moderate hybridisation in a recovering sympatric fur seal population. *BMC Evolutionary Biology* 10:143.
- [140] Ellner, S. P. and M. Rees. 2006. Integral projection models for species with complex demography. *The American Naturalist* 167:410–428.
- [141] Rees, M. and S. P. Ellner. 2016. Evolving integral projection models: evolutionary demography meets eco-evolutionary dynamics. *Methods in Ecology and Evolution* .
- [142] Ellner, S. P., D. Z. Childs, and M. Rees. 2016. *Data-driven Modelling of Structured Populations. A Practical Guide to the Integral Projection Model*. Springer International Publishing, Switzerland.
- [143] Barton, N. H., A. M. Etheridge, and A. Véber. 2016. The infinitesimal model. *bioRxiv* pp. 1–54.
- [144] Servedio, M. R., Y. Brandvain, S. Dhole, C. L. Fitzpatrick, E. E. Goldberg, C. A. Stern, J. Van Cleve, and D. J. Yeh. 2014. Not just a theory—The utility of mathematical models in evolutionary biology. *PLoS Biology* 12:e1002017–5.
- [145] Bonduriansky, R. 2001. The evolution of male mate choice in insects: a synthesis of ideas and evidence. *Biological Reviews* 76:305–339.
- [146] Dixon, P. M. 2013. Ripley’s *K* function. In A. H. El-Shaarawai and P. WW, eds., *Encyclopedia of Environmetrics*, pp. 2239–2248. Encyclopedia of environmetrics.

- [147] Malcolm, S. B. and M. P. Zalucki, eds. 1993. *Biology and Conservation of the Monarch Butterfly*. Natural History Museum of Los Angeles County.
- [148] Link, W. A. and J. R. Sauer. 1999. Controlling for varying effort in count surveys: an analysis of Christmas Bird Count data. *Journal of Agricultural, Biological, and Environmental Statistics* 4:116–125.
- [149] Vandenbosch, R. 2007. What do monarch population time series tell us about eastern and western population mixing? *Journal of the Lepidopterists Society* 61:28–31.
- [150] Link, W. A., J. R. Sauer, and D. K. Niven. 2006. A hierarchical model for regional analysis of population change using Christmas Bird Count data, with application to the American Black Duck. *The Condor* 108:13–24.
- [151] McIlroy, D., R. Brownrigg, T. P. Minka, and R. Bivand. 2017. `mapproj`: Map Projections .
- [152] Baddeley, A., E. Rubak, and R. Turner. 2015. *Spatial Point Patterns: Methodology and Applications with R*. Chapman and Hall/CRC Press, London.
- [153] Marx, C. J. and M. E. Lidstrom. 2001. Development of improved versatile broad-host-range vectors for use in methylotrophs and other Gram-negative bacteria. *Microbiology* 147:2065–2075.
- [154] Shanks, R. M. Q., N. C. Caiazza, S. M. Hinsa, C. M. Toutain, and G. A. O’Toole. 2006. *Saccharomyces cerevisiae*-based molecular tool kit for manipulation of genes from Gram-negative bacteria. *Applied and Environmental Microbiology* 72:5027–5036.
- [155] Deeraksa, A., S. Moonmangmee, H. Toyama, M. Yamada, O. Adachi, and K. Matsushita. 2005. Characterization and spontaneous mutation of a novel gene, *polE*, involved in pellicle formation in *Acetobacter tropicalis* SKU1100. *Microbiology* 151:4111–4120.